Quantec Geoscience Inc.
116 Spadina Ave., Suite 400
Toronto, ON, M5V 2K6
Phone (416) 306 1941
Fax (416) 306 1949

Geophysical Survey Report

Report Regarding the
Geophysical Survey INTERPRETATION of
Quantec TITAN-24 Distributed Array System
TENSOR-MT and DCIP SURVEYS

at

The Black Fox Project

on behalf of

Apollo Gold Corporation

R. Gordon
J. M. Legault
E. Martinez
W. Qian
August, 2003
Project QGI-285

EXECUTIVE SUMMARY

Introduction

A Titan-24 survey was commissioned by ***Apollo Gold*** to assist with their ongoing exploration program at the ***Black Fox Mine*** Property in Northern Ontario. At *Black Fox*, nine (**9**) survey lines, between 1.9 and 2.7km long, were acquired at 200m line-spacings and 100m stations, totaling 19.7 km of coverage. The MT and DCIP data were interpreted using 2D computer inversion and the results, in relation to the known geology, are described in this document.

The Titan system is a multi-channel, distributed acquisition survey, recording broad band Magnetotelluric resistivity data (AMT/MT), D.C. Resistivity data and Induced Polarization chargeability data. The system provides high multiplicity data sets utilizing 24bit Sigma Delta A/D conversion and Full waveform instantaneous Time series data acquisition. The Titan system consists of 3 main elements: 1) its acquisition system, 2) its digital signal processing, and 3) its 2D-3D interpretation capability.

The Titan-24 system is used to provide three independent data sets capable of accurately measuring subsurface resistivities to depths in excess of one kilometer, and chargeabilities (mineralization) to depths of 400-600 meters.

Survey Objectives

The primary objectives of this survey were:

1. Identify disseminated sulphide pods in the first 200m of depth
2. Look for flow type ore characterized by 5-10% massive disseminated sulphides in the 0-700m range with DCIP and deeper (700-1300m) with Titan MT Resistivity
3. Detect structural flexures within the subsurface
4. Provide additional structural information and targeting ability for deep (>400m) drill programs.

In addition, based on later discussions/geologic evidence provided by ***Apollo Gold***

5. Detect sulphide-poor/magnetite-depleted, *ankerite-altered* zones, along the Destor-Porcupine Break, with similar characteristics to the ultramafic volcanic-hosted ***Black Fox*** gold deposit.

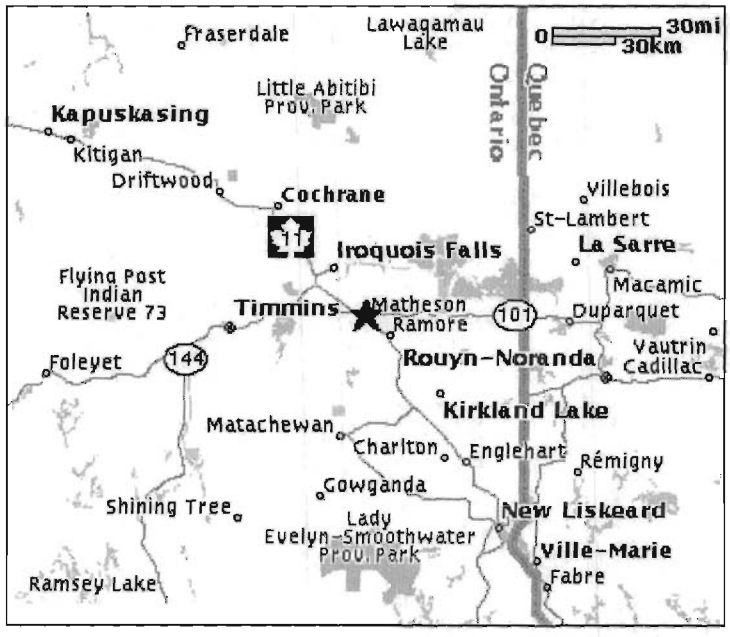

Figure 1: Black Fox Project General Location Map

Project Results

The ***Black Fox*** MT and DCIP Titan surveys have successfully mapped major structures potentially relating the Destor-Porcupine Break (DPB) and also identified numerous resistivity and chargeability anomalies for follow up.

Specifically, to the ***Black Fox Property,*** the Titan system responded as follows:

- In general the data quality is good to excellent, with an average error of <0.1% for the DC voltage and <0.1mrad for the IP phase, as well as <1/20TH of a decade for the MT resistivity and <3degrees for the MT phase – this, in spite of the close proximity of man-made and mine-site culture.
- The Titan surveys have identified as many as ***57*** separate DCIP and MT anomalies, including ***12*** highest priority features, which resemble the ***Black Fox*** sheared/altered/magnetite-depleted /sulphide-poor ultramafic-hosted target model, and are also aligned along the DPB. In addition, at least ***25*** high 2ND priority targets were identified. The remaining third of the targets (***20***) feature resistivity and chargeability combinations which differentiate these from the other primary targets.
- Based on the magnetite-depleted/low sulphide target model and the physical property data collected, the ***Black Fox*** type-response is a "chargeability low" and a major contact-type structural feature in the resistivity (*Type I*). Although unusual, it indeed appears to explain the Titan responses we obtained over the ***Black Fox/Glimmer*** mine site (see Figure 2and Figure 3).

  On nearly all the lines, several mod-large IP voids were identified which appear to lay along major DC-MT geoelectric structures - these seem to be strongest east of line 800E to 1600E, and in close proximity to the inferred *Destor-Porcupine Break* and it is believed these are the areas worth following. However, chargeability low targets are difficult to identify with assurance because they also closely resemble barren lithologic unit. Without the magnetics, it is hard to differentiate between the two.
- In addition, **3** other types of Titan targets were identified, all of which were based on chargeability highs, relating to possible disseminated to massive sulphides, with varying types of resistivity association – specifically, *Type II* = Destor-Porcupine stockwork-type (Res contact structure + IP high); *Type III* = Qtz-carbonate altered type (High Res + IP High) and, finally, *Type IV* = massive sulphide or clay-altered type (Low Res + IP High). Of the three types, *Type II* and, possibly also *Type III,* represent the target-classes which best describe the geologic model described in the initial survey objectives and is also most favoured in Archean gold environments.
- In general, the Titan targets are aligned along up to 3 separate horizons, which lie north, south and subparallel to the DPB. In addition ***1-2*** north-south chargeability trends have also been defined, which may represent mineralized structural breaks (Figure 3).
- In general the target size ranges from 100 x 100m to >400 x 400m, and the average depth of burial is >100m – with many DCIP-defined mineralized bodies extending below 500-750m and MT-defined structures and contacts mapped to below 1-1.5km.
- DCIP has proven to be the best indicator of anomalous chargeability relating to both the *presence and/or absence of disseminate sulphides* associated with ***Black Fox*** and other Archean lode-gold mineralization, within the upper ***350-750m*** of the bedrock. In the present evaluation, the IP chargeability has been used as the primary sulphide mapping and targeting tool.
- MT has proven to be the best indicator of geologic structure along the inferred ***Destor-Porcupine Break***. In the medium to lower depth range **(>300m-1.5km)**, the MT inversion results have been able to define major moderate to steeply-dipping resistivity contacts, likely ascribed to major structure and/or lithology, and which correlate well with the DCIP anomalies, but also often extending to great depth. As a result, the MT is used as the preferred structural mapping tool at ***Black Fox.***

Conclusions

The exploration objectives have been favourably answered, using the Titan-24 distributed acquisition technology and integrated geologic and geophysical interpretation. In response to the survey objectives, the following conclusions can be drawn:

- Several resistivity contacts down to 1 km have been mapped consistently by MT.
- Some low resistivity features on these contacts have been identified by DC inversions. Most of these features show up on MT sections as well.
- The most significant contacts correlate with the ***Destor-Porcupine Break (DPB)***.
- Numerous chargeability anomalies (highs and lows) have been identified, that likely define sulphides (or magnetite), which often lie on the structures defined by the resistivity contacts. They represent interesting drilling targets.

The interpretation consists of a schematic structural interpretation and our Titan targets overlain on each of the 3 or 4 types of 2D inversion models which were produced – however the interpretation mainly utilized the 2D MT Resistivity, for the structure, and the 2D Sharp Model DCIP Chargeability (see Figure 2), for the chargeability high & low features, which are primary indicators of sulphide mineralization and magnetite. Of note, the cross-sectional structural geophysical interpretation offered is crude (i.e., due to poor line-to-line continuity of some features) – the primary objective is to emphasize the various breaks and resistivity contacts in the MT models, which are then used to correlate against the IP highs and lows.

As a general rule, the MT resistivity and, to a less extent, the DC resistivity results appear to have identified various resistivity breaks and contacts, which could be used to correlate against the IP chargeability highs and lows, which are primary indicators of sulphide &/or magnetite content. In our opinion, the Titan results are defining major subvertical structures, particularly along the inferred Destor-Porcupine Break (DBP), as well as more subtle south-west dipping features. Similar geologic / geoelectric features have been identified in our OMET Titan studies in Red Lake (see Figure 5). Based on these results, it is believed that IP highs and/or lows, which lie along any MT or DC structural breaks, represent targets of interest for gold exploration (Figure 4).

A list of prioritized targets was produced and an explanation of the geologic model and also the borehole physical property results that the interpretation was based upon. These are listed in a line-by-line basis, with approx. 4-6 targets per line, and are prioritized from 1 to 4 - essentially representing the 4 main, contrasting types of Titan anomalies that have been identified on the ***Black Fox*** property. Each type has its own combination of physical properties (resistivity & chargeability).

Recommendations

The Titan-24 approach has had two valuable applications at ***Black Fox:*** A) Evaluation and Guiding drill targets, and B) Accountable and Scientific Analysis of geological concepts and ideas, geophysical results during and post-drilling to minimize follow-up holes. In addition, we recommend that:

a) Depending on various petrophysical models which are considered to be favourable in the ***Black Fox*** geologic context, these Titan anomalies need to be studied, drilled and calibrated to gain further geologic knowledge of the property. In particular, with regards to explaining the four contrasting anomaly types (*Types I to IV*) encountered, in order to confirm the source material and to focus drilling onto other favourable targets of a similar type/physical property mix.

b) That drill-testing of the Titan anomalies should be conducted in a systematic fashion, by: i) working from known geology to lesser known, ii) from the shallow to deeper targets, iii) from the center of coverage, where the geoelectric structure is best defined in the 2D inversions, to the outside of coverage, where it more poorly defined, due to 2D aperture, and iii) from the multi-parameter anomalies (IP+DC+MT) Titan-defined targets to the more poorly-correlated (or deep MT) single-parameter anomalies.

c) Any drilling should focus in on the center of the anomalies that we've described in our anomaly table and cross-sections. The overall dimensions and depths are added to facilitate the drilling effort.

d) The Titan coverage should be extended along strike, to the northwest and southeast, in order to identify other targets similar to ***Black Fox*** along the *Destor-Porcupine Break*. If the more

southern or northern anomalies also prove favourable, consideration should be given to extend or shift the future survey coverage, north and south, in order to provide adequate anomaly definition – extending the lines to a distance approximately 2X the desired depth of investigation.

e) Titan targets that are drilled should be logged using borehole Petrophysics, in order to determine the true geologic source of anomalies, and also surveyed with borehole transient EM (BHTEM) to detect off-hole conductors and to identify the nature and extent of in-hole sulphide mineralization.

f) A 3D Gocad model of the property should be built and queried for fully integrated drill targets. Other elements for the query may include geochemistry, assays, depth, etc. Following this, consideration should be given to perform additional geologically-constrained inversions, in order to further refine the interpretation, if there is sufficiently good geological control and petrophysical database for the property. If so, unknown and potentially important targets can be more easily discriminated from the known geology, particularly at depth.

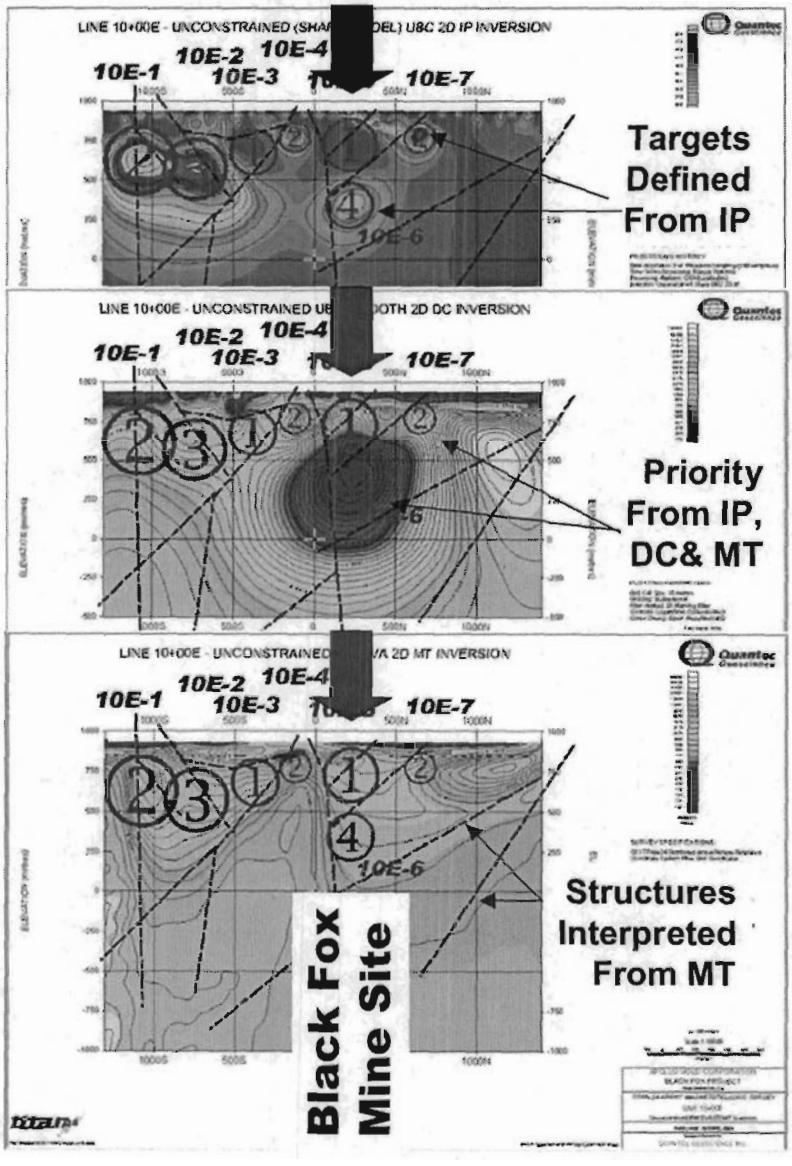

Figure 2: Cross-sectional view of Titan 2D Inversion Results Across Black Fox Line 1000E (Corresponds to Mine Grid ≈ L100+000E)

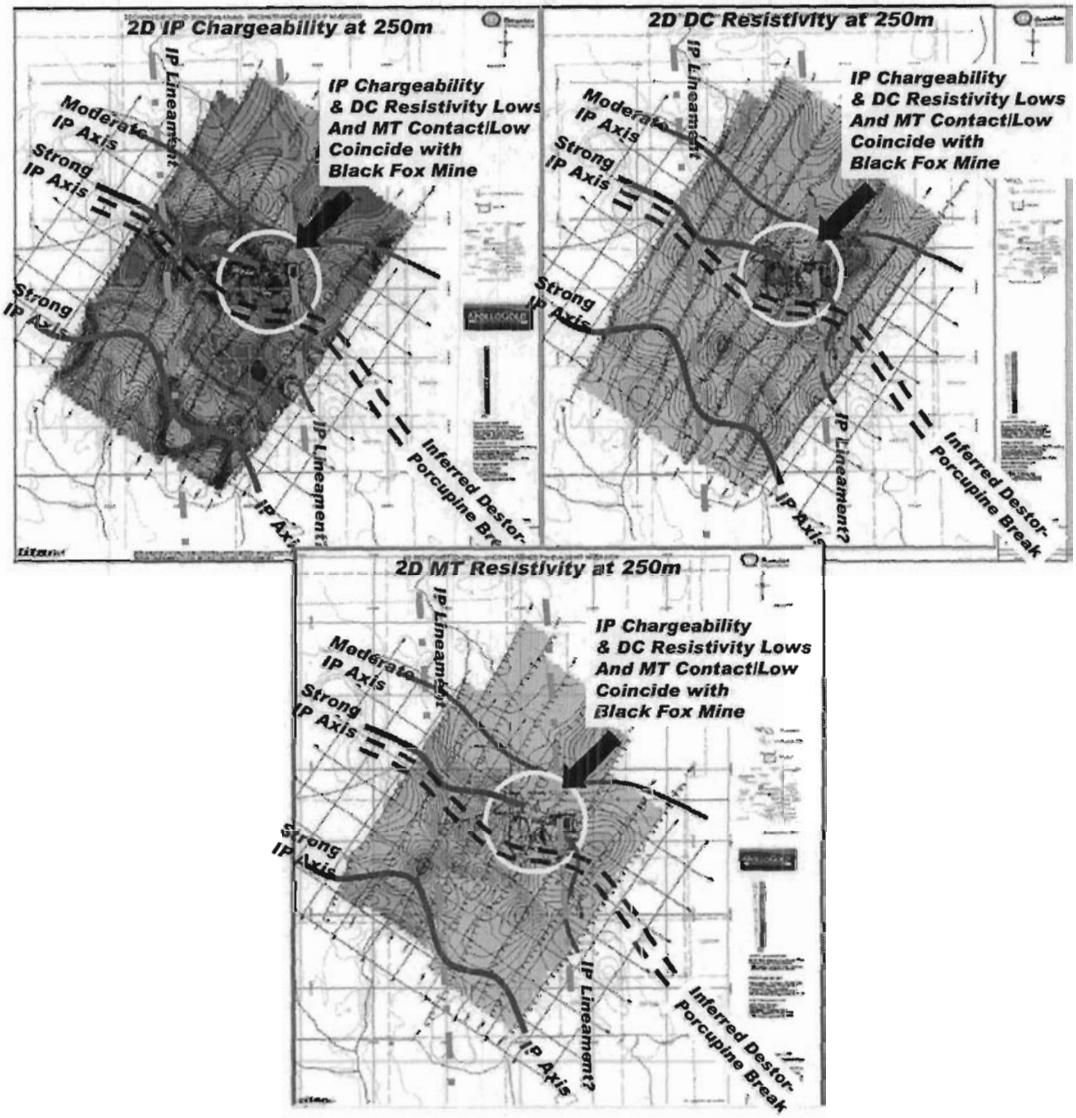

Figure 3: Plan-view of Titan 2D Inversion Results for 250m Depth Slice.

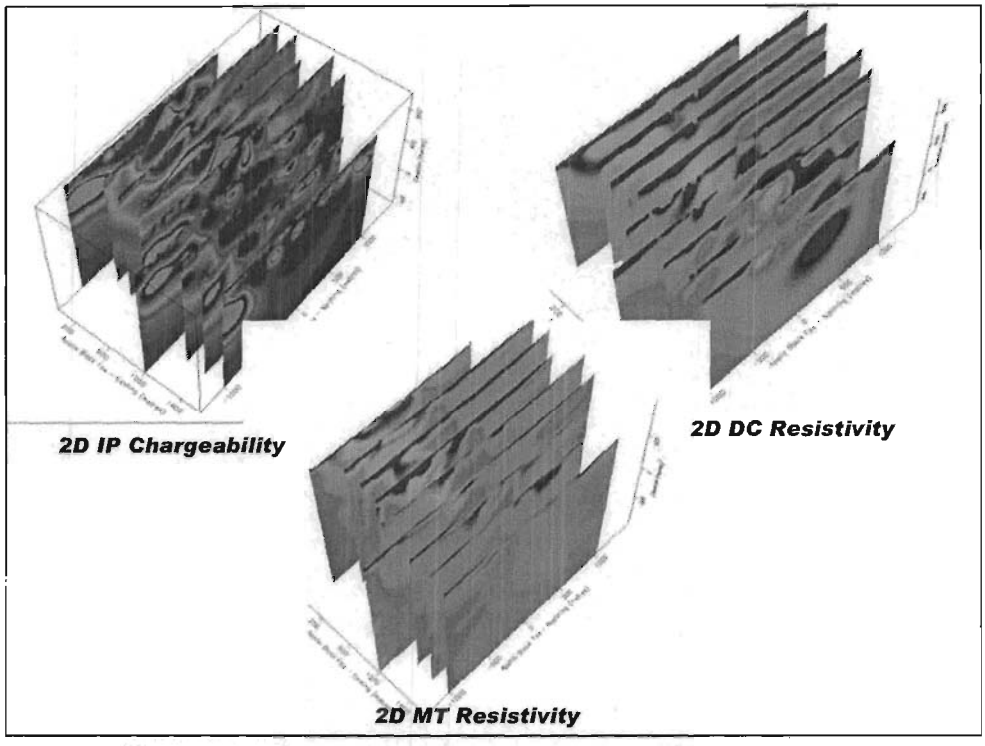

Figure 4: 3D Views of Black Fox 2D Inversion Results (View Looking North, from Above).

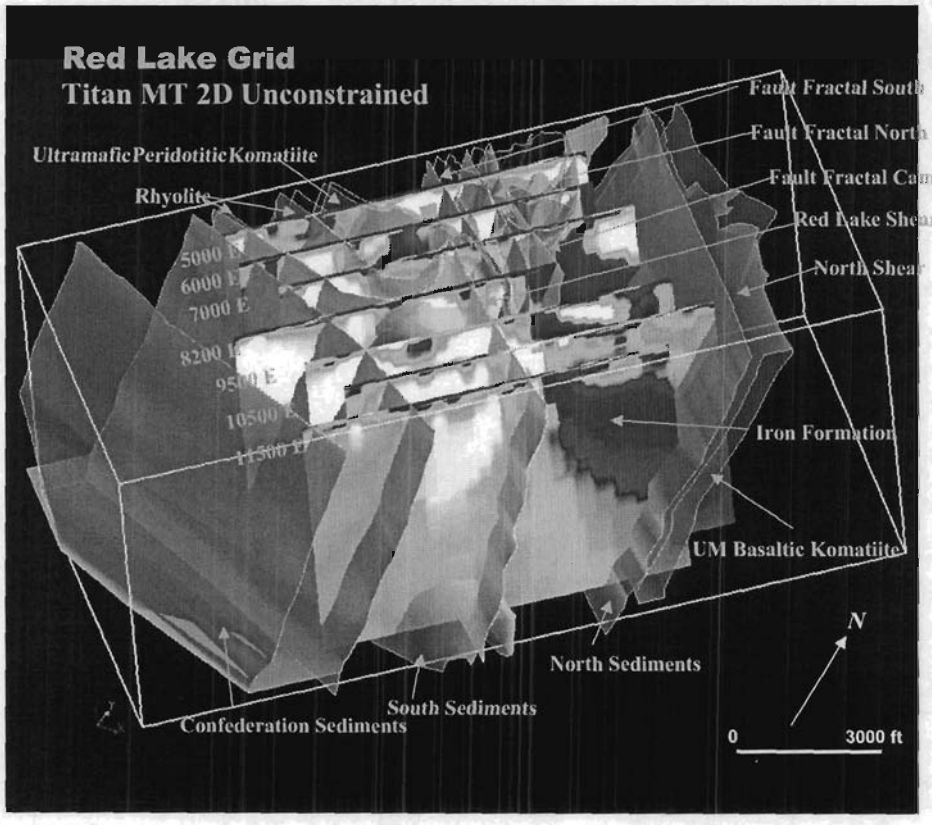

Figure 5: Unconstrained 2D MT Inversion Results at Goldcorp Red Lake Mine (OMET Project 14-2001)

TABLE OF CONTENTS

LIST OF TABLES AND FIGURES

1. INTRODUCTION

During the period of April 25th to May 4th, 2003, joint tensor magnetotelluric (MT) and dc resistivity\induced polarization (DCIP) surveys were undertaken for the Black Fox project of Apollo Gold Corp., using the Titan-24 distributed array system, developed by Quantec Geoscience Inc., of Toronto, ON. The survey is designed to characterize the geophysical response of the geologic environment, specifically the electrical resistivity and the chargeability of the underlying bedrock, extending to great depth.

The primary objectives of this survey were:

- Identify disseminated sulphide pods in the first 200m of depth
- Look for flow type ore characterized by 5-10% massive disseminated sulphides in the 0-700m range with DCIP and deeper (700-1300m) with Titan MT Resistivity
- Detect structural flexures within the subsurface
- Provide additional structural information and targeting ability for deep (>400m) drill programs- Identify disseminated sulphide pods in the first 200m of depth.

In addition, based on later discussions/geologic evidence provided by ***Apollo Gold***

- Detect sulphide-poor/magnetite-depleted, *ankerite-altered* zones, along the ***Destor-Porcupine Break***, with similar characteristics to the ultramafic volcanic-hosted ***Black Fox*** gold deposit (see Figure 6).

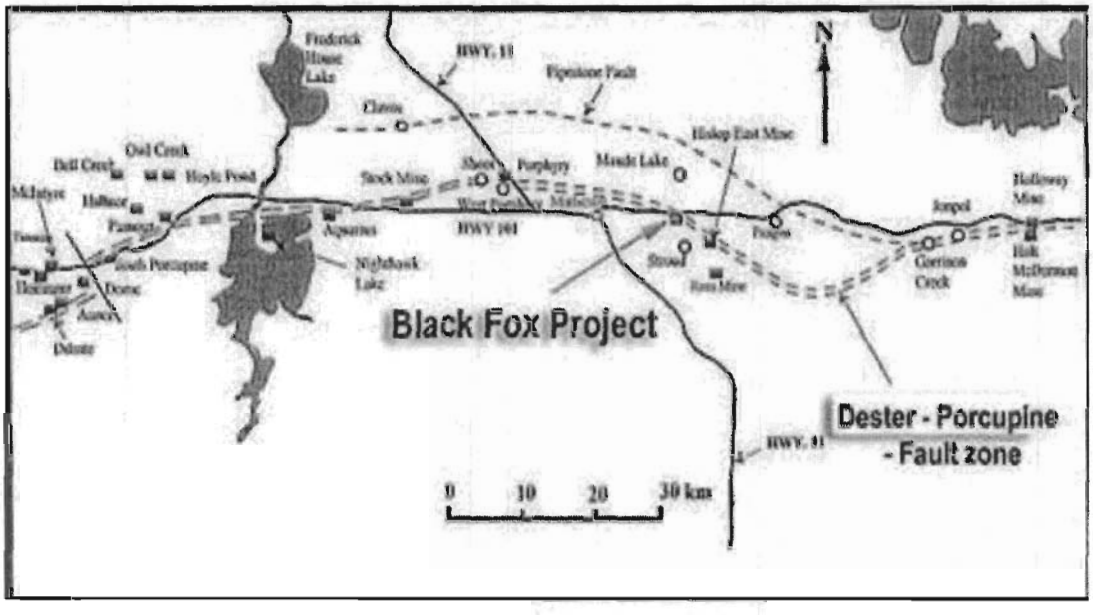

Figure 6: Black Fox Project Regional Structural Geologic Model.

2. SURVEY DESCRIPTION

- **Project/Grid Areas Surveyed:** ***Black Fox Mine***
- **Survey Types**: TITAN-24 DISTRIBUTED ARRAY TENSOR MAGNETOTELLURICS (MT) & DC RESISTIVITY AND INDUCED POLARIZATION (DCIP)
- **Survey Dates:** April 25 – May 4, 2003
- **Survey Coverage:** **9** lines (19.7 line-km)

2.1 LOCATION

- **General Location:** The Black Fox mine grid is located approx. 10 km east from Matheson. All lines are crossing the Hwy 101 (Figure 7 and Figure 8).
- **Township:** Beatty and Hislop Twp.
- **Province:** Ontario
- **Nearest Settlements:** Matheson and Iroquois Falls, On
- **Nearest Highway:** Hwy 101
- **UTM Zone:** 17
- **Latitude/Longitude:** Approx.: N 48° 32' 18.75", W 80° 20' 29.53"
- **UTM position**[1]**:** Approx.: 548605mE, 5376369mN

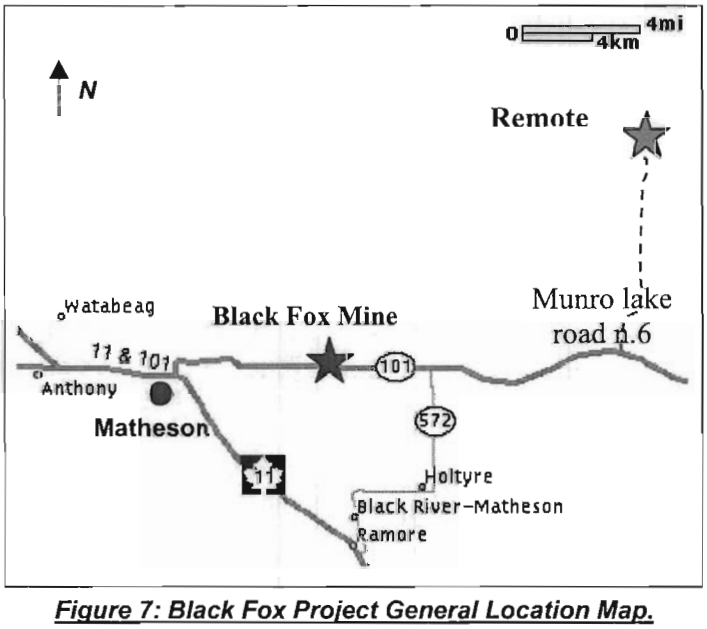

Figure 7: Black Fox Project General Location Map.

[1] UTM coordinates (NAD83) positioning (GPS) supplied by Apollo Gold Corp. 05-2003).

2.2 *SURVEY GRID.*

- **Established by:** Previously established for Apollo Gold Corporation.
- **Coordinate Reference System:** Survey Grid Coordinates referenced to UTM (NAD83) Coordinates (Table I)[2].
- **Line Direction:** Azimuth N-035^0
- **Line Separation:** 200 meters
- **Station Interval:** 100 meters
- **Method of Chaining:** Metric, secant distance (GPS)

Line No.	Survey/Array Coord. Start	Survey/Array Coord. End	UTM Coord. Start	UTM Coord. End
0+00E	1000S	900N	547144E 5375450N	548121E 5377098N
2+00E	800S	1500N	547443E 5375510N	548538E 5377529N
4+00E	800S	1500N	547664E 5375401N	548725E 5377427N
6+00E	800S	1300N	547772E 5375343N	548826E 5377150N
8+00E	1000S	1500N	547850E 5375021N	549121E 5377236N
10+00E	1300S	1400N	547837E 5374743N	549251E 5377034N
12+00E	1000S	1100N	548172E 5374854N	549231E 5376707N
14+00E	1000S	800N	548300E 5374824N	549333E 5376290N
16+00E	1000S	1000N	548438E 5374718N	549600E 5376437N

Table I: Survey Line Locations and UTM Reference

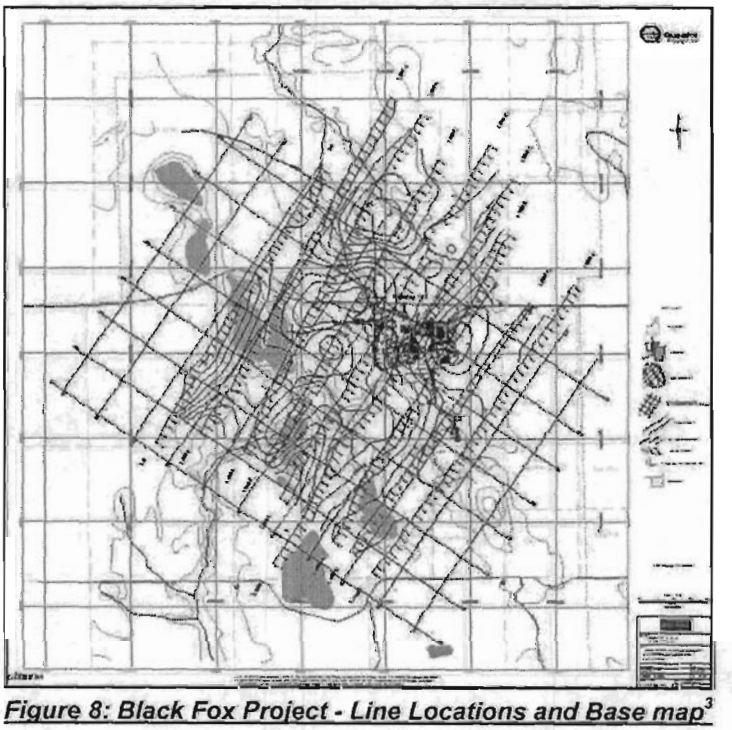

Figure 8: Black Fox Project - Line Locations and Base map[3]

[2] Note: Survey Grid and existing Mine Grid approx. subparallel; Survey coord. 1025E/225N corresponds to Mine coord. 10000E/10110N.
[3] Note: Titan survey lines overlain onto digital basemap of mine-site translated to UTM (Nad83/Zone 17) using basepoints (Nad27/U17) supplied by Apollo Gold Corp. (G. Quigley, APG, pers. comm., July-2003). Claim and topographic base from OMNDM claimap3 website (ref., http://www.mndm.gov.on.ca/mndm/mines/slides/claimap3; E. Martinez, QGI, pers. comm., July-2003).

2.3 *SURVEY PERSONNEL*

- **Project Manager:** Kevin Blackshaw
- **Data Processing (office):** Kevin Smith, Susanna Scappin
- **In-Field Crew Chief/Observer:** Neil Maukonen
- **Geophysical Technicians:** Claude Chiasson, Trent Retallick
- **Field Technicians:** Alain Dufour, Eric Dufour, Jacques Frenette, Eric Hotvedt, Donny Maclaren, Jason Ploeger, Pat Van De Kraats, Carmen Vouko

2.4 *SURVEY COVERAGE*

2.4.1 DCIP Surveys

LINE	SETUP	MINIMUM C1	MAXIMUM C1	MINIMUM P1	MAXIMUM P2
0+00E	1	1050S	950N	1000S	1000N
2+00E	1	800S	1450N	750S	1500N
4+00E	1	850S	1450N	800S	1500N
6+00E	1	850S	1250N	800S	1300N
8+00E	1	1050S	1450N	1000S	1500N
10+00E	1	1250S	1350N	1300S	1400N
12+00E	1	1050S	1050N	1000S	1100N
14+00E	1	1050S	750N	1000S	800N
16+00E	1	1050S	1050N	1000S	1000N
					TOTAL: 19.75 km

Table II: Maximum and Minimum DCIP Center-Pole Electrode Position.

2.4.2 MT Surveys

LINE	MIN EXTENT	MAX EXTENT	TOTAL (m)
0+00E	1000S	900N	1900
2+00E	750S	1500N	2250
4+00E	800S	1500N	2300
6+00E	800S	1300N	2100
8+00E	1000S	1500N	2500
10+00E	1300S	1400N	2700
12+00E	1000S	1100N	2100
14+00E	1000S	800N	1800
16+00E	1000S	1000N	2000
			TOTAL: 19.65 km

Table III: MT Survey Coverage (Pot-to-Pot).

2.5 SURVEY SPECIFICATIONS

2.5.1 DCIP Surveys

- **Survey Array:** Pole-Dipole-Dipole Array (see Figure 9).
- **Receiver Configuration:** 20 to 28 Ex = Continuous In-line voltages (Figure 10)
  11 to 14 Ey = Alternating (2-station) cross-line voltages[4]
- **Array Length:** 1800 to 2700 meters
- **Number of Arrays/line:** 1
- **Dipole spacing:** 100 meters
- **Sampling Interval:** Ex = 100 meters
  Ey = 200 meters
- **Rx-Tx Separation:** N-spacing (P_N-C_N min) = 0.5 to 26.5
  with maximum varying according to line-length
- **Infinite Location:** Approx. 9.5km north of grid.
- **Spectral Domain:** Tx = Frequency-domain square-wave current
  Rx = Full waveform time-series acquisition
  Data processing/output in frequency-domain.

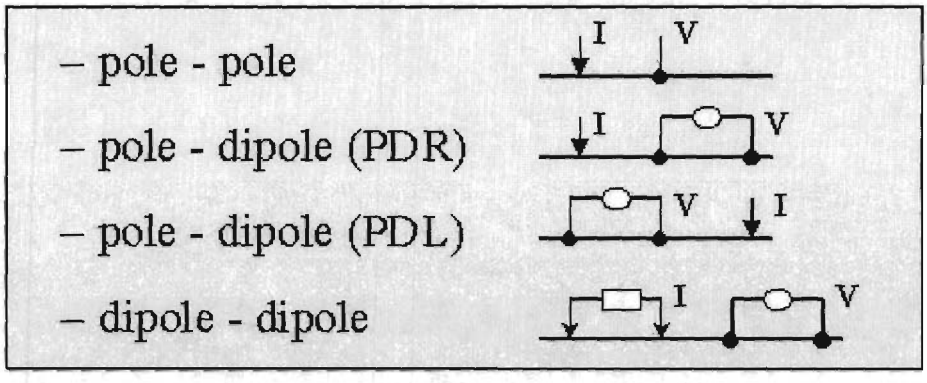

Figure 9: Common IP Electrode Arrays

2.5.2 MT Surveys

- **Technique:** Tensor soundings, remote-referenced
- **Base Configuration:** 18 to 28 Ex = Continuous In-line E-fields (Figure 11)
  10 to 14 Ey = Alternating (2-station) cross-line E-fields
  1 pair LF coils
  1 pairs HF coils
- **Remote Configuration:** 1 Ex = in line E-fields
  1 Ey = cross-line E fields
  1 pair LF coils
  1 pair HF coils
- **Array Length:** 1800 and 2700 meters
- **Number of Arrays/line:** 1

[4] Note: Cross-Line Ey voltages obtained for future reference purposes – not presented in cross-sectional plots.

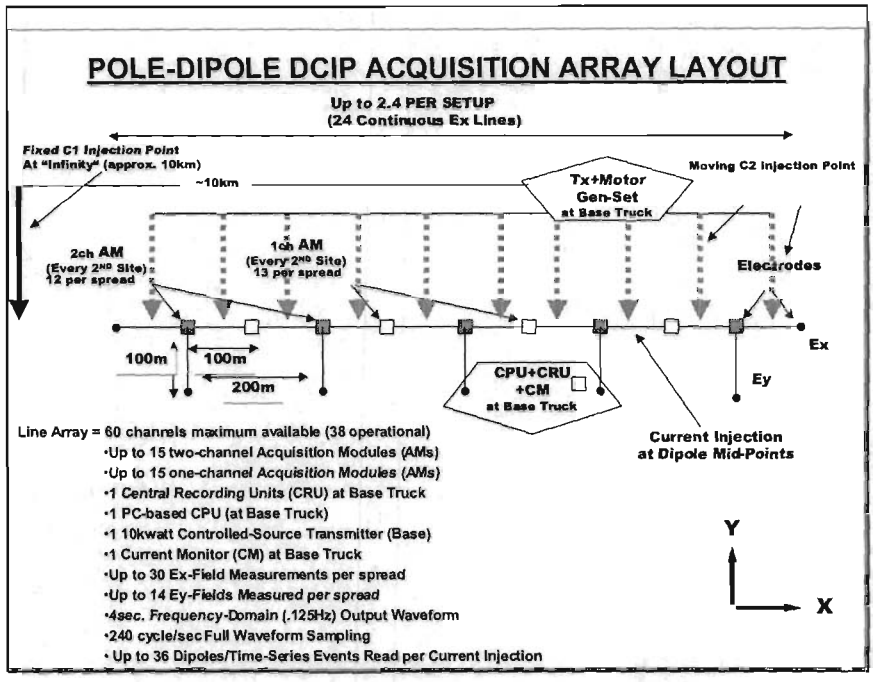

Figure 10: DCIP Survey Layout for Pole - Dipole Array

- **Dipole Spacing:** 100 meters
- **Sampling Interval:** Ey = 200 meters
  Ex = 100 meters
- **Ex/Ey Sampling Ratio:** Ey = 9 to 14
  Ex = 18 to 28
- **E/H Sampling Ratio:** 2 (see Figure 11)
- **Remote-reference Measurements:** 1 Hx/Hy set (1 Ey/Ex set for verification/monitoring)
- **Remote reference Position:** UTM 0564989E, 5388578N (NAD27, Zone 17)
  From Porcupine take the Highway 101 to Matheson.
  Turn left onto Highway 101 east and travel 15.4Km past the Apollo Gold mine to the Munro Lake n.6 road.
  Turn left onto this gravel road and follow North for about 12 Km to a clear-cut area.
  The remote site is located 100m off the right side of the road, in the clear-cut (see Figure 7).
- **Data Acquisition:** Full-waveform time-series acquisition
  Data processing/output in frequency-domain

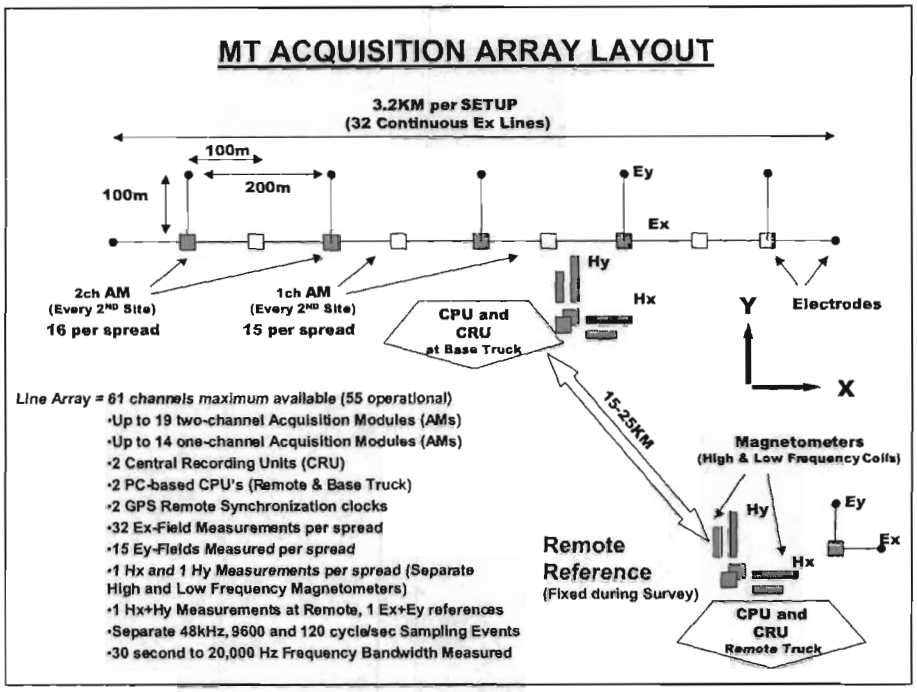

Figure 11: MT Survey Coverage (Pot to Pot)

2.6 *SURVEY PARAMETERS*

2.6.1 DCIP Surveys

- **Transmitter Waveform:** 30/256 Hz square waves at 100% duty cycle (~4sec Pos./Neg.)
- **Transmitter Output Current:** 0.1 amperes to 3.4 amperes
- **Receiver Sampling Speed:** 240 samples/second (24 bit A/D @ 120 db dynamic range)
- **Tx-Rx Synchronization:** using current monitor (10 μsec time-accuracy)
- **Time-Series Stacking:** 20 cycles (full-waveform)
- **Read Time:** 7.5 to 10 minutes per event
- **Post-Processing:** using QGI QuickLay™ v2.01.6
  1) Time-series stacking
  2) Robust statistics
  3) Current waveform deconvolution
  4) Digital filtering (60Hz + harmonics)
- **Spectral Chargeability Model:** Decay parameters using Halverson-Wait model fit
- **Time-Domain Decay Window:** T_O to T_F= 800 to 2000 milliseconds
- **Final Raw Data Output:**
  1) X/Y Position of Tx and Rx Dipoles
  2) Normalized voltage (volts/ampere)
  3) Voltage error (percent)
  4) Phase (milliradians)
  5) Phase error (milliradians)
  6) Apparent Resistivity (ohm-metres).

2.6.2 MT Surveys

- **Frequency Bandwidth:** Operating: 0.01 to 48000 Hz
  Effective: 10s to 20000 Hz
- **Time-series Sampling:** High Range: 48000 samples/sec
  Mid-Range: 9600 samples/sec or 12000 samples/sec
  Low Range: 120 samples/sec
- **Remote-Base Synchronization:** GPS clocks (10μsec time-accuracy)
- **Time-Series Stacking:** High Range: 1,534,999 samples
  Mid-Range: 20^{20} (1,048,576) samples
  Low Range: 2^{19} (524,288) samples
- **Sample/Record Time:** High Range: min. 3 events @ 30 seconds per event
  Mid Range: 2 events @ 1.5 minutes per event
  Low Range: 1 event @ 80 minutes per event
  (total recording and retrieving time approx. 4 hours)
- **Post-Processing:** using QGI Quicklay™

  1) Coherent noise rejection using remote-reference
  2) Proprietary digital filtering (scrubbing)
  3) Coherency sorting
  4) Impedance estimate stacking
- **Final Data Output:** Auto and cross-power spectral estimates
  (0.1-20,000 Hz @ 8 pts/decade) in EDI format

2.7 *SURVEY INSTRUMENTATION*

- **Receiver System:** Quantec Titan-24 Distributed Array Acquisition System, comprising:
  - 61channels max. per system (up to 55ch operationally) with internal A/D conversion (24bit @120db / dual speed @120-48kHz), and buffer memory (6Mb).
  22 x 2-channel Acquisition Modules (AMs)
  17 x 1-channel Acquisition Modules (AMs)
  AM data transmission using LAN cabling
  - 2 Central Recording Units (QCRU), at base & remote (MT surveys) reference sites (140Gb data storage)
  - 2 GPS synchronization clocks (10nsec precision / 12.3MHz clock-speed), at base & remote (MT) CPU's
  - 2 PC-based Central Processing Units (base & remote)
- **Transmitter (DCIP Surveys):** ZONGE GGT-10 (10kW) with frequency/waveform control, using CPU, and Current Monitor (CM); with truck-mounted Westinghouse 30kwatt alternator (400 Hz @ 3-phase / 220V) with Kohler Command 25 engine (25Hp / 2 cyl) and Zonge VR-1 voltage-regulator.
- **Receiver Electrodes:** Ground contacts using stainless steel rods
- **Receiver Coils (MT Surveys):** 4 EMI model BF-4 (100sec to 600Hz) magnetometers (Hx-Hy -2 at base / 2 at remote)
  8 EMI model BF-6 (10Hz to 20kHz) magnetometers (Hx-Hy -2 at remote / 2-6 at base).

3. RESULTS AND INTERPRETATION

3.1 OVERVIEW

The Titan-24 surveys at ***Black Fox*** were designed to provide deep structural and lithologic information, below conventional geophysical penetration depths (>200-250m), associated with potential Au-mineralized zones along the Destor-Porcupine Break, as well as possible extensions to the ***Black Fox Mine***. This summary interpretation report presents the Titan data and 2D inversion results, in cross-section and in plan, providing a brief description of these results, as well as selected targets which are based on prioritized geologic models.

The Titan-24 system acquires three types of geophysical data – magnetotelluric (MT), direct current resistivity (DC), and induced polarization (IP). The MT and DC data both measure the same physical property – resistivity – which is sometimes an indicator of metallic mineralization, but is more often than not controlled by the rock porosity. IP measures "chargeability" and is a near-direct indicator of the presence of metallic mineralization, either massive or disseminated, most commonly various sulfides and graphite – making it a useful tool for gold exploration. For this survey, all three data acquisition capabilities of the Titan-24 system were utilized.

A detailed introduction to DCIP, specifically the Titan approach to DCIP, is included in **Appendix D**. DCIP is an electrical method which uses the injection of current and the measurement of voltage and decay to determine the subsurface resistivity and chargeability. Depth of investigation is controlled by array geometry and transmitted current. The Titan surveys typically image DC resistivity to depths of 500-750 metres, and the IP images to 350-500m, in subvertical tabular geologic settings. The difference in penetration is a function of the relative physical property contrasts and relative signal-to-noise levels between the two measurements. In fact, in certain conditions, several drill-tested examples with Titan DCIP have demonstrated resolution depths exceeding 750m for the chargeability.

A detailed introduction to MT, specifically the Titan-24 approach to MT, can be found in **Appendix E**. MT is an electromagnetic method which measures the subsurface resistivity to great depths. Natural time variations in the Earth's magnetic field, due to oscillations of the ionosphere and lightning, induce electric currents in the ground. MT measures these natural signals. The depth of investigation is determined primarily by the frequency of the measurement, and it can be to great depth. Depth estimates from any individual sounding may easily exceed 20 km. However, the data can only be confidently interpreted when the "aperture" of the array is comparable to the depth of investigation, so the inversion depth is generally limited to about half the length of the profile – presently, 1-1.5km depths.

The primary tool for evaluating the Titan-24 data is two-dimensional (2D) inversion. A discussion of inversion, focusing on the Titan-24 approach, is presented in **Appendix F**. The critical points are that an inversion models depends on the data, but also the data errors, and the "model norm". The inversion models are not unique, may contain "artifacts" of the inversion process, and may not accurately reflect all of the information apparent in the actual data. Inversions are a tool, a very powerful tool, but not a "solution". Inversion models need to be reviewed in a context of the data, model fit, and with an understanding of the model norm used.

For each profile, in **Appendix B**, in addition to the raw pole-dipole-dipole apparent resistivity and phase results, 2D inversion results are also presented. The UBC DCInv2D^{TM} algorithm was used with smooth- and sharp- model parameters. The purpose is to address model ambiguity. For the DC resistivity inversion using a "smooth" model norm, but dispense with the corresponding "sharp" DC model. This is because the sharp model of the DC resistivity inversion tends to push all the features in the model close to surface. And so, for this reason, it is not very much useful in the data interpretation exercise, although it does provide a model, which explains the data. However, in contrast, for the IP chargeability inversion, we show both the sharp and smooth 2D models. We do this in order to compare the two models and determine which features are absolutely needed to explain the data and which features are made up by the inversion process (artifacts). We can use both models to also better assess the uncertainties for each feature. For the DCIP inversions, data error adjustment and bad data rejection are used jointly to achieve inversion convergence – in all cases, model convergence was achieved by minimizing the model misfit to the number of points. All three DC and IP inversion models also are shown in scaled Geosoft plan and cross-sectional forms in **Appendix A**.

For the MT portion of the Titan survey, first the raw data pseudo-sections are shown in **Appendix B**. The apparent resistivity and phase pseudo-sections provide a useful summary of the data. The pseudo-sections consist of the apparent resistivity or phase data at each site as a function of frequency. The horizontal axis is site location along the profile. The vertical axis for each plot is the log of frequency. This indirectly corresponds to depth, i.e. that low frequency signals penetrate deeper into the earth.

For the raw MT, there are four sections, the upper two are for the in-line dipoles and the lower two are the cross-line dipoles. Phase pseudo-sections for each mode are shown immediately below the resistivity sections. The phase sections are closely related in information content to the resistivity sections. Phase sections indicate the change in resistivity with respect to frequency. Low phases indicate areas of resistivity increase with frequency while high phases indicate resistivities decrease with frequency. . As a general rule, for MT, deep resistivity lows are always accompanied by MT phase highs. However, very shallow conductivity structure can cause static-like (frequency independent) resistivity lows without accompanying phase highs. Such feature in TE mode is removed before the inversion.

On the same page immediately after, we show the MT pseudo-sections of EVA processed data. The data processing is somewhat interpretive and it is important to review the data processing approach and impact. The four sections here no longer represent in-line and cross-line, they now represent geologic strike (TM) apparent resistivity and phase in the upper two plots and geologic dip (TE) in the lower two plots. These data have been "EVA" processed, including topographic stripping, rotation, eigenvector decomposition, static shifts, static stripping and fitting the data with 1D models. The data pseudo-sections are now more consistent with the 2D assumption inherent in the inversion.

For the MT inversions, we will show two models, RLM based on the smooth-conjugate gradient and PW, developed by Quantec using a finite-element, Gauss-Newton solution – providing sharper, high-resolution cross-section resistivity images. Again from the comparison of these two models, we can assess the model feature uncertainties. Only the PW MT 2D models also are shown in scaled Geosoft plan and cross-sectional forms in **Appendix A**.

The DCIP and MT data were inverted independently. In the *Discussion of Results,* in the following section, the overall interpretation for the profile follows on a line-by-line, and method-by-method basis. In the *Prioritized Targets* section, the three Titan 2D inversion results are combined and geophysical features of interest, based on favourable physical property combinations, based on the geologic target model and according to the physical property results, are identified for further follow-up.

In the images that follow, for the DC and MT resistivity, cool colors represent resistivity highs and warm colors resistivity lows, i.e. conductive features. Alternatively, for the MT phase and for the IP, warm colours represent chargeability highs and cool colours represent chargeability lows.

The data quality for this survey is excellent, due in part to the noise rejection capabilities of the Titan technology, as well as the relatively high injected currents levels and bulk resistivities at ***Black Fox*** for the DC, and also to good natural field signal levels for the MT. In fact, weak natural fields in the 300-3k Hz bandwidth, known as the "dead band", are either absent or minimized in the *Black Fox* sounding curves.

3.2 *Discussion of Results*

Shown below are images of the complete set of raw data and 2D inversion results for the DCIP and MT surveys, for Line 0E, accompanied by a discussion of the results for each of the technologies. The digital images for the remaining lines (2E to 16E) are presented in Appendix B, for brevity sake. Scaled Geosoft cross-sections and plans of the 2D inversion results are also presented in Appendix A.

3.2.1 Line 0+00 E

DC Resistivity

The observed and calculated DC Apparent Resistivity pseudosections and the final 2D smooth body DC Resistivity inversion, for Line 0E, are shown in Figure 12. The excellent quality of the data and the model fits are clearly evident.

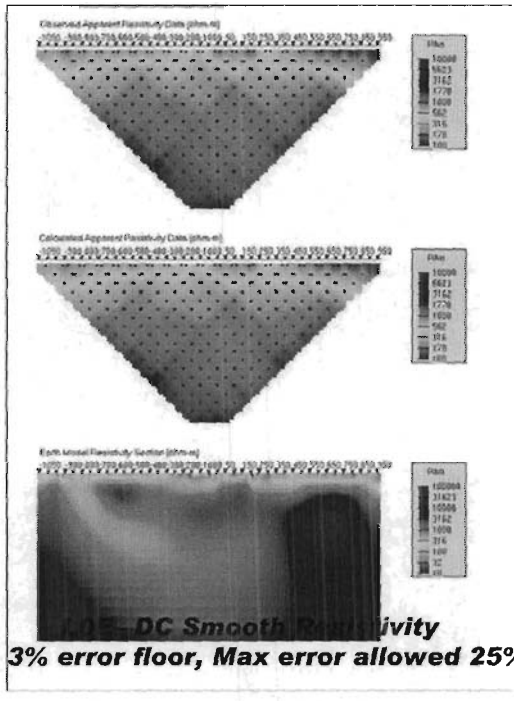

Figure 12: Line 0E – UBC 2D Smooth DC Inversion Results.

IP Chargeability

The observed and calculated IP Phase pseudosections and the final 2D sharp body IP Chargeability inversion, for Line 0E, are shown in Figure 13. The corresponding 2D smooth body inversion results are shown in Figure 14. The excellent quality of the data and the model fits are clearly evident.

There are well defined chargeability anomaly at sites 750S, 200N and 750N.

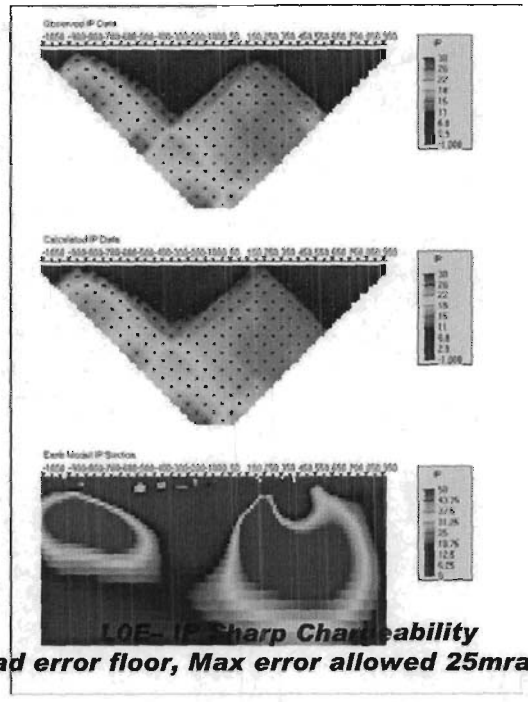

Figure 13: Line 0E – UBC 2D Sharp model IP Inversion results.

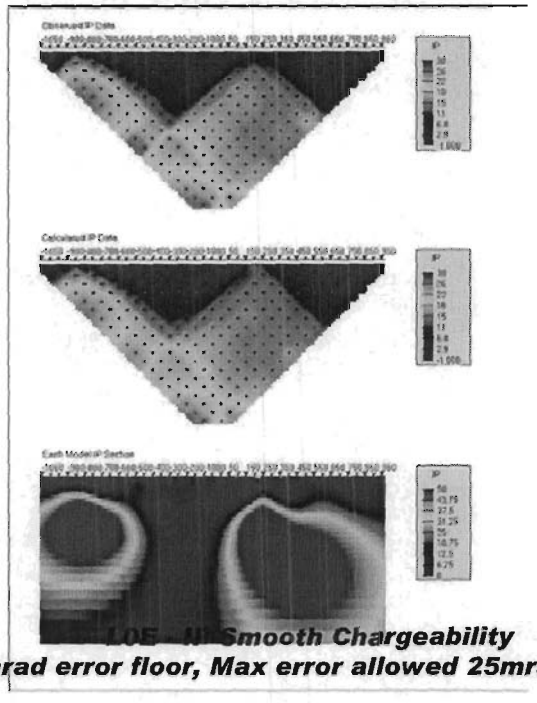

Figure 14: Line 0E – UBC 2D Sharp Model IP Inversion Results

MT Resistivity

The raw (measured) MT frequency pseudosections for Line 0E are presented in Figure 15, from top to bottom: a) the In-line (XY) apparent resistivity, b) In-line (XY) phase, c) Cross-line (YX) apparent resistivity and d) Cross-line (YX) phase. The corresponding EVA processed Along-strike (TE) and Across-strike (TE) MT pseudosections are shown in Figure 16. The excellent data quality is clearly

evident.

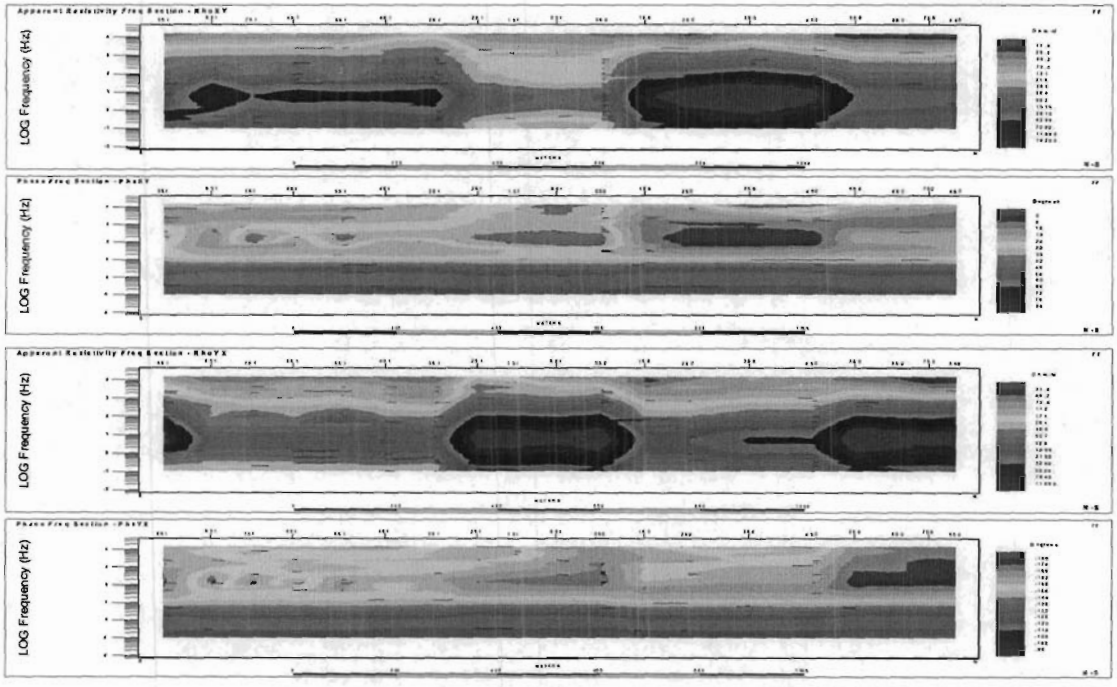

Figure 15: L0E - Raw MT Apparent Resistivity and Phase Frequency Pseudosections

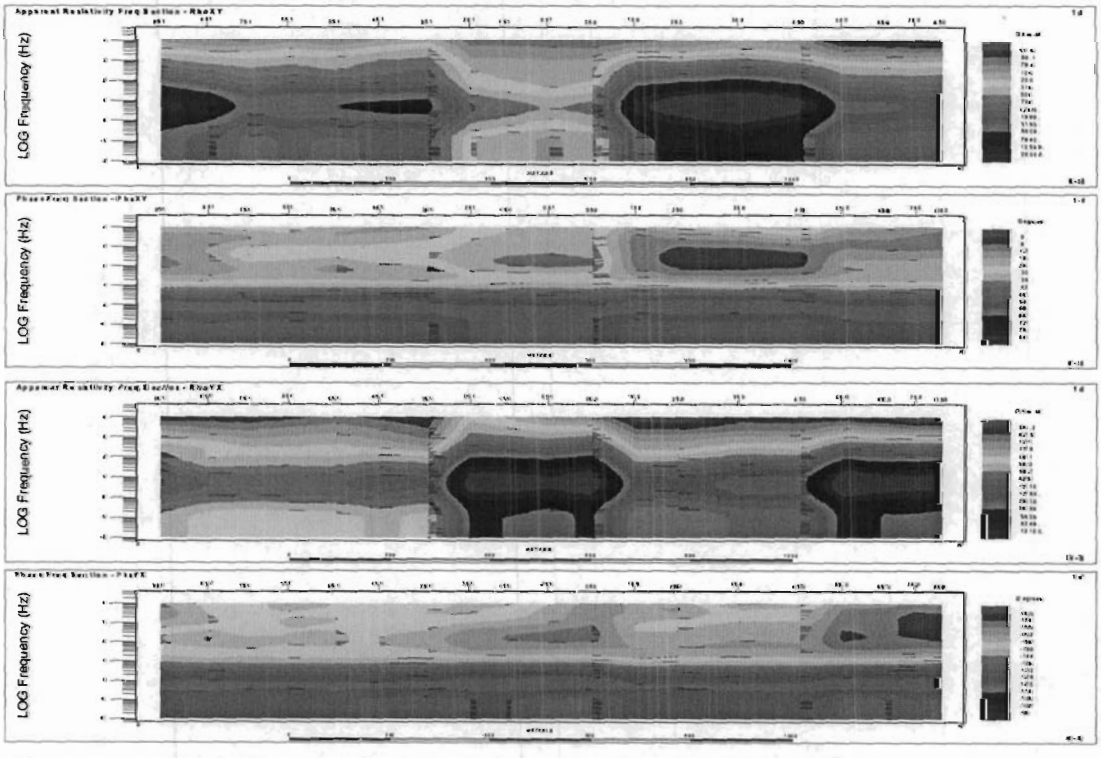

Figure 16: L0E - EVA-processed MT Apparent Resistivity and Phase Frequency Pseudosections

The 2D smooth-conjugate RLM MT resistivity inversion results for Line 0E are shown in Figure 17 and the corresponding 2D Gauss-Newton PW MT resistivity inversion results are shown in Figure 18.

Relatively good (~8% rms) model-convergences were obtained.

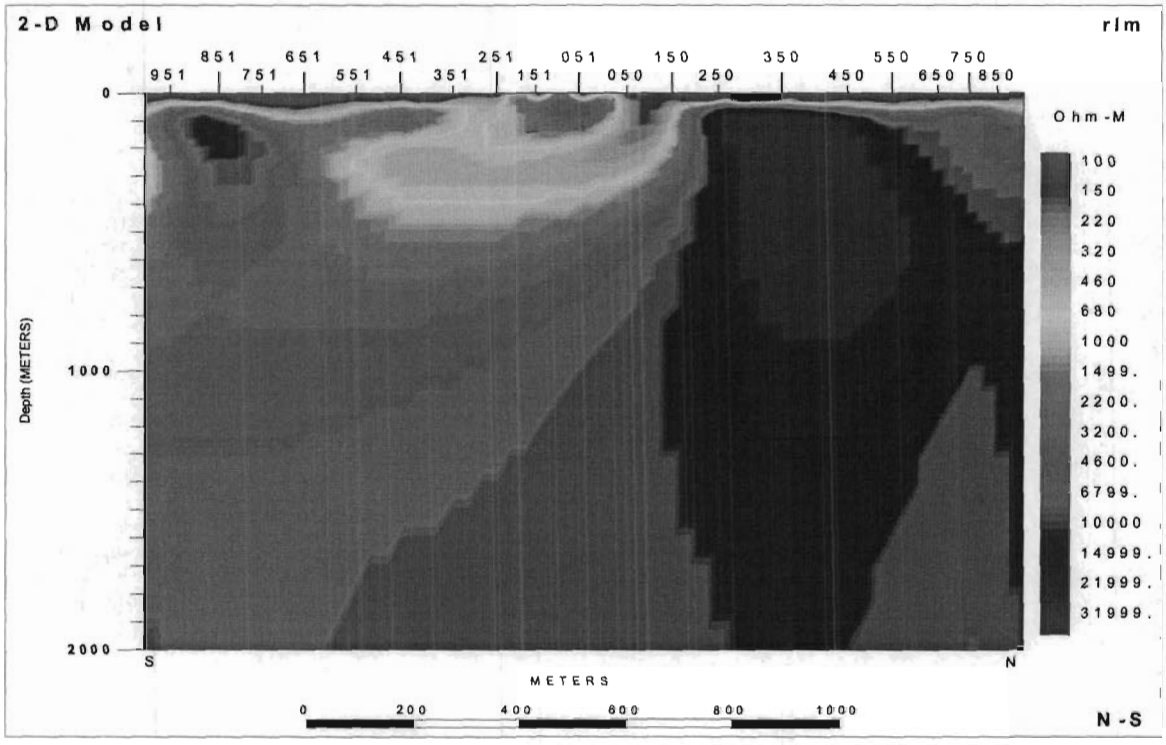

Figure 17: L0E - 2D RLM Smooth-Conjugate MT Resistivity Inversion.

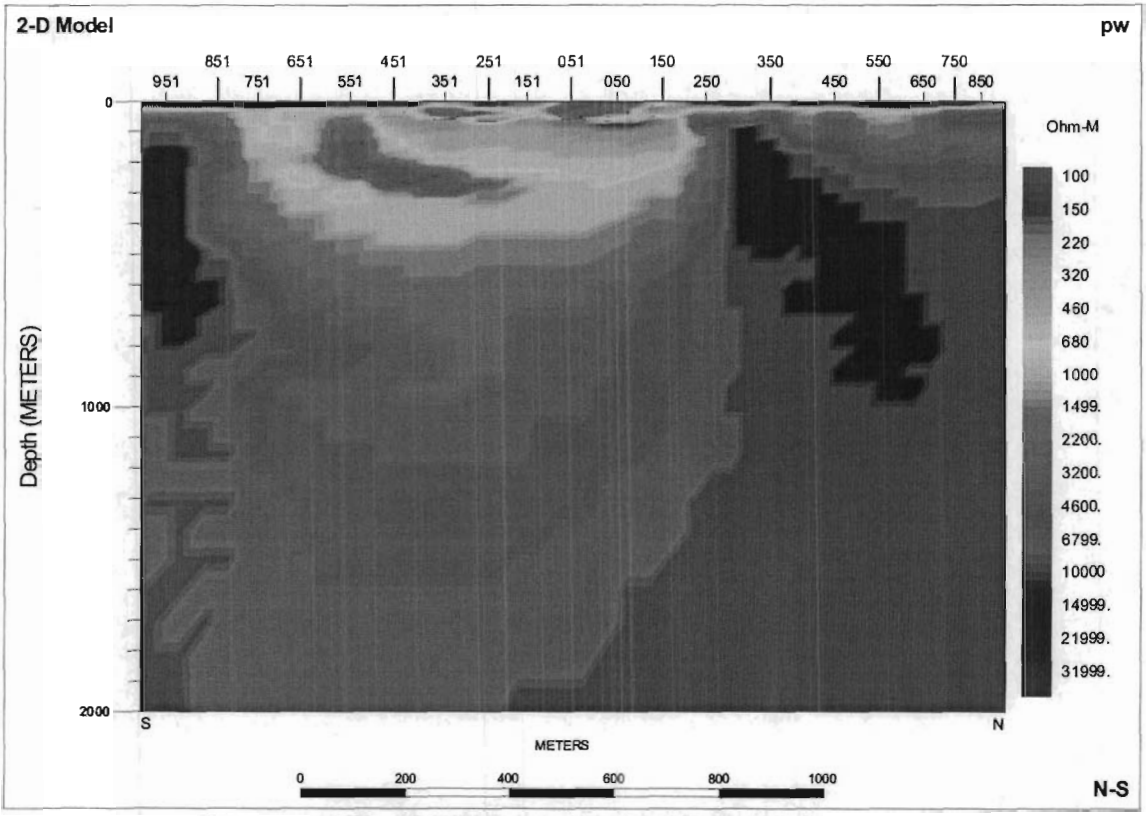

Figure 18: L0E - 2D PW Gauss Newton MT Resistivity Inversion.

Discussion of Results

This line, which lies ≈1km northwest of the ***Black Fox Mine***, cross-cuts the *Destor-Porcupine Break* (DPB) and hwy 101 approximately near its center. The MT data and inversion models clearly define two major resistivity contacts at 750S and 250 N - the latter which may represent the *DPB* - and it confirms the north dipping conductive feature shown on the DC section. The presence of the low resistivity block may or may not continue to depth, contrary to what the image has shown. The TE apparent resistivity increase in this conductive block can be explained by high resistivity truncation of the conductive block along the strike (EW) direction.

Due to limited depth of penetration in DC resistivity, these two contacts, particularly the southern one, are not well defined in the DC model. In fact the DPB appears to coincide with a weak, fault-like, low resistivity zone near 300N. The thickness of the conductive overburden is exaggerated due to the smoothness regularization of the inversions.

Comparing the two IP inversions leads to the impression that the IP data are sensing to an effective depth of about 700 meters and there are four dominant chargeable bodies along the profile. The top and lateral extent of these major chargeable anomalies are well defined. But their depth extent is far less certain. The DPB appears to straddle the northernmost IP anomaly at 300N. The rock body or bodies caused these anomalies can be anywhere within the center of the contour highs.

3.2.2 Line 2+00 E[5]

This MT profile is very similar to profile 0, except the southern contact has been moved to 500 S. The *DPB* may correspond to the horst-like resistivity high, centred near 300N. The DCIP inversion model shows overburden and thickening of it at 0 and also a major contact near 300 N, which correlates with the

[5] For profiles 200E to 1600E, refer to Appendix B for images of raw DCIP and MT data and 2D inversion models, and to Appendix A for 2D Geosoft plots.

MT horst near the inferred *DPB*.

The chargeability anomalies seen from the previous line seem to converge to 0 on this line, near the inferred DPB. The resolution of the data is insufficient to make this judgment conclusive. The moderate south dip of this large IP anomaly agrees with the geologic trends and may correspond to a disseminated-sulphide or magnetite rich unit – possibly ultramafics.

3.2.3 Line 4+00 E

This profile, which lies 500m west of the ***Black Fox Mine***, again, falls into the paradigm of the previous two profiles, with the DC and MT identifying a major horst-like structure or contact near the inferred DPB. In contrast, there is a contact to low resistivity MT feature towards the far north of the line, that comes into the picture at around 400 N. Again the depth extent of these contacts is unclear/uncertain from the comparison of RLM to PW models

The major chargeability anomaly, also defined on previous lines and lying at depth near the centre of the profile, has a dip which agrees with the known geology and may represent a mineralized lithologic unit or structure, which marks the DPB.

3.2.4 Line 6+00 E

This profile confirms the model of previous profiles, but the RLM model shows almost 1D like structure while the PW model indicates the contact goes as deep as 500 – 2000 m. This is almost entirely due to the inversion methodology differences between RLM and PW. However from the differences of the model, we can conclude that the depth extends of these contacts are between 200 –2000 m. In northern Ontario resistive terrain, the MT wavelength is too large to discriminate the depth extend better.

A prominent DCIP resistivity contact, which corresponds to the MT horst near 300N, appears to define the DPB. A large, strong IP high appears to lie at depth, below the DC and MT structures.

3.2.5 Line 8+00 E

This line, which skirts the NW edge of the ***Black Fox Mine*** (situated near stn 300N), shows a good correlation of resistivities derived from DC, PW and RLM of MT. There are low resistivity features at 250S and 450N and high resistivity in between. Comparing the two IP inversions, we can conclude that there are two large chargeable anomalies in close proximity to resistivity contacts, and a smaller but stronger IP anomaly which is on-strike with the *Black Fox Mine*. This IP anomaly appears to be steeply dipping but does not extend below 300-400m depths. The top of the northern and central anomalies are close to the surface and the top of the southern anomaly is about 250 m.

3.2.6 Line 10+00 E

This line straddles the ***Black Fox Mine*** (situated near stn 250N – see Figure 19). The DC model suggests that there is a large, significant low resistivity feature at 200-800m depths between 0 – 500N, which lies below the *Black Fox Mine*, and is consistent with a large clay-altered zone. This anomaly also shows up on RLM, but on the PW section, it becomes insignificant. A weak IP anomaly also corresponds to this DC low, but may represent an off-line, edge effect. Again, as observed on previous lines, the PW inversion appears to define a steeply dipping horst-like resistivity high feature across the DPB.

In the IP results, the *Black Fox Mine* and DPB coincide with a thin, shallow-north dipping IP high feature in the near surface, and a large, well defined, pronounced IP low at depth– which is in agreement with the magnetite-depleted, low-sulphide nature of the known gold mineralization at *Black Fox*, as well as the borehole physical property data. Significantly, the prominent, west dipping IP anomalies, observed in nearly all the previous profiles and identified as a possible mineralized ultramafic, are noticeably absent 0 which clearly distinguishes L1000E from these other lines. Comparing the two types of IP inversions leads to the impression that there are three IP anomalies with the major one sits on the southern side of the MT resistivity contact and the other two sitting on the resistivity contact clearly defined by the PW model – with much of the deeper northern half of the profile apparently devoid of polarizeable rocks.

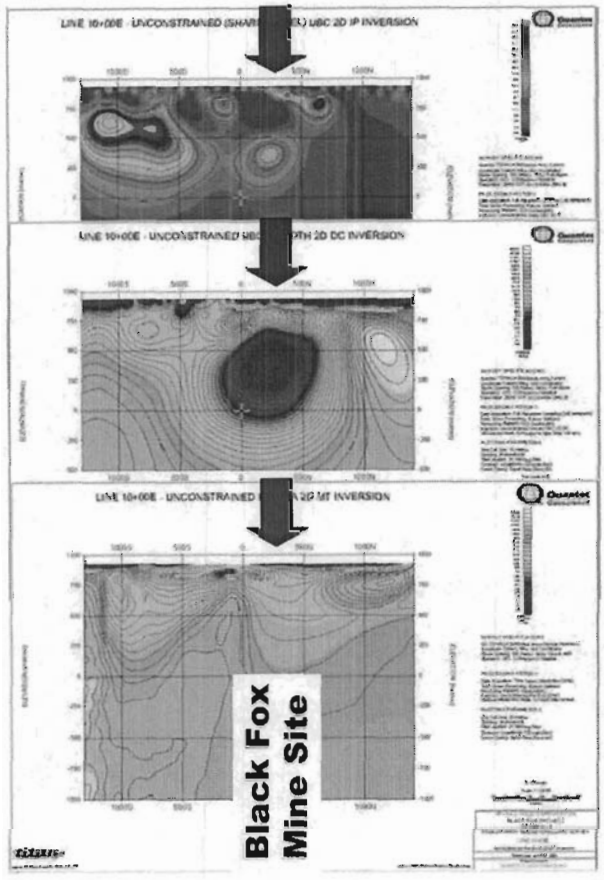

Figure 19: Titan 2D Inversion results across Black Fox Mine along L1000E.

3.2.7 Line 12+00 E

The RLM model for this line, lying approx. 100m east of the ***Black Fox Mine***, clearly defines the two major resistivity contacts at 400S and 250N – the latter which coincides with the DPB. On the north side of 250N, there is a low resistive feature showing up in DC, RLM and PW – similar to that identified below the *Black Fox Mine*, along L1000E. The PW and DC model didn't define the southern contact very clearly. There are IP anomalies associated with contacts and northern low resistivity feature, but most of the highest chargeabilities occur in the south.

3.2.8 Line 14+00 E

The correlation of resistivities derived from RLM and PW is excellent at this line. The south dipping conductive feature on DC at 400N shows up vaguely on RLM and PW. . This can well explained by the low resolution of MT compared to DC. This feature which was also defined below ***Black Fox Mine***, along L1000E, has moved north and deeper, relative to the previous 2-3 profiles. The IP shows anomalies on contacts, but again the largest, strongest IP anomaly occurs along the southern end of the profile.

3.2.9 Line 16+00E

Along this easternmost profile, which lies >500m southeast of the ***Black Fox Mine,*** the correlation of resistivities derived from RLM and PW is slightly worse than the previous line. However, the south dipping conductive feature observed in the DC at 400N shows up better on RLM and PW. Again, this low resistivity DC feature was also defined below ***Black Fox Mine***, along L1000E and is consistent with either a porous, clay-altered zone. The IP shows up anomalies in the upper resistive regions of the section, but chargeabilities are noticeably absent in the deep DC resistivity low to the north – consistent with low

sulphides &/or magnetite.

3.2.10 Plan View

The Titan 2D inversion results, when viewed in plan along selected depth slices (z=100m, 250m, 500m, ±1000m), generally support the same lateral variations with depth as those observed in the cross-sectional results – although the strike-continuity is poorly resolved due to their dipping nature.

The plan view 2D chargeability results, at shallow depths, define the main, central NW-SE trending IP high axis, possibly a mineralized ultramafic unit or structure, which extends along the *Destor-Porcupine Break,* from the northwest but ends abruptly at the *Black Fox Mine* site (see Figure 20). Here the IP high becomes a circular chargeability low and coincident DC resistivity low – consistent with alteration and magnetite or sulphide depletion. The south-east extension of this IP axis is poorly defined. At progressively deeper depths (see Appendix B), this chargeability low/resistivity low feature progressively occupies a larger region, east of the mine site and along the *DPB* near 0N – again indicating the absence of polarizeable material at depth and implying an extension of large, structurally-controlled alteration zone at depth and east of *Black Fox Mine.*

Two other, strike-extensive and sinuous IP axes of significance, which subparallel this ultramafic/*DPB* – related chargeability zone, are also defined: a) a weaker, shallower zone, best defined in the 100m-level plans and lying 350m further north, which is unexplained, but possibly marks a volcano-sedimentary contact; and b) a buried, larger, stronger zone, lying 800-1200m further south, which is also unexplained but which coincides with a mapped ultramafic intrusive in regional compilations – likely possibly magnetite &/or sulphide-rich.

The DC and MT resistivity depth-level plans at shallow depth also define long, sinuous, northwest-southeast resistivity lineaments, similar to those defined in the shallow chargeability – likely identifying concordant geologic structures and lithologic units, most of which are not polarizeable/unmineralized. At depth, however, the resistivity contrasts are weaker and the NW-SE direction also appears to be replaced by more oblique NS and NE-SW trends – possibly reflecting cross-cutting structural control. However, the most notable feature is the pronounced, DC resistivity low in the ***Black Fox*** mine area which extends northeast and southeast along the baseline– explained as a possible clay-altered zone – increasing in size & strength with progressive depth,. The horst-like MT resistivity high feature which coincides with the *Destor-Porcupine Break* in nearly all the 2D MT profiles is more readily defined as a sinuous, z-shaped feature in the deeper MT level plans - *Black Fox* lies in a weak resistivity low, along a well-defined contact.

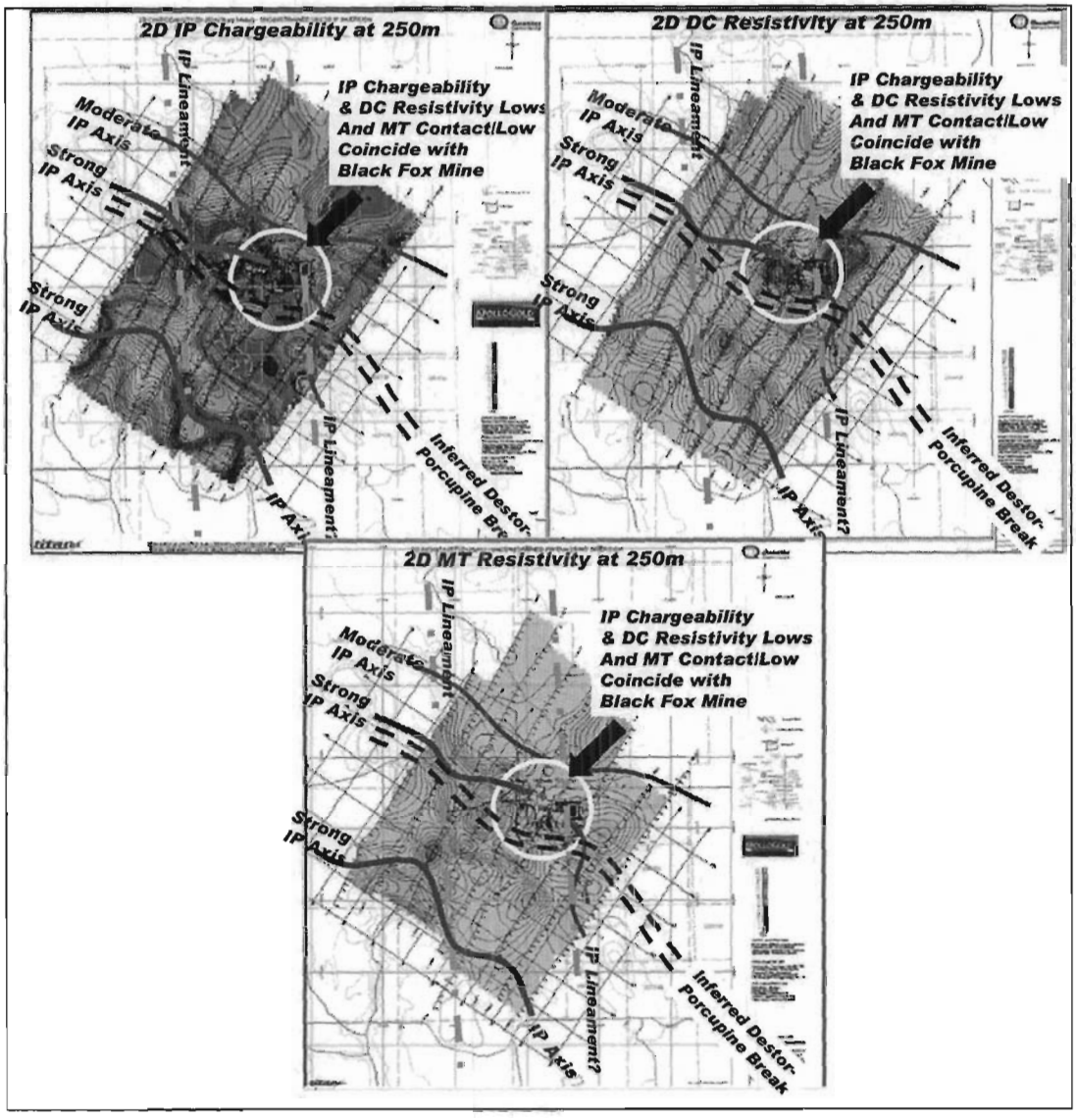

Figure 20: Cross-sectional view of Titan 2D Results at 250m Depth Level.

3.3 TARGETING RESULTS

The following Titan geophysical anomalies of interest at ***Black Fox Project*** have been identified, on each of the survey lines, using information drawn from all four 2D inversion modeling results, but primarily based on both a) the *2D Sharp Model DCIP Chargeability*, as an primary indicator of the presence &/or non-presence (see below) of sulphide mineralization and/or magnetite, and b) the *2D PW MT Resistivity*, as a primary indicator of geoelectric structure – the remaining 2D inversion products (i.e., *2D Smooth Model IP Chargeability,* and *2D Smooth Model DC Resistivity*) being used in support/validation of the main inversion indicators.

The geophysical characteristics used in the target prioritization/identification of anomalies is based on the description of the ***Black Fox/Glimmer Mine*** geologic model, provided by ***Apollo Gold***[6],wh ich consists of structurally controlled ankerite to qtz-carbonate altered ultramafic rocks – characterized by magnetite-depletion, weak sulphide content, and, hence, low chargeability. Also important is the likely nearby presence of a major resistivity structure, as well as likely also a moderate increased resistivity associated

[6] Ref: E. Berentson, APC, pers. comm., 07-2003 and 1:500 scale Vertical Composite Geologic section for L100+00E (21-Jan-00).

with the lower relative porosity. These are interpreted to correspond to moderate to high resistivity, low chargeability and low magnetics – which is also supported in the borehole petrophysical evidence, in **3** boreholes recently logged by Quantec Logging Services (ref. Qls Project L139 – June, 2003), as shown in Figure 21, below.

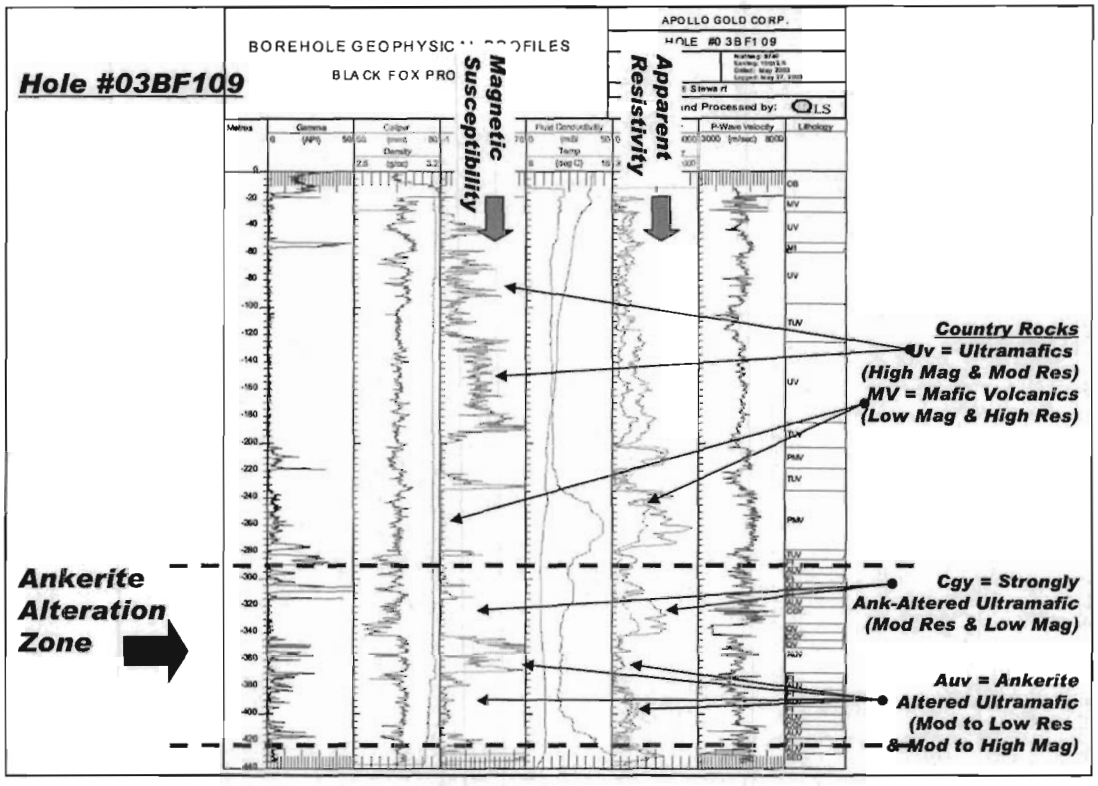

Figure 21: Borehole Physical Property Log at Black Fox Project

The following table describes the combination of physical properties associated with the target-model type and priority obtained at ***Black Fox.*** Because the predicted absence of chargeability is a relatively unusual target model, the other common model types, which offer contrasting physical property characteristics, are also described and prioritized.

Type 1. Black Fox Type (1St Priority)*: Carbonate altered ultramafics, without magnetite or disseminated sulphides* – characterized by a major resistivity contact, low chargeability and possibly moderate to low resistivity).

Type 2. Destor-Porcupine Type (2ND Priority): *Altered Stockwork with disseminated sulphides* – characterized by major resistivity contact and high chargeability.

Type 3. Quartz-Carbonate Altered Model (3RD Priority): *with disseminate sulphides* – characterized by high chargeability, high resistivity and proximal to major resistivity structure.

Type 4. Massive Sulphide Model (4TH Priority): *with stringer to massive sulphides & or clay alteration* – characterized by high chargeability, low resistivity and proximal to major resistivity structure.

Using this target prioritization, the following tables describe all the Titan targets identified at ***Black Fox*** on a line-by-line basis. As previously mentioned, the prioritization is based primarily on the chargeability evidence from the *2D Sharp Model Chargeability Inversions*, as well as the structural resistivity obtained

from the *2D PW MT Resistivity Inversions* - these two products offering higher resolution information than the other 2 smooth model inversion results (*2D Smooth IP and 2D Smooth DC)*. Included for each of the targets is a description of the line and station where the targets are centred, as well as the approximate depth to the top and middle of each of the chargeability anomalies, their approximate dimension, the strength of the IP response and the associated resistivity structure. The corresponding anomalies are identified in the accompanying PowerPoint diagram, in which the interpreted resistivity and chargeability structures are superimposed on each of the **4** (four) inversion sections.

No.	*Line*	*Station*	*Depth (m)*	*Size (metres)*	*IP Strength (milliradians)*	*Resistivity Structure (From 2D MT)*	*Priority / Type*
0E–1	0E	750S	Top= 50m Mid= 250m	550 x 350 m	>90millirads	Contact Low	2
0E–2	0E	475S	Top= 30m Mid= 75m	100 x 100 m	20millirads	Contact	2
0E–3	0E	200S	Top= 150m Mid= 250m	300 x 300 m	0	Contact Low	1
0E–4	0E	225N	Top= 100m Mid= 300m	450 x 300 m	>90millirads	Contact High	2
0E–5	0E	650N	Top= 60m Mid= 500m	650 x 400 m	>60millirads	Contact High	3
2E-1	200E	550S	Top= 50m Mid=275m	550 x 250m	>30millirads	Contact Low	2
2E-2	200E	0N	Top= 170m Mid= 400m	750 x 350 m	>70millirads	Contact High	2
2E-3	200E	120N	T< 30m Mid= 100m	150 x 150 m	0	Contact Low	1?
2E-4	200E	525N	Top= 100m Mid= 150m	300 x 200 m	<30millirads	Contact Low	2
2E-5	200E	1000N	Top= 30m Mid= 70m	150 x 150 m	<20millirads	Contact Low	2
4E-1	400E	650S	Top= 75m Mid= 250m	650 x 350 m	>30millirads	High	3
4E-2	400E	375S	Top= 0m Mid= 75m	150 x 100 m	0	Contact Low	1?
4E-3	400E	100S	Top= 150m Mid= 400m	850 x 400 m	>70millirads	Contact Low	2
4E-4	400E	025N	Top= 0m Mid= 75m	400 x 400 m	<20millirads	Contact High	2
4E-5	400E	575N	Top= 50m Mid= 250m	450 x 350 m	<30 millirads	Low	4
4E-6	400E	1175N	T < 30m Mid= 150m	150 x 200 m	>10 millirads	Contact Low	2
6E-1	600E	700S	Top= 50m Mid= 250m	400 x 300 m	>30 millirads	High	3
6E-2	600E	400S	Top= 150m Mid= 350m	400 x 350 m	>30 millirads	Contact High	2
6E-3	600E	0	T> 30m Mid= 130m	250 x 200 m	0	Contact	1
6E-4	600E	200N	Top= 75m Mid= 250m	300 x 450 m	>100 millirads	Contact High	2
6E-5	600E	650N	Top= 70m Mid= 300m	450 x 450 m	<50 millirads	Contact High	2
6E-6	600E	1050N	Top= 50m Mid= 150m	250 x 250 m	<20 millirads	High	3

Table IV: Prioritized Titan Anomaly Table for Black Fox (see accompanying figures).

No.	Line	Station	Depth (m)	Size (metres)	IP Strength (milliradians)	Resistivity Structure (From 2D MT)	Priority / Type
8E-1	800E	850S	Top=120m Mid= 400m	450 x 400 m	>60 millirads	Contact High	2
8E-2	800E	575S	Top= 200m Mid= 450m	650 x 400 m	>50 millirads	Low	4
8E-3	800E	175S	Top= 50m Mid= 200m	300 x 250 m	<20 millirads	Contact High	2
8E-4	800E	050N	Top= 150m Mid= 300m	500 x 350 m	0	Contact High	1
8E-5	800E	300N	T< 50m Mid= 250m	500 x 200 m	>70millirads	Contact High	2
8E-6	800E	500N	Top= 400m Mid= 600m	400 x 400 m	0	Contact High	1?
8E-7	800E	650N	Top= 100m Mid= 300m	400 x 250 m	<30millirads	Contact High	2
8E-8	800E	1275N	Top= 75m Mid= 150m	400 x 200 m	20millirads	Contact High	2
10E-1	1000E	1050S	Top= 120m Mid= 300m	450 x 450 m	>50millirads	Contact Low	2
10E-2	1000E	750S	Top= 120m Mid= 350m	450 x 400 m	<50millirads	Contact High	3
10E-3	1000E	375S	Top= 50m Mid= 200m	350 x 200 m	0	Contact Low	1
10E-4	1000E	130S	Top= 100m Mid= 150m	175 x 175 m	>20millirads	Contact High	2
10E-5	1000E	200N	Top= 100m Mid= 200m	450 x 300 m	0	Contact Low	1
10E-6	1000E	240N	Top= 450m Mid= 600m	350 x 250 m	<20millirads	Low	4
10E-7	1000E	650N	Top= 75m Mid= 125m	250 x 175 m	>30millirads	Contact High	2
12E-1	1200E	950S	Top= 125m Mid= 250m	350 x 250 m	<50millirads	High	3
12E-2	1200E	750S	Top= 50m Mid= 400m	600 x 300 m	>40millirads	Contact High	2
12E-3	1200E	150S	T< 50m Mid= 200m	350 x 450 m	0	Contact High	1
12E-4	1200E	100S	Top= 350m Mid= 650m	600 x 350 m	<20millirads	High	3
12E-5	1200E	275N	Top= 250m Mid= 400m	250 x 300 m	0	Contact Low	1
12E-6	1200E	375N	Top= 50m Mid= 125m	275 x 175 m	>40millirads	Low	4
12E-7	1200E	550N	Top= 300m Mid= 450m	250 x 275 m	<20millirads	Contact High	2
12E-8	1200E	700N	Top= 75m Mid= 150m	200 x 225 m	>40millirads	Low	4
14E-1	1400E	875S	Top= 60m Mid= 350m	700 x 450 m	<60millirads	Contact High	2
14E-2	1400E	150S	Top= 50m Mid= 200m	250 x 300 m	>20millirads	High	3
14E-3	1400E	075N	Top= 275m Mid= 425m	350 x 500 m	0	Contact Low	1

Table III (cont): Prioritized Titan Anomaly Table for Black Fox (see accompanying figures)

No.	Line	Station	Depth (m)	Size (metres)	IP Strength (milliradians)	Resistivity Structure (From 2D MT)	Priority / Type
14E-4	1400E	350N	Top= 60m Mid= 150m	400 x 175 m	>50millirads	Low	4
14E-5	1400E	400N	Top= 475m Mid= 650m	600 x 250 m	>10millirads	Low	4
14E-6	1400E	780N	T< 10m Mid= 125m	300 x 150 m	>50millirads	High	3
16E-1	1600E	950S	Top= 60m Mid= 375m	600 x 400 m	>70millirads	High	3
16E-2	1600E	370S	Top= 130m Mid= 250m	270 x 200 m	>70millirads	High	3
16E-3	1600E	070S	Top= 120m Mid= 190m	175 x 150 m	>70millirads	Contact High	2
16E-4	1600E	250N	Top= 200m Mid= 450m	800 x 450 m	0	Contact Low	1
16E-5	1600E	290N	Top= 70m Mid= 130m	200 x 150m	>40millirads	Contact High	2
16E-6	1600E	760N	Top= 75m Mid= 175m	400 x 200m	>100 millirads	High	3

Table III (cont): Prioritized Titan Anomaly Table for Black Fox (see accompanying figures).

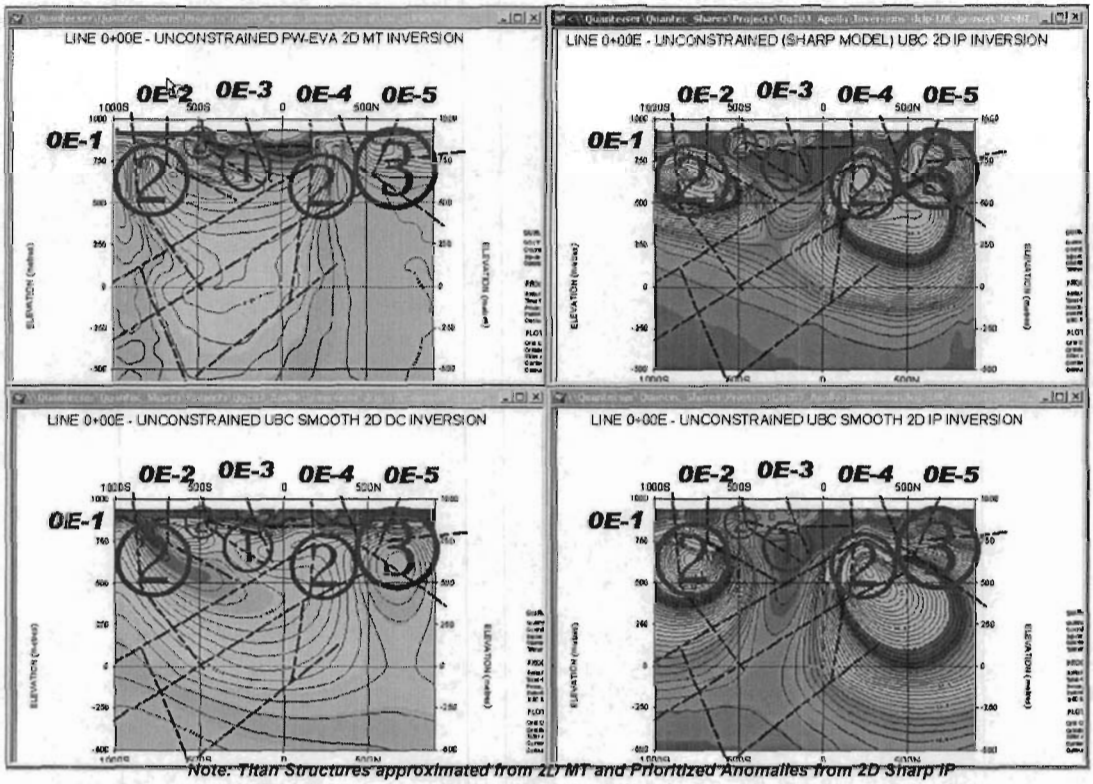

Note: Titan Structures approximated from 2D MT and Prioritized Anomalies from 2D Sharp IP

Figure 22: Prioritized Targets and Interpreted Structural Overlay onto 2D Inversions for Line 0E (Shown, clockwise from upper left, PW 2D MT, Sharp 2D IP, Smooth 2D IP & Smooth 2D DC).

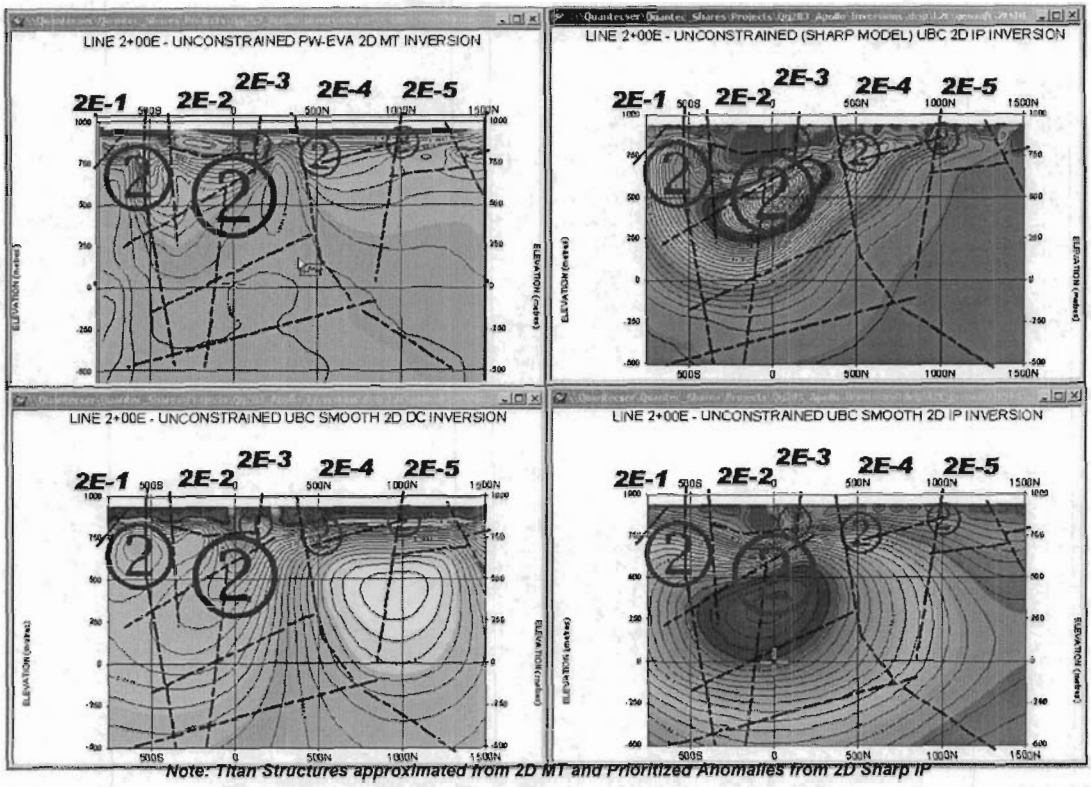

Note: Titan Structures approximated from 2D MT and Prioritized Anomalies from 2D Sharp IP

Figure 23: Prioritized Targets and Interpreted Structural Overlay onto 2D Inversions for Line 200E.

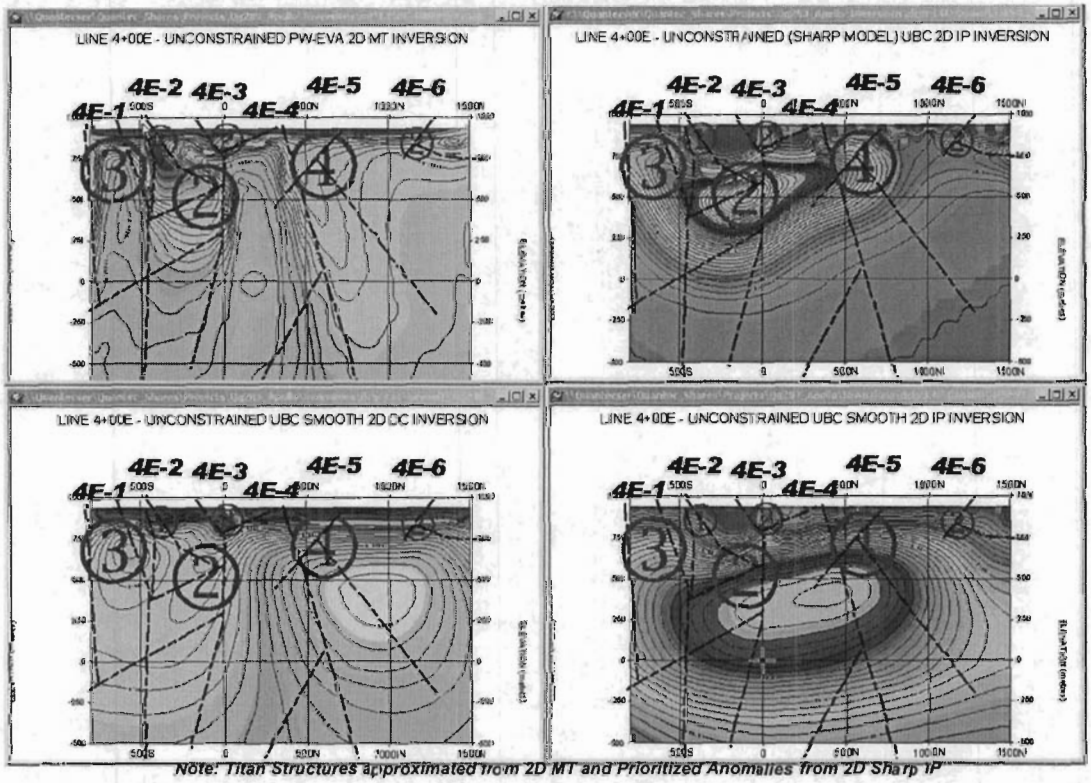

Note: Titan Structures approximated from 2D MT and Prioritized Anomalies from 2D Sharp IP

Figure 24: Prioritized Targets and Interpreted Structural Overlay onto 2D Inversions for Line 400E.

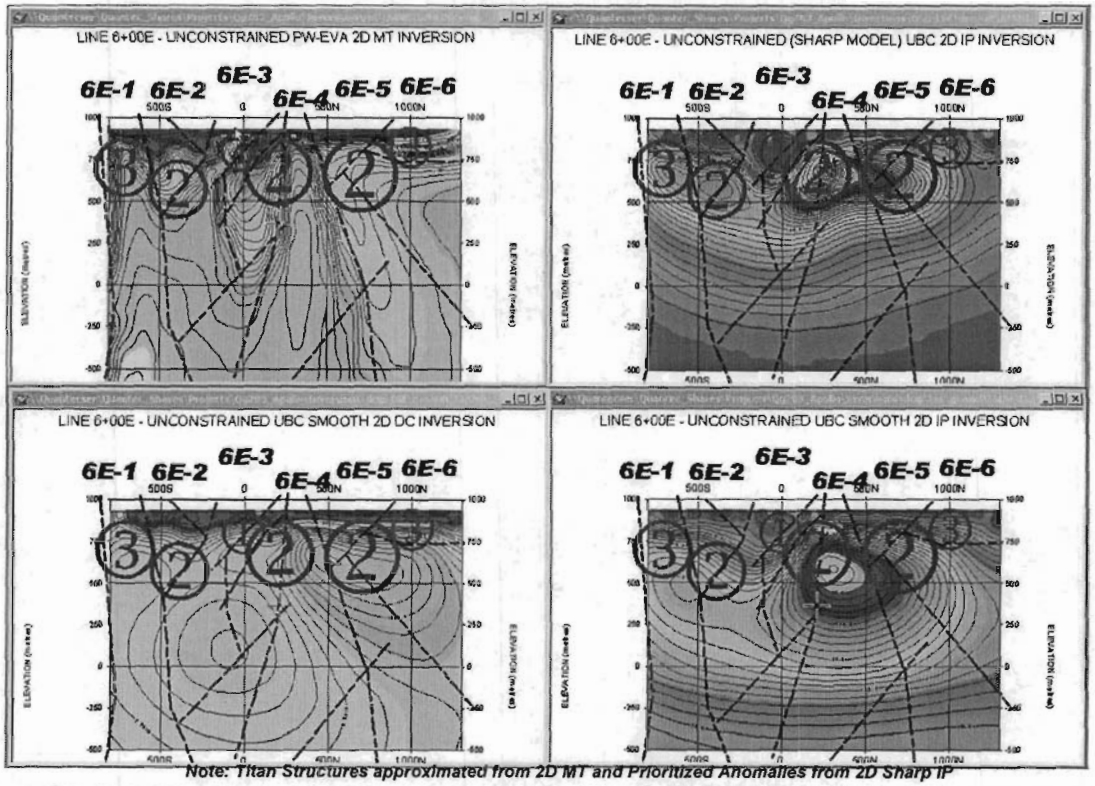

Note: Titan Structures approximated from 2D MT and Prioritized Anomalies from 2D Sharp IP

Figure 25: Prioritized Targets and Interpreted Structural Overlay onto 2D Inversions for Line 600E.

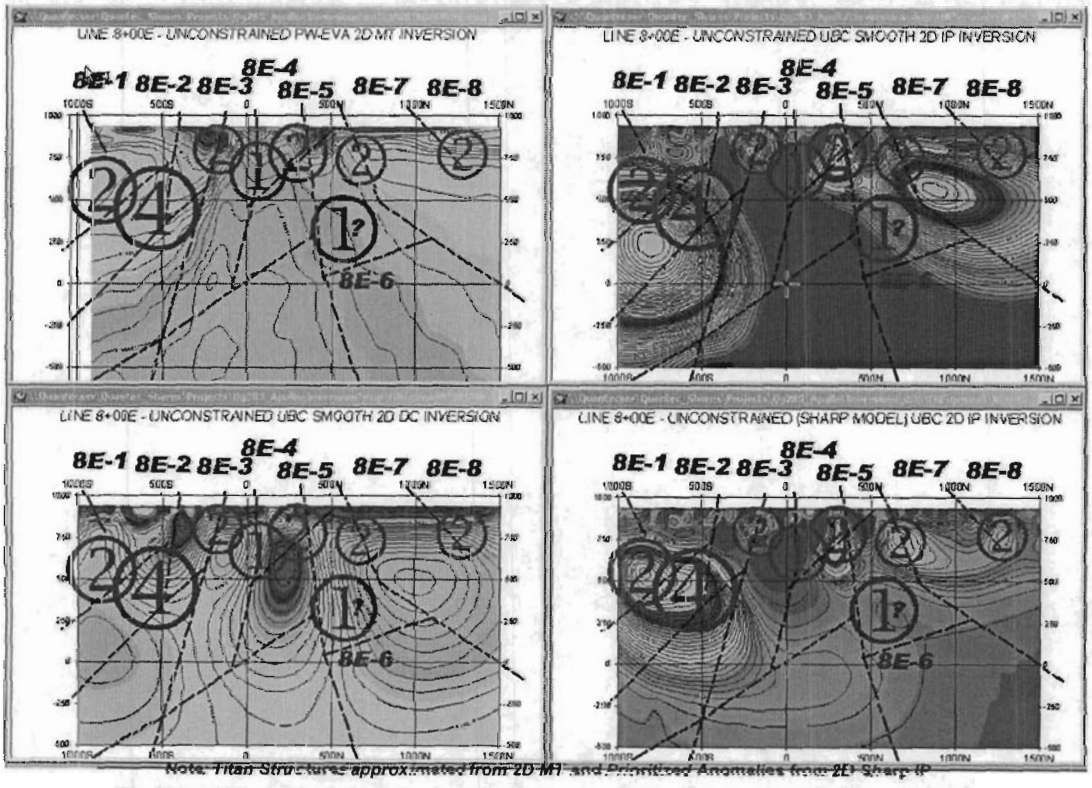

Note: Titan Structures approximated from 2D MT and Prioritized Anomalies from 2D Sharp IP

Figure 26: Prioritized Targets and Interpreted Structural Overlay onto 2D Inversions for Line 800E.

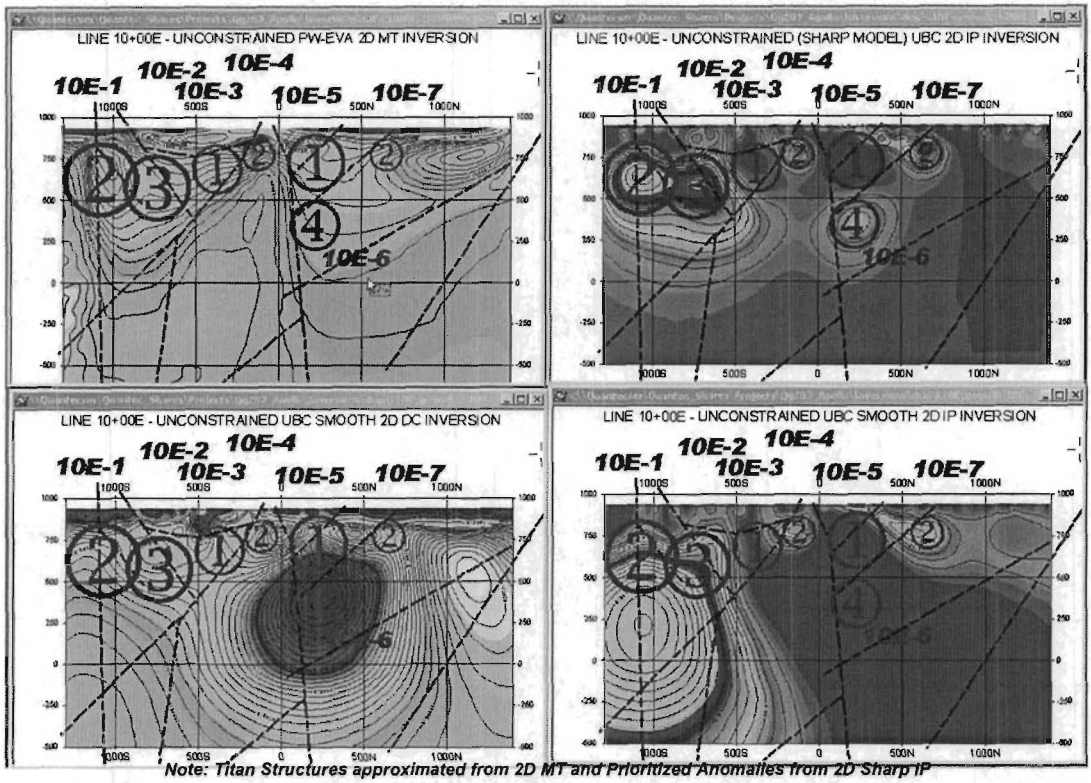

Note: Titan Structures approximated from 2D MT and Prioritized Anomalies from 2D Sharp IP

Figure 27: Prioritized Targets and Interpreted Structural Overlay onto 2D Inversions for L1000E.

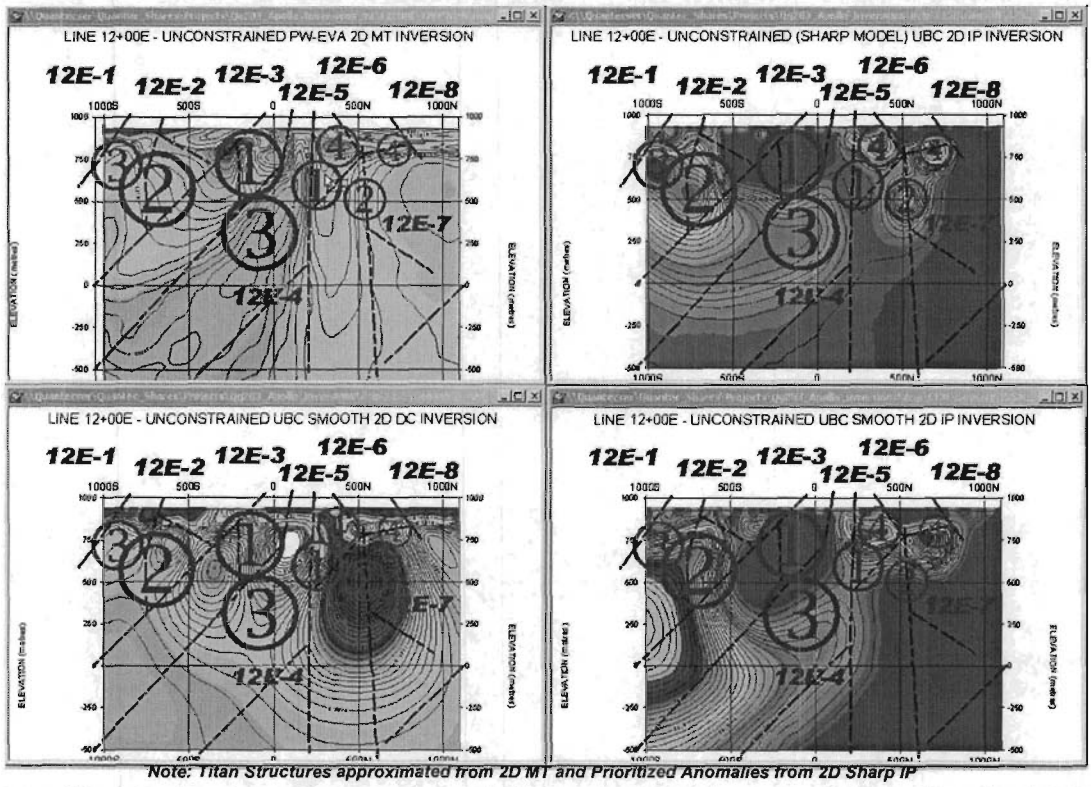

Note: Titan Structures approximated from 2D MT and Prioritized Anomalies from 2D Sharp IP

Figure 28: Prioritized Targets and Interpreted Structural Overlay onto 2D Inversions for L1200E.

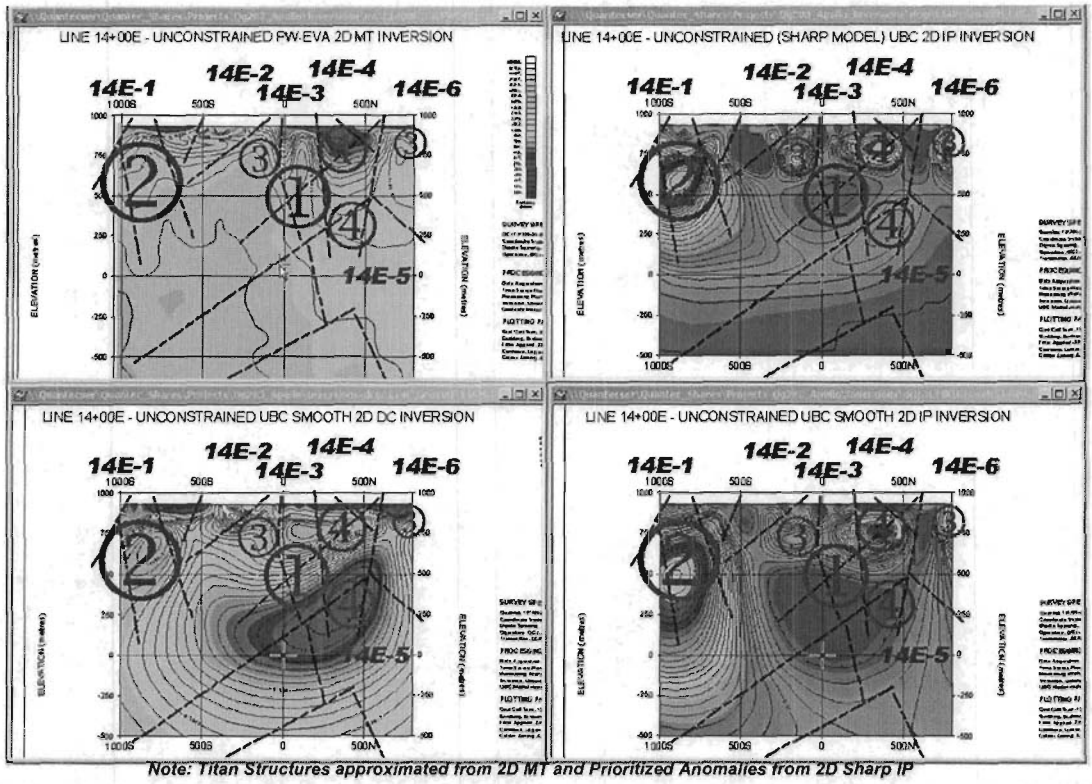

Note: Titan Structures approximated from 2D MT and Prioritized Anomalies from 2D Sharp IP

Figure 29: Prioritized Targets and Interpreted Structural Overlay onto 2D Inversions for L1400E.

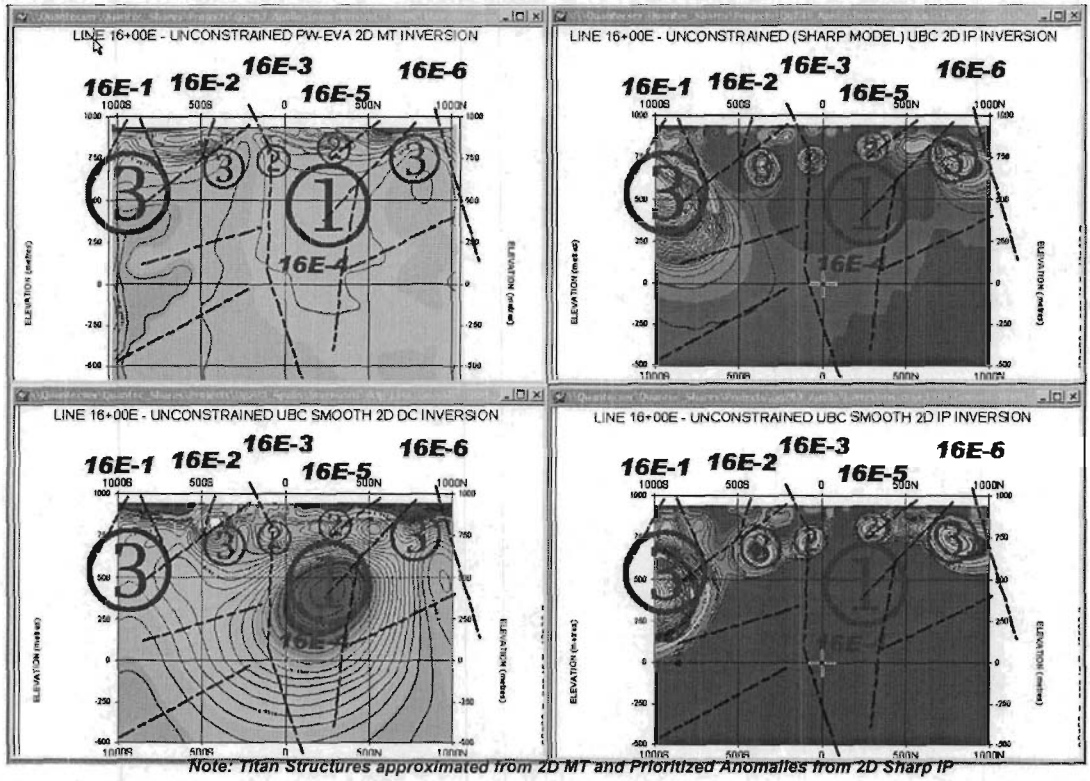

Note: Titan Structures approximated from 2D MT and Prioritized Anomalies from 2D Sharp IP

Figure 30: Prioritized Targets and Interpreted Structural Overlay onto 2D Inversions for L1600E.

4. CONCLUSIONS AND RECOMMENDATIONS

4.1 CONCLUSIONS

The Titan 3D-Quest approach is a systematic methodology for integrating and reconciling all of the available information. The purpose is not a 100% drilling success rate; it is a dramatically improved exploration program through an overall improved understanding of the deep subsurface and the ability to focus drilling through data integration. Key to this is ongoing re-evaluation of existing data, geophysical and otherwise, as the exploration program evolves.

At present, the exploration objectives have been favourably answered, using the Titan-24 distributed acquisition technology and integrated geologic and geophysical interpretation. The Titan system is a viable exploration tool for providing deep chargeability information and deep resistivity information in the near mine environment and provides an effective targeting tool when combined with geologic information and insight. In response to the survey objectives, the following conclusions can be drawn:

- Several resistivity contacts down to 1 km have been mapped consistently by MT.
- Some low resistivity features on these contacts have been identified by DC inversions. Most of these features show up on MT sections as well.
- Numerous chargeability anomalies (highs and lows) have been identified on the structures defined along resistivity contacts. They represent interesting drilling targets.
- The most significant contacts correlate with the ***Destor-Porcupine Break (DPB)***.

The Titan system has delineated responses on each of the survey lines that indicate significant resistivity and chargeability contrasts exist within the survey block – including ranges of 10^5 in resistivity (0.1-100k ohm-m) and >100mrads in chargeability. These are indicative and consistent with elevated levels of alteration, both clay &/or quartz, as well as sulphides (&/or magnetite), both massive and disseminated.

The interpretation consists of a schematic structural interpretation and our Titan targets overlain on each of the four types of 2D inversion models which were produced – however the interpretation mainly utilized the 2D MT Resistivity, for the structure, and the 2D Sharp Model DCIP Chargeability, for the chargeability high & low features, which are primary indicators of sulphide mineralization and magnetite. Of note, the cross-sectional structural geophysical interpretation offered is crude (i.e., due to poor line-to-line continuity of some features) – the primary objective is to emphasize the various breaks and resistivity contacts in the MT models, which are then used to correlate against the IP highs and lows.

Specifically, to the ***Black Fox Property***, the system responded as follows:

- In general the data quality is good to excellent, with an average error of <0.1% for the DC voltage and <0.1mrad for the IP phase, as well as <1/10 of a decade for the MT resistivity and <3degrees for the MT phase – this, in spite of the close proximity of man-made and mine-site culture..

- The Titan surveys have identified as many as ***57*** separate DCIP and MT anomalies, including ***12*** highest priority features (***Type I***) which resemble the ***Black Fox*** sheared/altered/magnetite-depleted/sulphide-poor ultramafic-hosted target model, whose physical property combinations (Resis. Contact + IP low+ Mag low) were confirmed in borehole physical property analyses and in comparisons with the known ***Black Fox/Glimmer*** orebody on sections 800E-1000E. In fact, the ***Black Fox*** deposit itself coincides with a pronounced 2D IP chargeability low and DC resistivity low, as well as a weaker contact/low MT feature, when viewed in plan. Similar anomalies have been defined along the DPB.

  In addition, at least ***25*** high 2ND priority targets were identified which resemble the structurally-controlled, quartz-carbonate altered, shear-hosted disseminate sulphide targets (***Type II*** = Resis Contact + IP high) which were also defined as geologically favourable in the survey objectives. These generally are aligned along 3 major axes, which subparallel and coincide with the DPB.

  The remaining third of the targets (***20***) feature resistivity and chargeability combinations which liken them to largely disseminate (***Type III*** = Resis. High/IP High) or largely massive (or clay-altered) sulphide bodies (***Type IV*** = Resis. Low/IP High).

- Based on the magnetite-depleted/low sulphide target model and the physical property data collected, the ***Black Fox*** type-response is a "chargeability low" and a major contact-type structural feature in the resistivity (*Type I*). Although unusual, it indeed appears to explain the Titan responses we obtained over the ***Black Fox/Glimmer*** mine site.

  Indeed, on nearly all the lines, several mod-large IP voids were identified which appear to lay along major DC-MT geoelectric structures - these seem to be strongest east of line 800E to 1600E, and in close proximity to the inferred *Destor-Porcupine Break* and it is believed these are the areas worth following. However, chargeability low targets are difficult to identify with assurance because they also closely resemble barren lithologic unit. Without the magnetics, it is hard to differentiate between the two.

- In addition, **3** other types of Titan targets were identified, all of which were based on chargeability highs, relating to possible disseminated to massive sulphides, with varying types of resistivity association – specifically, *Type II* = Destor-Porcupine stockwork-type (Res contact structure + IP high); *Type III* = Qtz-carbonate altered type (High Res + IP High) and, finally, *Type IV* = massive sulphide or clay-altered type (Low Res + IP High). Of the three types, *Type II* and, possibly also *Type III,* represent the target-classes which best describe the geologic model described in the initial survey objectives, and is also most favoured in Archean gold environments.

- In general the target size ranges from 100 x 100m to >400 x 400m, and the average depth of burial is >100m – with many DCIP-defined mineralized bodies extending below 500-750m and MT-defined structures and contacts mapped to below 1-1.5km.

- In general, the Titan targets are aligned along 3 separate horizons, which lie north, south and subparallel to the DPB. In addition ***1-2*** north-south chargeability trends have also been defined which may represent mineralized structural breaks.

- DCIP has proven to be the best indicator of anomalous chargeability relating to both the *presence and/or absence of disseminate sulphides* associated with ***Black Fox*** and other Archean lode-gold mineralization, within the upper ***350-750m*** of the bedrock. Benefiting from superior shallow to moderate-depth resolution, due to high redundancy data acquisition and, thanks to the IP parameter, a greater sensitivity to smaller, more weakly mineralized Au-bearing zones. The IP chargeability has been used as the primary sulphide mapping and targeting tool.

- MT has proven to be the best indicator of geologic structure along the inferred ***Destor-Porcupine Break***. Benefiting from superior depth penetration (>300m-1.5km) and advanced interpretation algorithms, the MT inversion results, in particular, have been able to define major subvertical to steeply-dipping resistivity contacts, likely ascribed to structure and/or lithology, below the thick overburden blanket and often extending to great depth.

  In the upper 100-500m, as expected, the DC resistivity results also generally agree with the MT-defined resistivity structures. However, with increasing depth and towards the edges of coverage, the results from both methods appear to diverge, as the DC method becomes progressively/adversely affected of off-diagonal 2D and 3D geology. As a result, the MT is used as the preferred structural mapping tool at ***Black Fox.***

As a general rule, the MT resistivity and, to a less extent, the DC resistivity results appear to have identified various resistivity breaks and contacts, which could be used to correlate against the IP chargeability highs and lows, which are primary indicators of sulphide &/or magnetite content. In our opinion, the Titan results are defining major subvertical structures, particularly along the inferred Destor-Porcupine Break (DBP), as well as more subtle south-west dipping features. Similar geologic / geoelectric features have been identified in our OMET Titan studies in Red Lake (see Figure 5). Based on these results, it is believed that IP highs and/or lows, which lie along any MT or DC structural breaks, represent targets of interest for gold exploration.

A list of prioritized targets was produced and an explanation of the geologic model and also the borehole physical property results that the interpretation was based upon. These are listed in a line-by-line basis, with approx. 4-6 targets per line, and are prioritized from 1 to 4 - essentially representing the 4 main, contrasting types of Titan anomalies that have been identified on the ***Black Fox*** property. Each type has

its own combination of physical properties (resistivity & chargeability).

4.2 RECOMMENDATIONS

The Titan-24 approach has had two valuable applications at ***Black Fox:*** A) Evaluation and Guiding drill targets, and B) Accountable and Scientific Analysis of geological concepts and ideas, geophysical results during and post-drilling to minimize follow-up holes. In addition, we recommend that:

a) Depending on various petrophysical models which are considered to be favourable in the ***Black Fox*** geologic context, these Titan anomalies need to be studied, drilled and calibrated to gain further geologic knowledge of the property. In particular, with regards to explaining the four contrasting anomaly types (*Types I to IV*) encountered, in order to confirm the source material and to focus drilling onto other favourable targets of a similar type/physical property mix.

b) That drill-testing of the Titan anomalies should be conducted in a systematic fashion, by: i) working from known geology to lesser known, ii) from the shallow to deeper targets, iii) from the center of coverage, where the geoelectric structure is best defined in the 2D inversions, to the outside of coverage, where it more poorly defined, due to 2D aperture, and iii) from the multi-parameter anomalies (IP+DC+MT) Titan-defined targets to the more poorly-correlated (or deep MT) single-parameter anomalies.

c) Any drilling should focus in on the center of the anomalies that we've described in our anomaly table and cross-sections. The overall dimensions and depths are added to facilitate the drilling effort.

d) The Titan coverage should be extended along strike, to the northwest and southeast, in order to identify other targets similar to ***Black Fox*** along the *Destor-Porcupine Break*. If the more southern or northern anomalies also prove favourable, consideration should be given to extend or shift the future survey coverage, north and south, in order to provide adequate anomaly definition – extending the lines to a distance approximately 2X the desired depth of investigation.

e) Titan targets that are drilled should be logged using borehole Petrophysics, in order to determine the true geologic source of anomalies, and also surveyed with borehole transient EM (BHTEM) to detect off-hole conductors and to identify the nature and extent of in-hole sulphide mineralization.

f) A 3D Gocad model of the property should be built and queried for fully integrated drill targets. Other elements for the query may include geochemistry, assays, depth, etc. Following this, consideration should be given to perform additional geologically-constrained inversions, in order to further refine the interpretation, if there is sufficiently good geological control and petrophysical database for the property. If so, unknown and potentially important targets can be more easily discriminated from the known geology, particularly at depth.

RESPECTFULLY SUBMITTED

QUANTEC GEOSCIENCE INC.

Wei Qian, PHD
Senior geophysicist – QGI

Jean Legault, P. Eng., P.Geo. (ON)
Senior geophysicist – QGI

Robert Gordon – P.Eng.
Senior geophysicist – QGI

Evelio Martinez, M.Sc.
Geophysicist - QGI

Toronto, ON

APPENDIX A: PLAN AND SECTION PLOTS

APPENDIX B: INVERSION RESULTS

LINE 0+00 E

DC Resistivity

The observed and calculated DC Apparent Resistivity pseudosections and the final 2D smooth body DC Resistivity inversion, for Line 0E, are shown in Figure 31. The excellent quality of the data and the model fits are clearly evident.

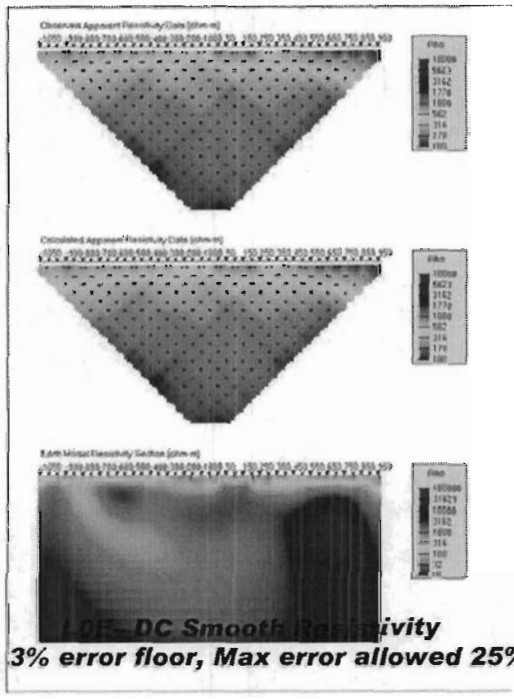

Figure 31: Line 0E – UBC 2D Smooth DC Inversion Results.

IP Chargeability

The observed and calculated IP Phase pseudosections and the final 2D sharp body IP Chargeability inversion, for Line 0E, are shown in Figure 32. The corresponding 2D smooth body inversion results are shown in Figure 33. The excellent quality of the data and the model fits are clearly evident.

There is a well defined chargeability anomaly at sites 750S, 200N and 750N.

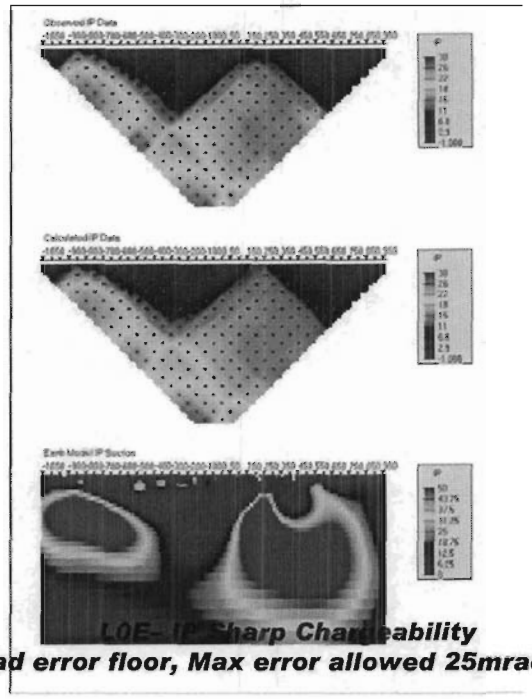

Figure 32: Line 0E – UBC 2D Sharp model IP Inversion results.

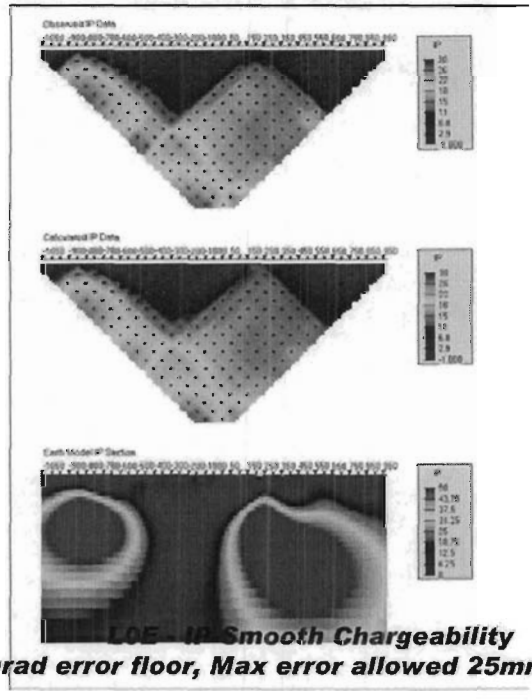

Figure 33: Line 0E – UBC 2D Sharp Model IP Inversion Results

MT Resistivity

The raw (measured) MT frequency pseudosections for Line 0E are presented in Figure 34, from top to bottom: a) the In-line (XY) apparent resistivity, b) In-line (XY) phase, c) Cross-line (YX) apparent resistivity and d) Cross-line (YX) phase. The corresponding EVA processed Along-strike (TE) and Across-strike (TE) MT pseudosections are shown in Figure 35. The excellent data quality is clearly

evident.

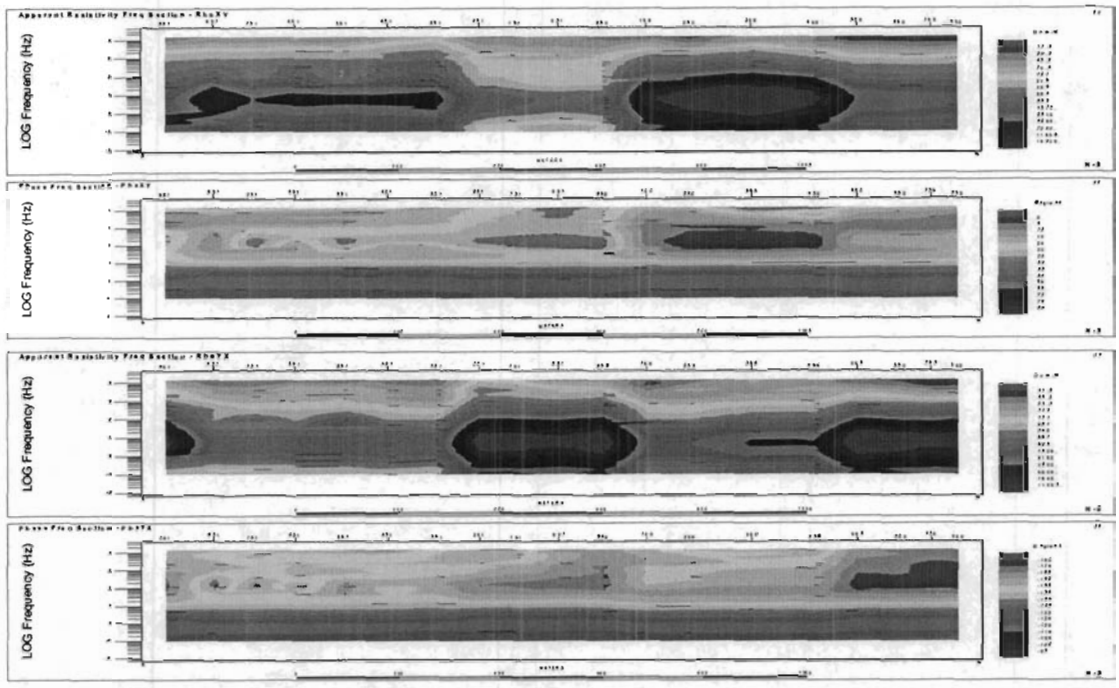

Figure 34: L0E - Raw MT Apparent Resistivity and Phase Frequency Pseudosections

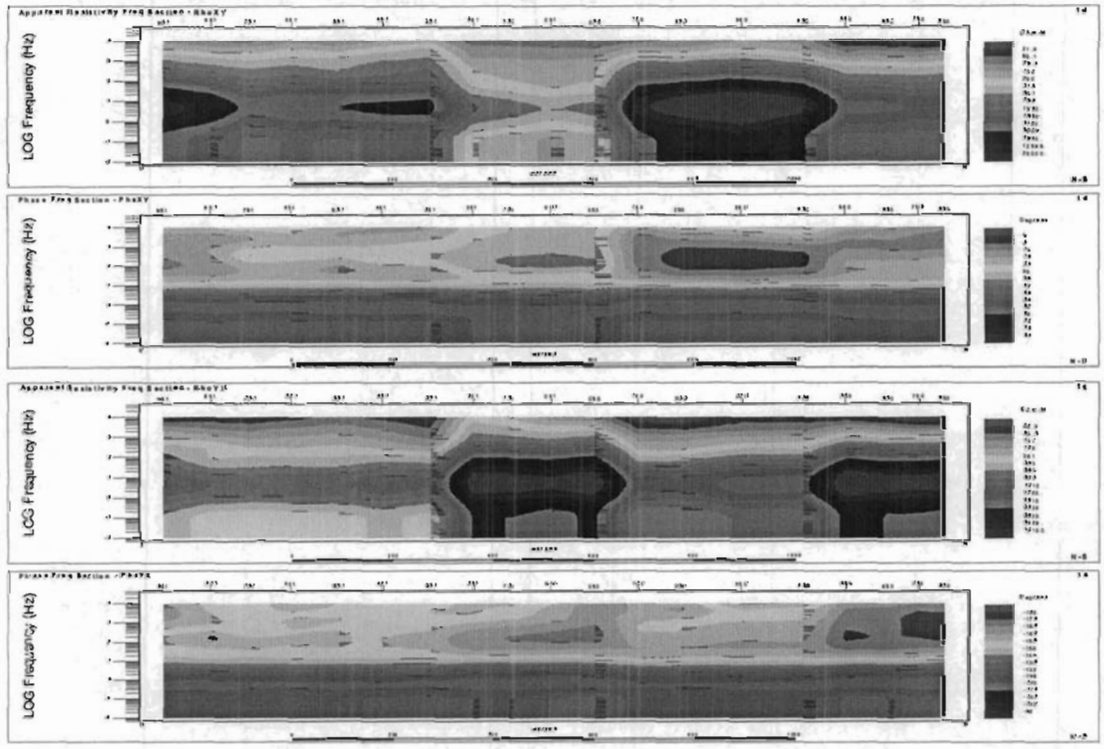

Figure 35: L0E - EVA-processed MT Apparent Resistivity and Phase Frequency Pseudosections

The 2D smooth-conjugate RLM MT resistivity inversion results for Line 0E are shown in Figure 36 and the corresponding 2D Gauss-Newton PW MT resistivity inversion results are shown in Figure 37. Relatively good (~8% rms) model-convergences were obtained.

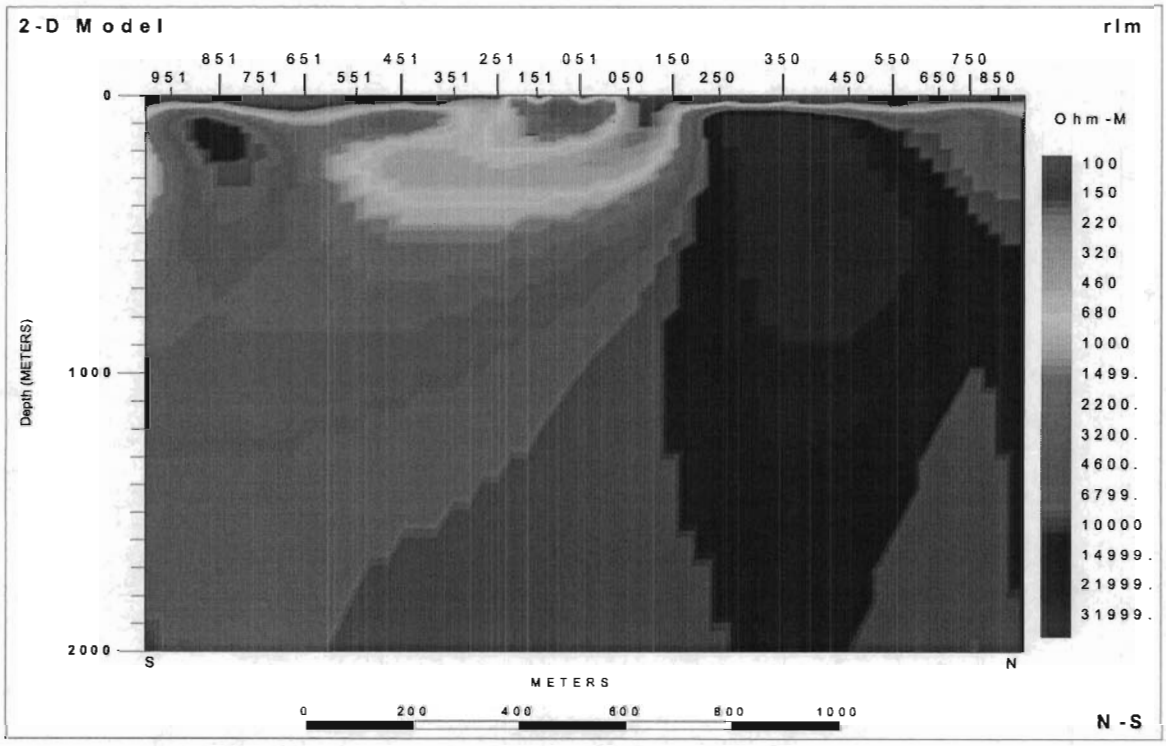

Figure 36: L0E - 2D RLM Smooth-Conjugate MT Resistivity Inversion.

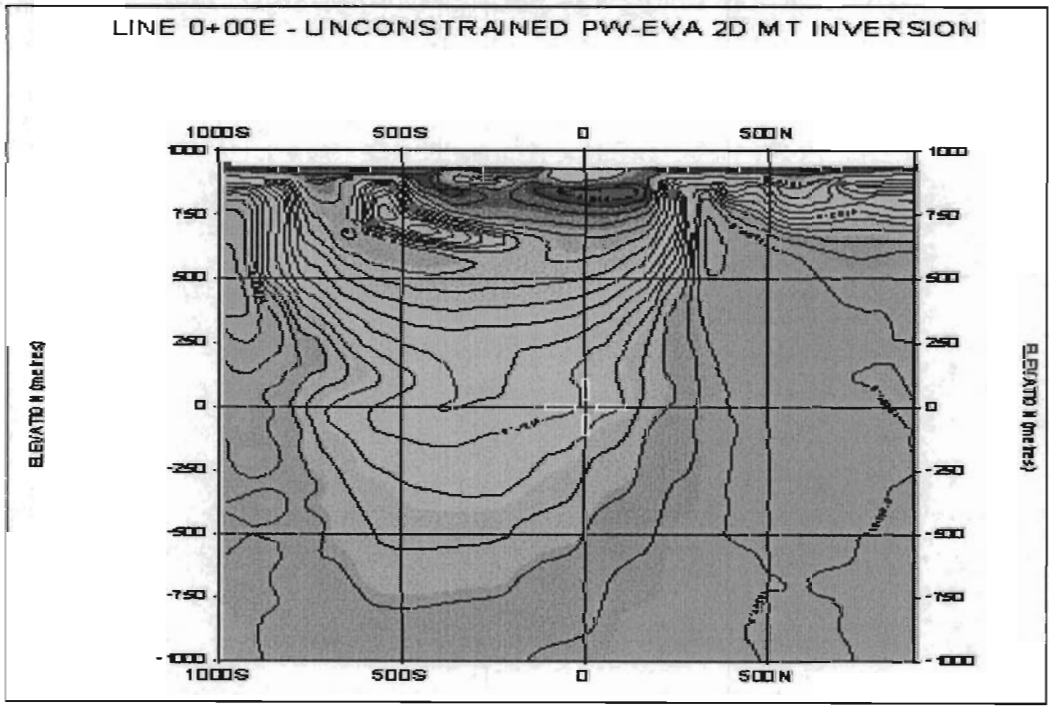

Figure 37: L0E - 2D PW Gauss Newton MT Resistivity Inversion.

Discussion of Results

The MT data and inversion models clearly demonstrate that there are two resistivity contacts at 750S and 250 N and it confirms the north dipping conductive feature shown on the DC section. The presence of the low resistivity block may or may not continue to depth, contrary to what the image has shown. The TE apparent resistivity increase in this conductive block can be explained by high resistivity truncation of the conductive block along the strike (EW) direction.

Due to limited depth of penetration in DC resistivity, these two contacts, particularly the southern one is not well defined in the DC model. The thickness of the conductive overburden is exaggerated due to the smoothness regularization of the inversions.

Comparing the two IP inversions leads to the impression that the IP data are sensing to an effective depth of about 700 meters and there are four dominant chargeable bodies along the profile. The top and lateral extend of these major chargeable anomalies are well defined. But their depth extend is far less certain. The rock body or bodies caused these anomalies can be anywhere within the center of the contour highs.

LINE 2+00 E

DC Resistivity

The observed and calculated DC Apparent Resistivity pseudosections and the final 2D smooth body DC Resistivity inversion, for Line 200E, are shown in Figure 38. The excellent quality of the data and the model fits are clearly evident.

This inversion model shows overburden and thickening of it at 0 and contact at 250 N.

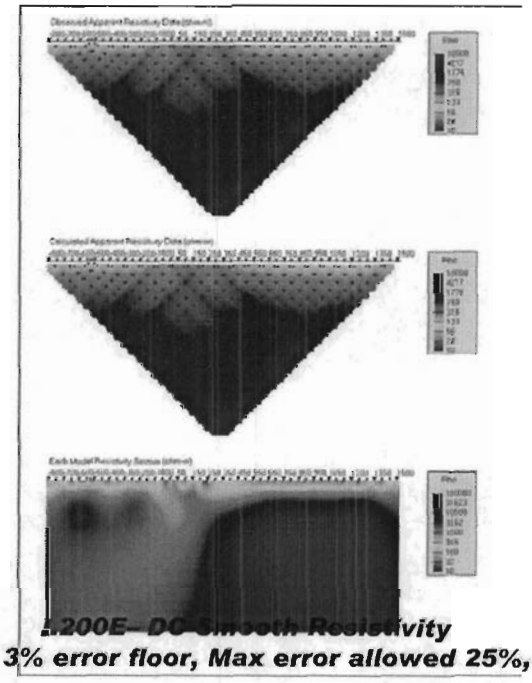

Figure 38: Line 200E – UBC 2D Smooth DC Inversion Results.

IP Chargeability

The observed and calculated IP Phase pseudosections and the final 2D sharp body IP Chargeability inversion, for Line 200E, are shown in Figure 39. The corresponding 2D smooth body inversion results are shown in Figure 40. The excellent quality of the data and the model fits are clearly evident.

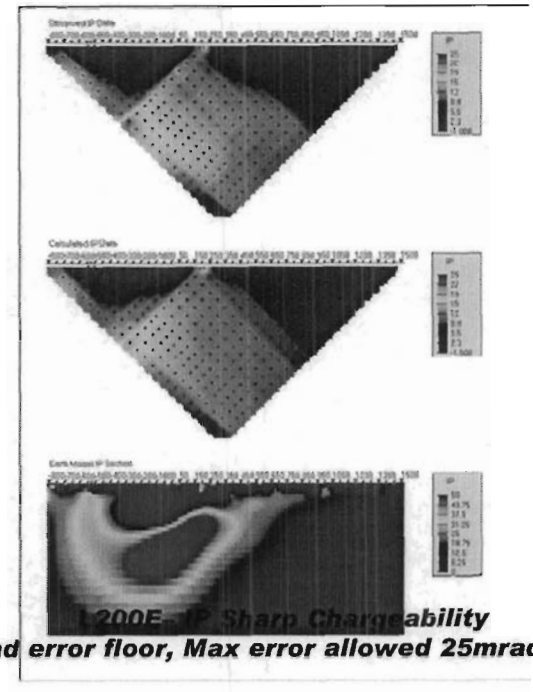

Figure 39: Line 200E – UBC 2D Sharp model IP Inversion results.

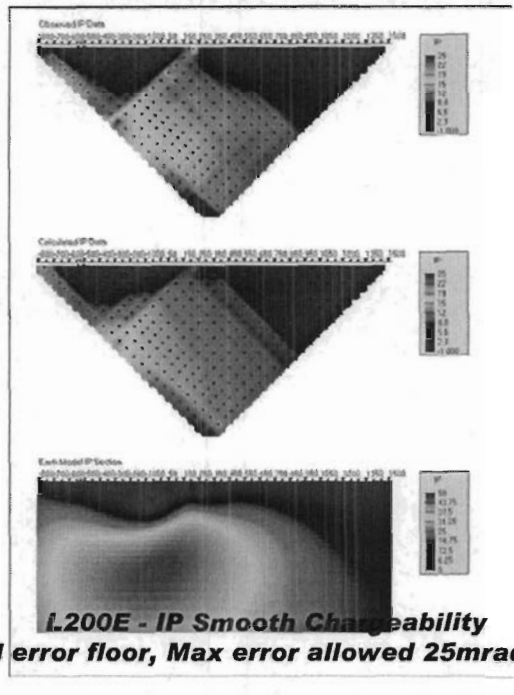

Figure 40: Line 200E – UBC 2D Smooth model IP Inversion results.

MT Resistivity

The raw (measured) MT frequency pseudosections for Line 200E are presented in Figure 41, from top to bottom: a) the In-line (XY) apparent resistivity, b) In-line (XY) phase, c) Cross-line (YX) apparent resistivity and d) Cross-line (YX) phase. The corresponding EVA processed Along-strike (TE) and Across-strike (TE) MT pseudosections are shown in Figure 42. The excellent data quality is clearly evident.

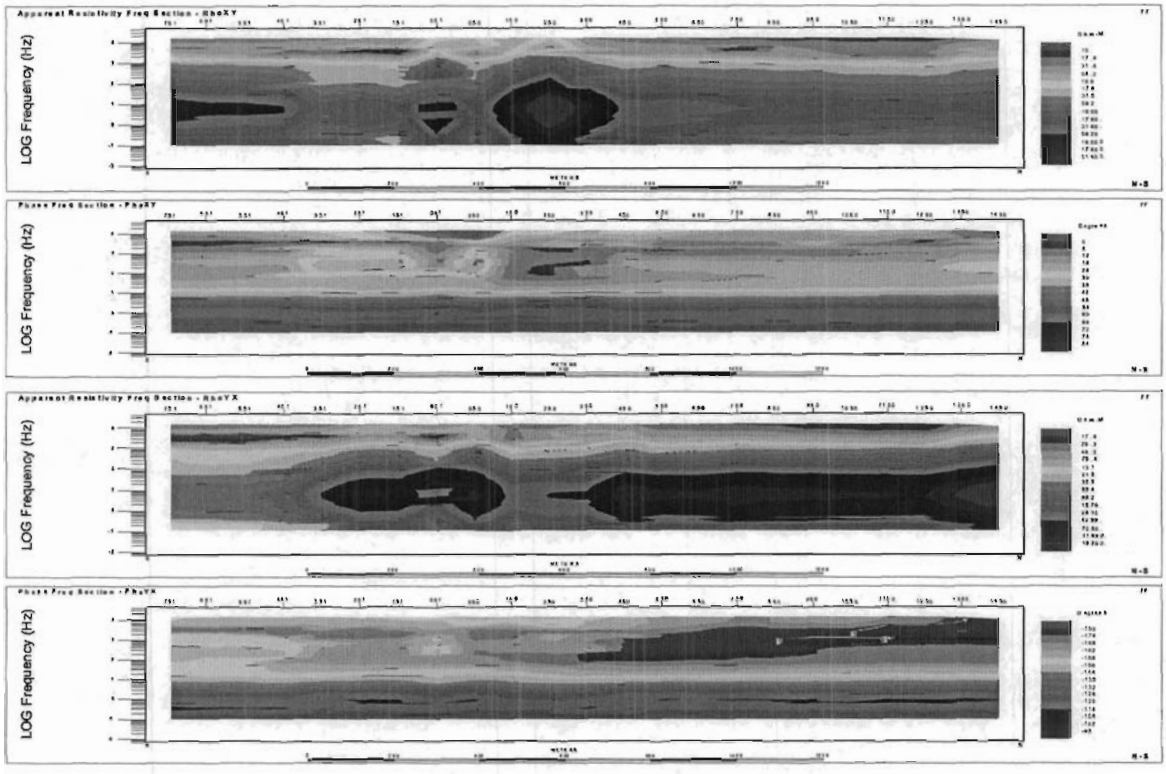

Figure 41: L200E - Raw MT Apparent Resistivity and Phase Frequency Pseudosections.

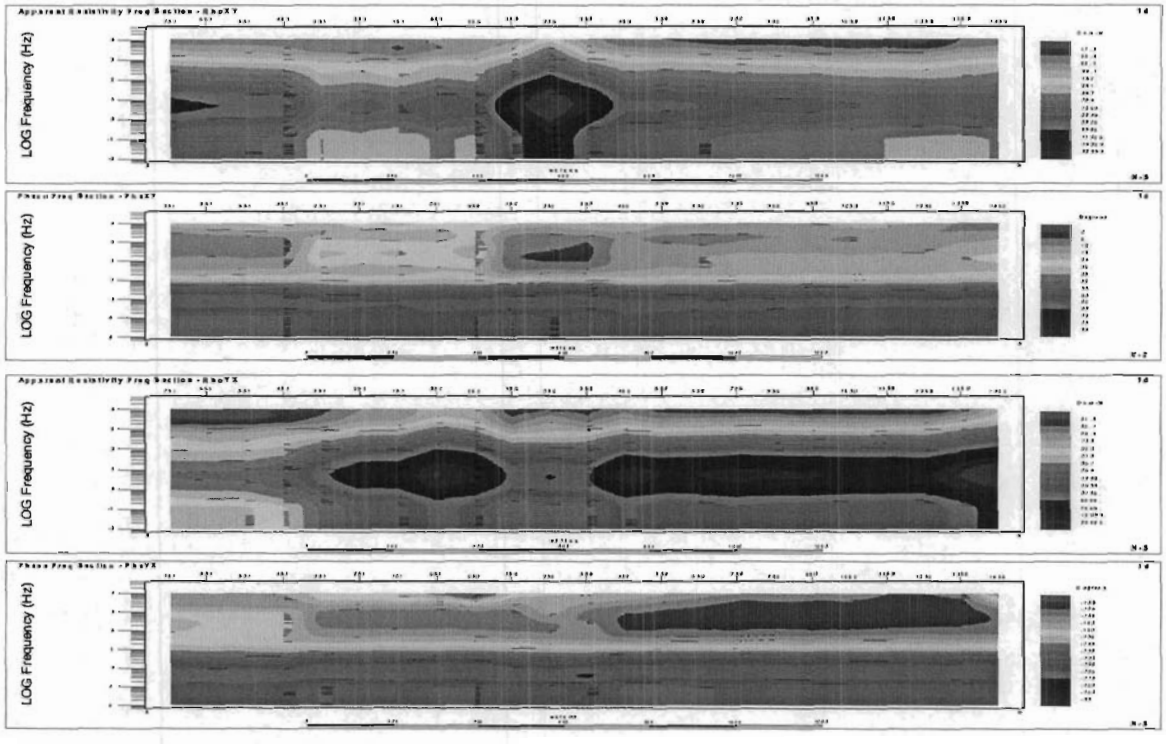

Figure 42: L200E - EVA-processed MT Apparent Resistivity and Phase Frequency Pseudosections

The 2D smooth-conjugate RLM MT resistivity inversion results for Line 200E are shown in Figure 43and the corresponding 2D Gauss-Newton PW MT resistivity inversion results are shown in Figure 44. Relatively good (~8% rms) model-convergences were obtained.

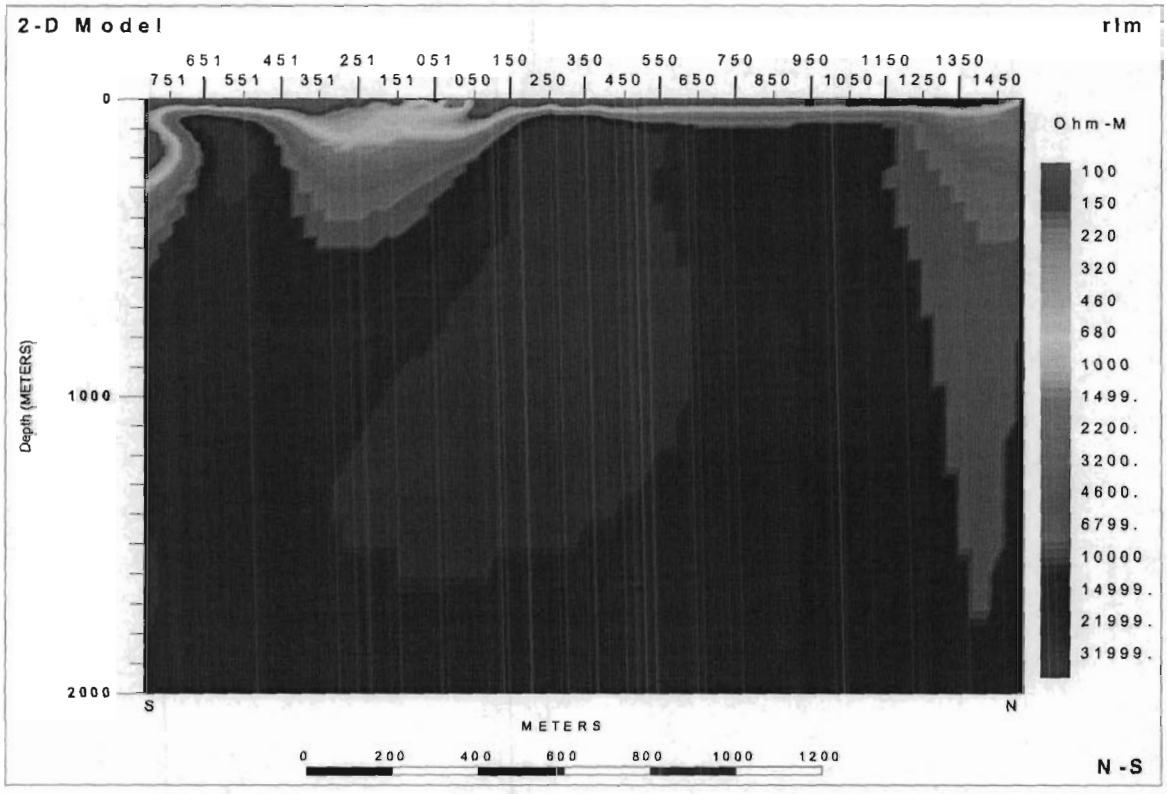

Figure 43: L200E - 2D RLM Smooth-Conjugate MT Resistivity Inversion.

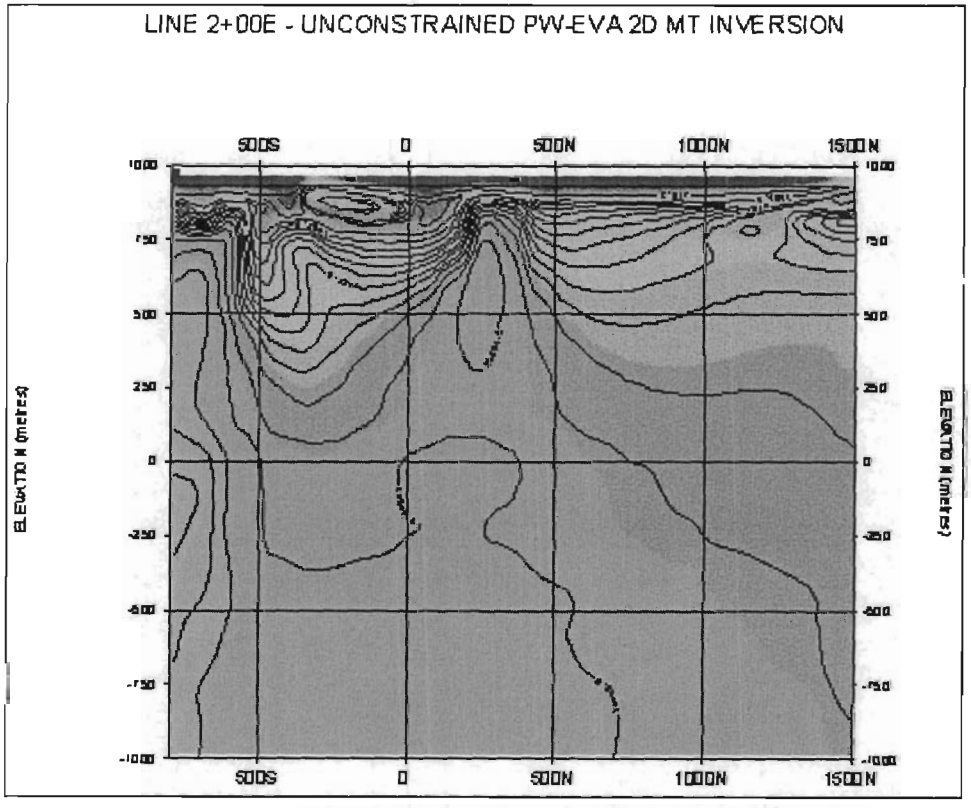

Figure 44: L200E - 2D PW Gauss Newton MT Resistivity Inversion.

Discussion of Results

This profile is very similar to profile 0, except the southern contact has been moved to 500 S. The chargeability anomalies seen from the previous line seem to converge to 0 on this line. The resolution of the data is insufficient to make this judgment conclusive.

LINE 4+00 E

DC Resistivity

The observed and calculated DC Apparent Resistivity pseudosections and the final 2D smooth body DC Resistivity inversion, for Line 400E, are shown in Figure 45. The excellent quality of the data and the model fits are clearly evident.

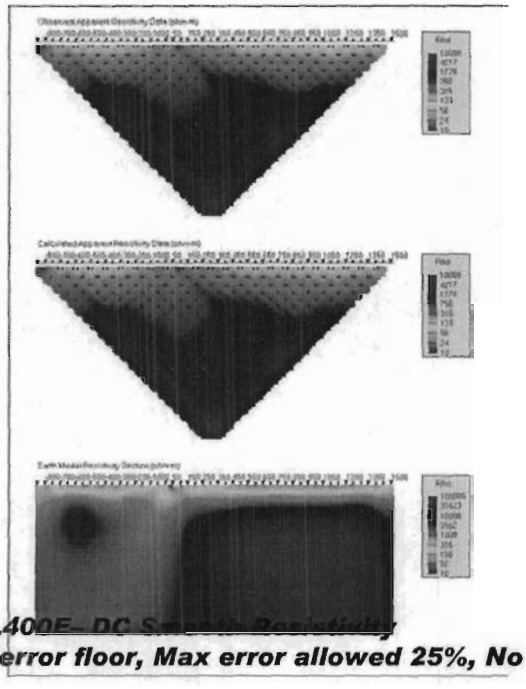

Figure 45: Line 400E – UBC 2D Smooth DC Inversion Results.

IP Chargeability

The observed and calculated IP Phase pseudosections and the final 2D sharp body IP Chargeability inversion, for Line 400E, are shown in Figure 46. The corresponding 2D smooth body inversion results are shown in Figure 47. The excellent quality of the data and the model fits are clearly evident.

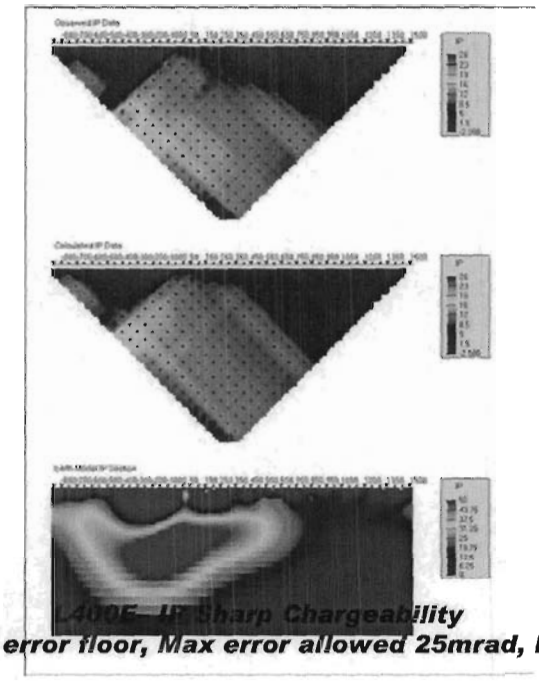

Figure 46: Line 400E – UBC 2D Sharp model IP Inversion results.

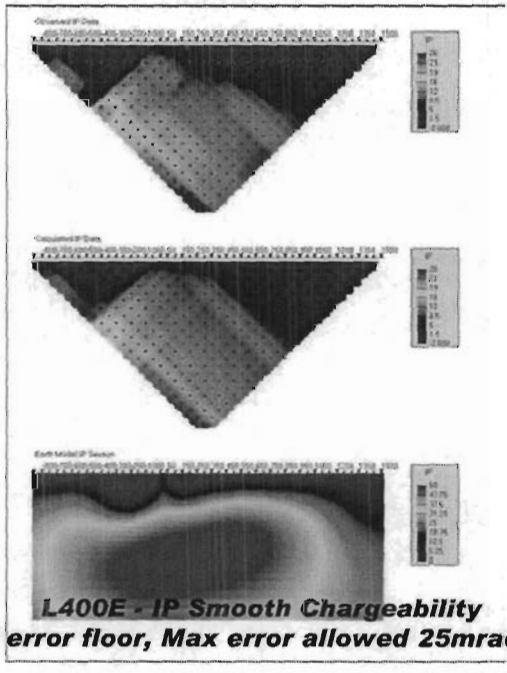

Figure 47: Line 400E – UBC 2D Smooth model IP Inversion results.

MT Resistivity

The raw (measured) MT frequency pseudosections for Line 400E are presented in Figure 48 – shown from top to bottom: a) the In-line (XY) apparent resistivity, b) In-line (XY) phase, c) Cross-line (YX) apparent resistivity and d) Cross-line (YX) phase. The corresponding EVA processed Along-strike (TE) and Across-strike (TE) MT pseudosections are shown in Figure 49. The excellent data quality is clearly evident.

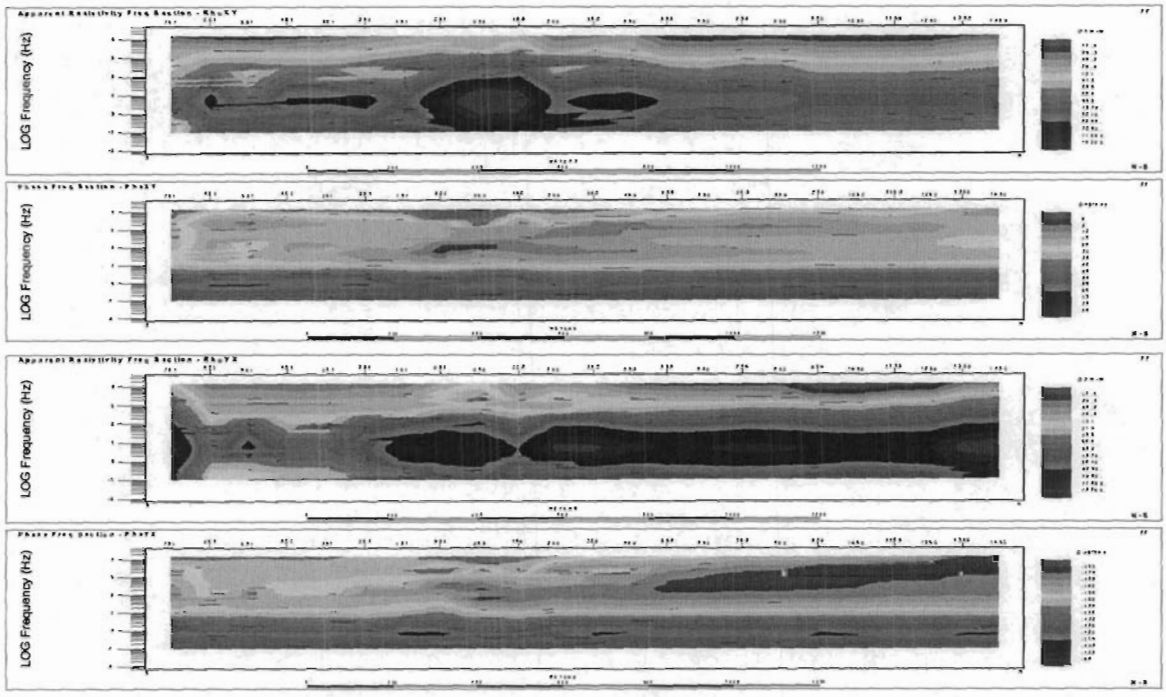

Figure 48: L400E - Raw MT Apparent Resistivity and Phase Frequency Pseudosections.

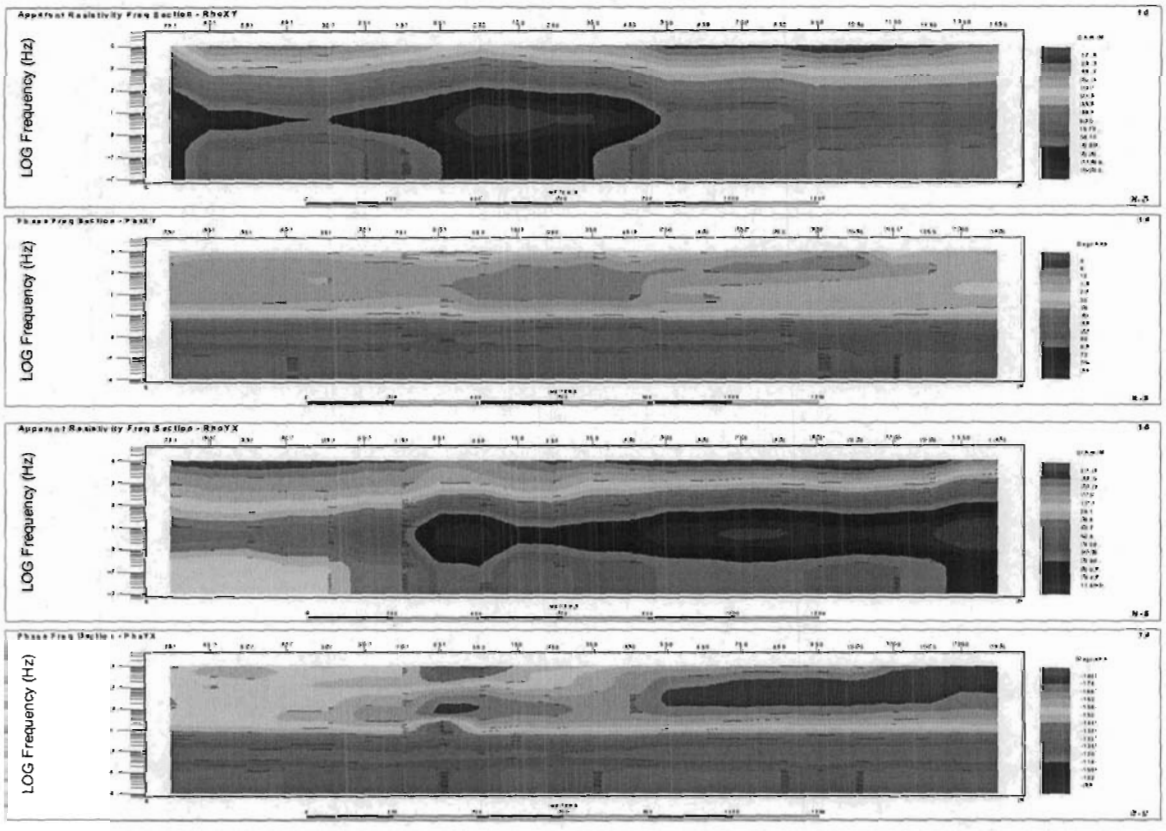

Figure 49: L400E - EVA-processed MT Apparent Resistivity and Phase Frequency Pseudosections

The 2D smooth-conjugate RLM MT resistivity inversion results for Line 400E are shown in Figure 43 and the corresponding 2D Gauss-Newton PW MT resistivity inversion results are shown in Figure 44. Relatively good (~8% rms) model-convergences were obtained.

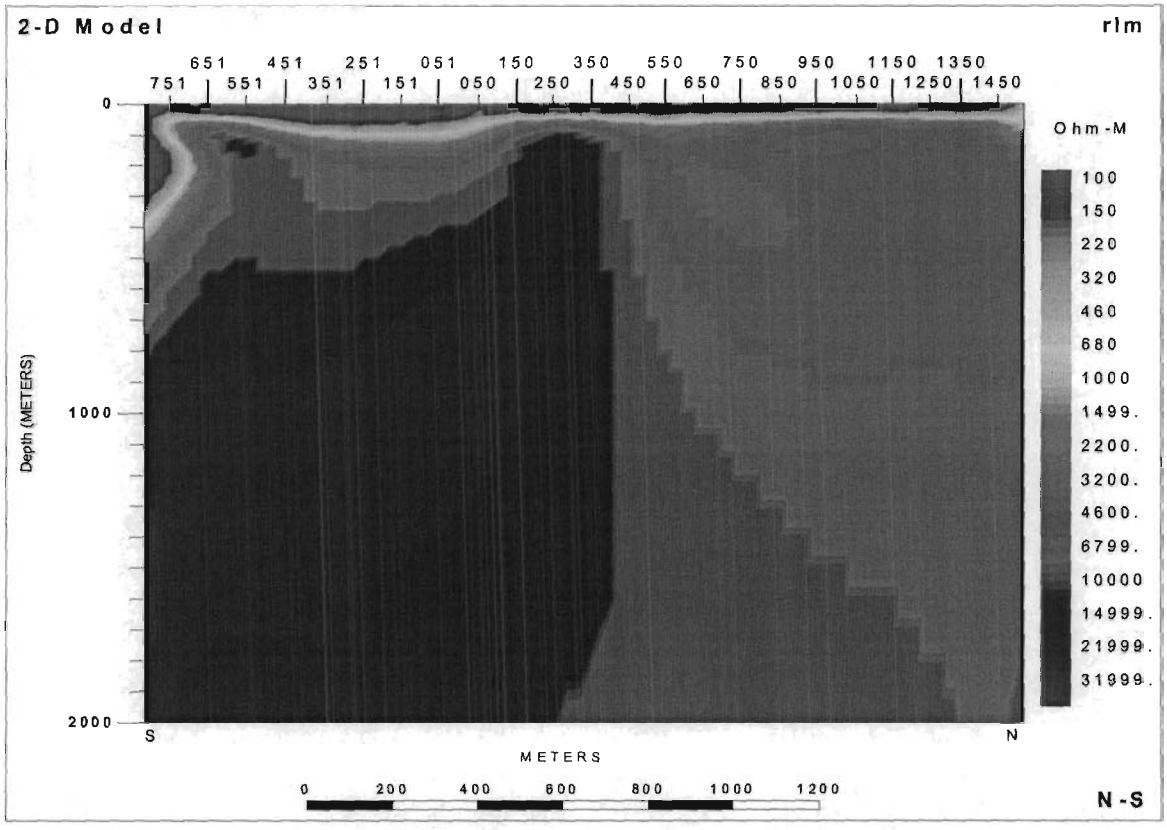

Figure 50: L400E - 2D RLM Smooth-Conjugate MT Resistivity Inversion.

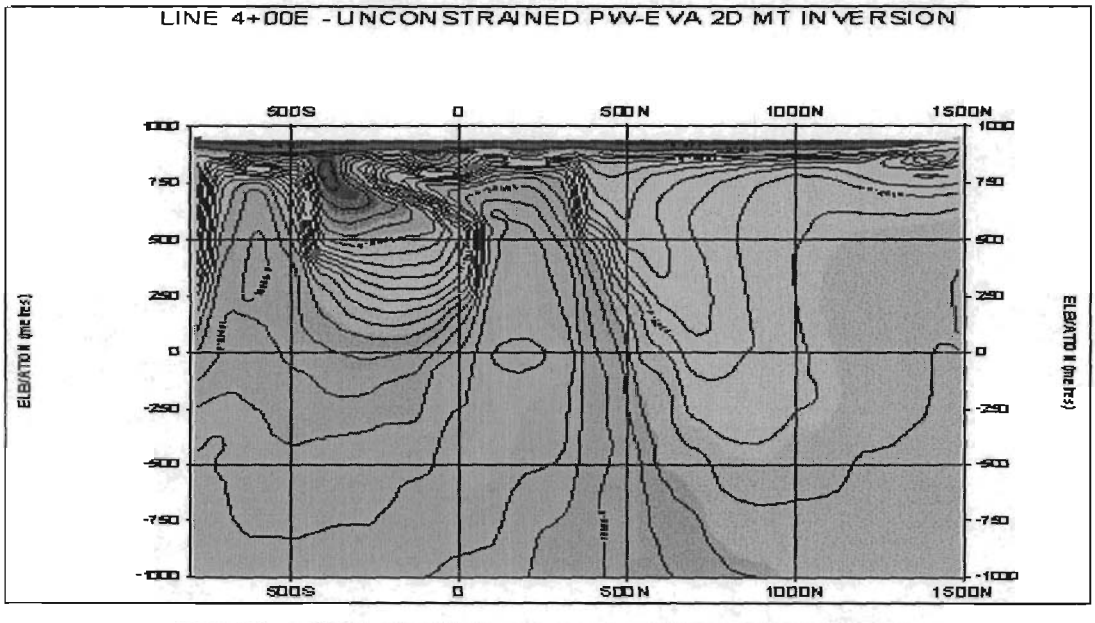

Figure 51: L400E - 2D PW Gauss Newton MT Resistivity Inversion.

Discussion of Results

This profile again, falls into the paradigm of the previous two profiles, but there is a contact to low resistivity at far north come into the picture at around 400 N. Again the depth extend of these contacts are not certain from the comparison of RLM to PW models.

LINE 6+00 E

DC Resistivity

The observed and calculated DC Apparent Resistivity pseudosections and the final 2D smooth body DC Resistivity inversion, for Line 600E, are shown in Figure 52. The excellent quality of the data and the model fits are clearly evident.

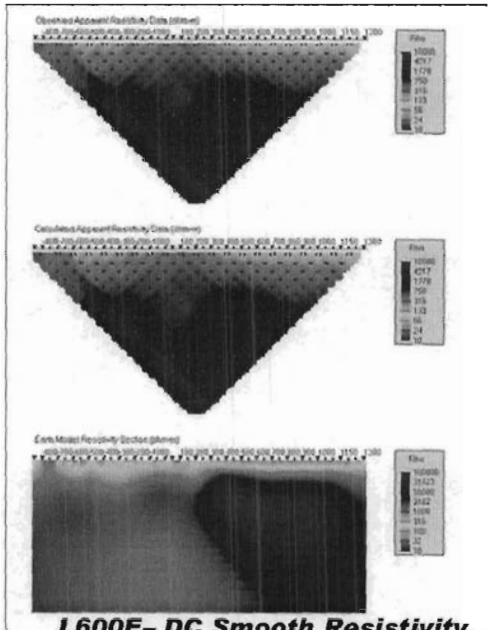

Observed

Calculated

2D Res

L600E– DC Smooth Resistivity
(10k start, 3% error floor, Max error allowed 25%, No Cull)

Figure 52: Line 600E – UBC 2D Smooth DC Inversion Results.

IP Chargeability

The observed and calculated IP Phase pseudosections and the final 2D sharp body IP Chargeability inversion, for Line 600E, are shown in Figure 53. The corresponding 2D smooth body inversion results are shown in Figure 54. The excellent quality of the data and the model fits are clearly evident.

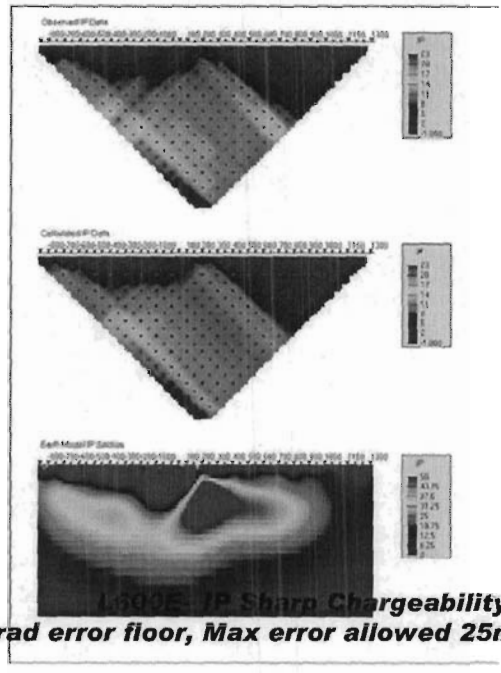

Figure 53: Line 600E – UBC 2D Sharp model IP Inversion results.

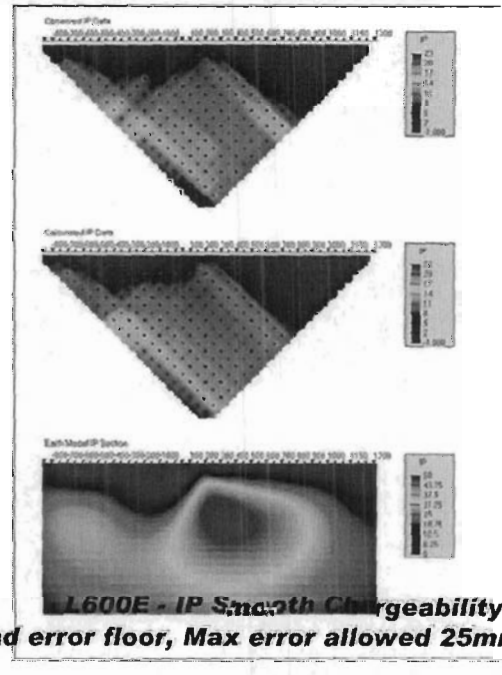

Figure 54: Line 600E – UBC 2D Smooth model IP Inversion results.

MT Resistivity

The raw (measured) MT frequency pseudosections for Line 600E are presented in – shown Figure 55 from top to bottom: a) the In-line (XY) apparent resistivity, b) In-line (XY) phase, c) Cross-line (YX) apparent resistivity and d) Cross-line (YX) phase. The corresponding EVA processed Along-strike (TE) and Across-strike (TE) MT pseudosections are shown in Figure 56. The excellent data quality is clearly evident.

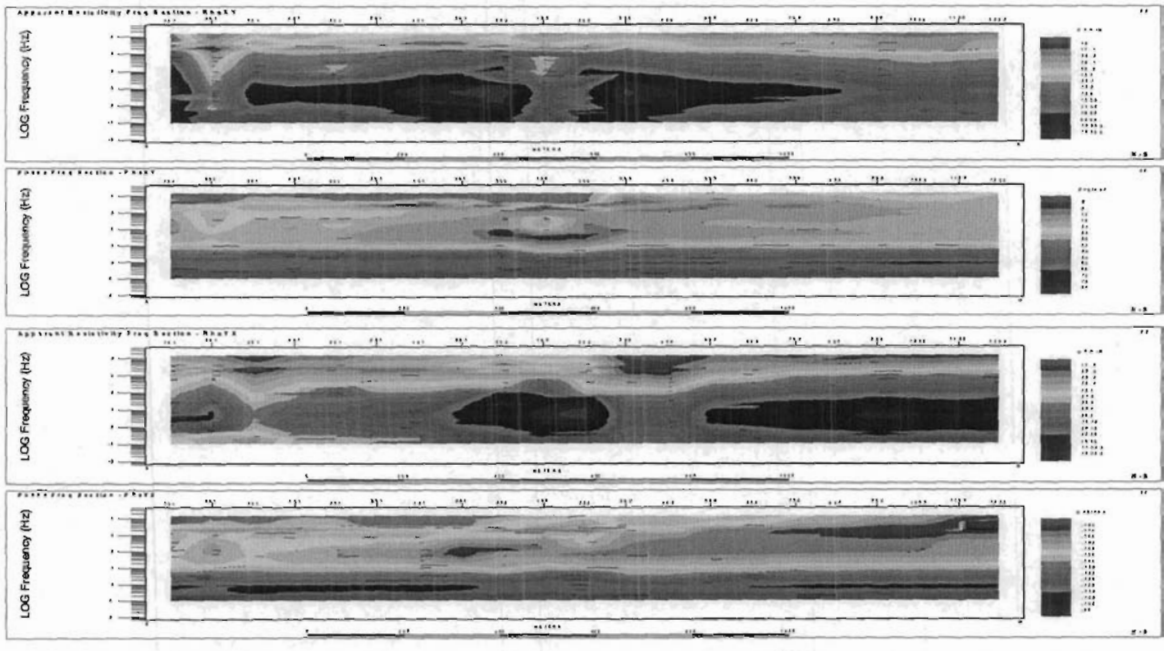

Figure 55: L600E - Raw MT Apparent Resistivity and Phase Frequency Pseudosections.

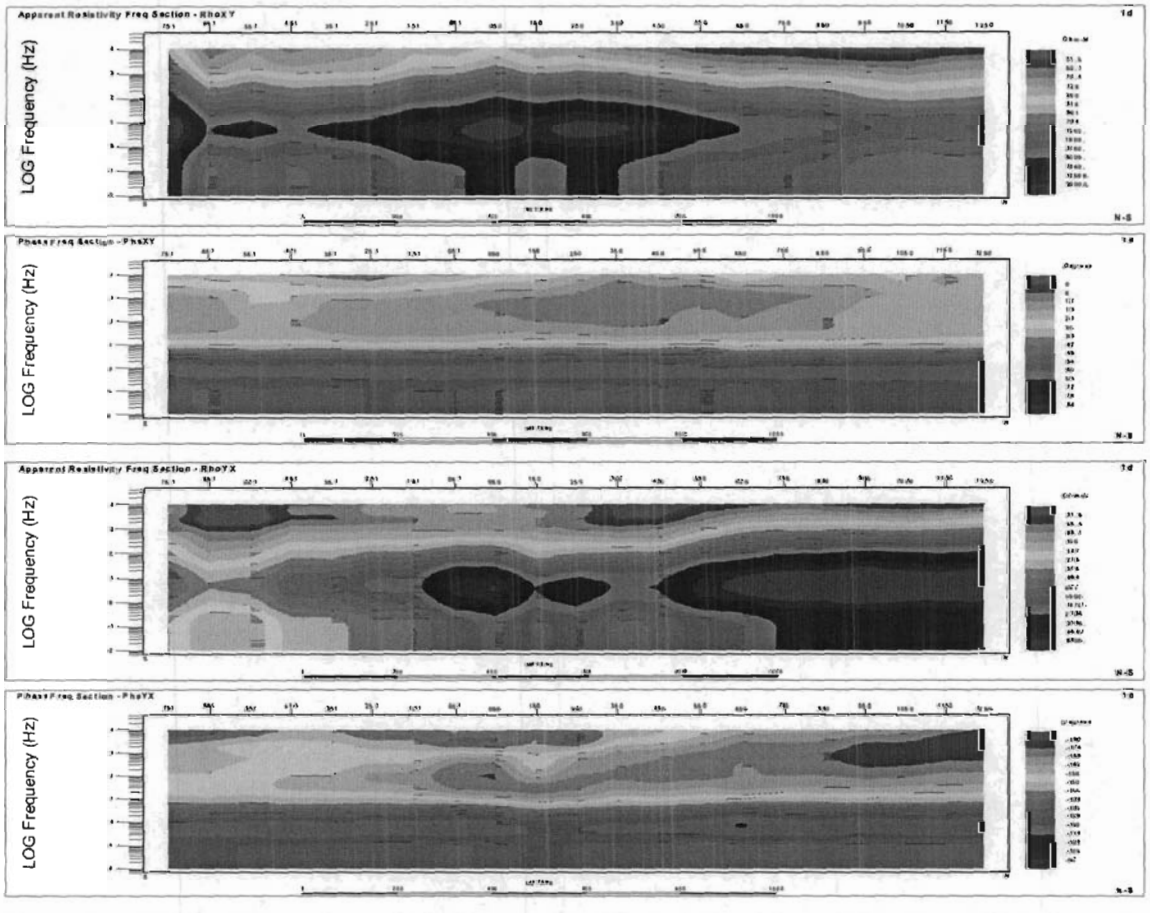

Figure 56: L600E - EVA-processed MT Apparent Resistivity and Phase Frequency Pseudosections

The 2D smooth-conjugate RLM MT resistivity inversion results for Line 600E are shown in Figure 43 and the corresponding 2D Gauss-Newton PW MT resistivity inversion results are shown in Figure 44. Relatively good (~8% rms) model-convergences were obtained.

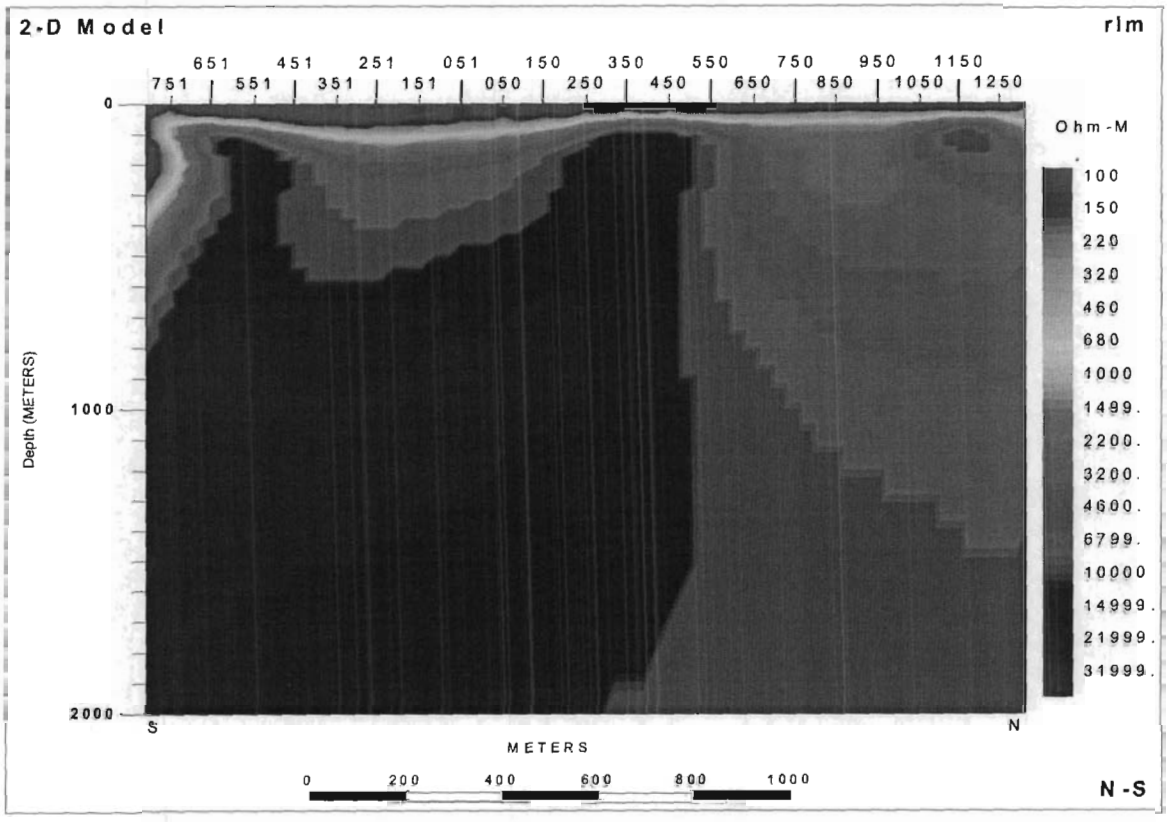

Figure 57: L600E - 2D RLM Smooth-Conjugate MT Resistivity Inversion.

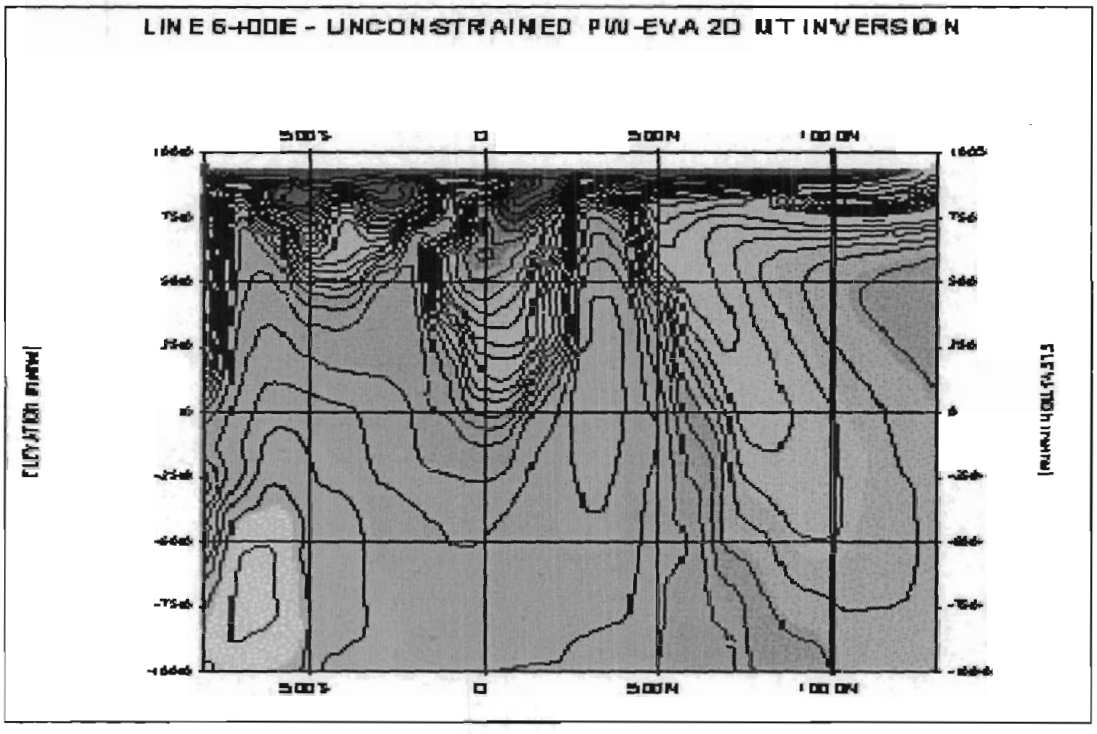

Figure 58: L600E - 2D PW Gauss Newton MT Resistivity Inversion.

Discussion of Results

This profile confirms the model of previous profiles, but the RLM model shows almost 1D like structure while the PW model indicates the contact goes as deep as 500 – 2000 m. This is almost entirely due to the inversion methodology differences between RLM and PW. However from the differences of the model, we can conclude that the depth extends of these contacts are between 200 –2000 m. In northern Ontario resistive terrain, the MT wavelength is too large to discriminate the depth extend better.

LINE 8+00 E

DC Resistivity

The observed and calculated DC Apparent Resistivity pseudosections and the final 2D smooth body DC Resistivity inversion, for Line 800E, are shown in Figure 59. The excellent quality of the data and the model fits are clearly evident.

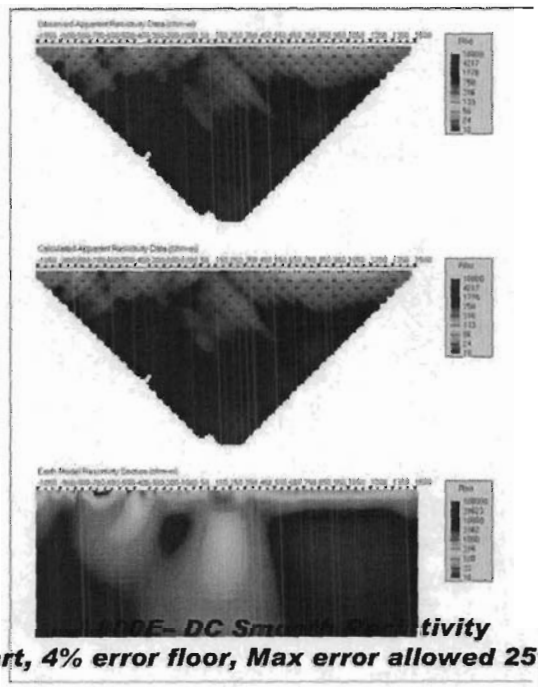

Figure 59: Line 800E – UBC 2D Smooth DC Inversion Results.

IP Chargeability

The observed and calculated IP Phase pseudosections and the final 2D sharp body IP Chargeability inversion, for Line 800E, are shown in Figure 60. The corresponding 2D smooth body inversion results are shown in Figure 61. The good to excellent quality of the data and the model fits are clearly evident.

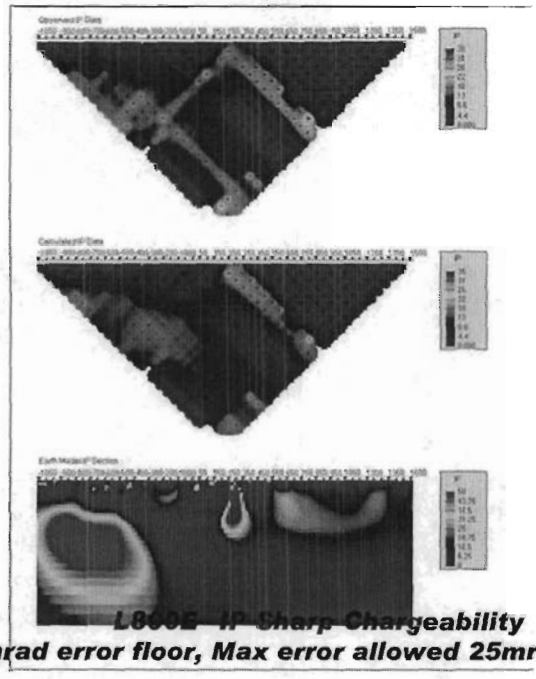

Figure 60: Line 800E – UBC 2D Sharp model IP Inversion results.

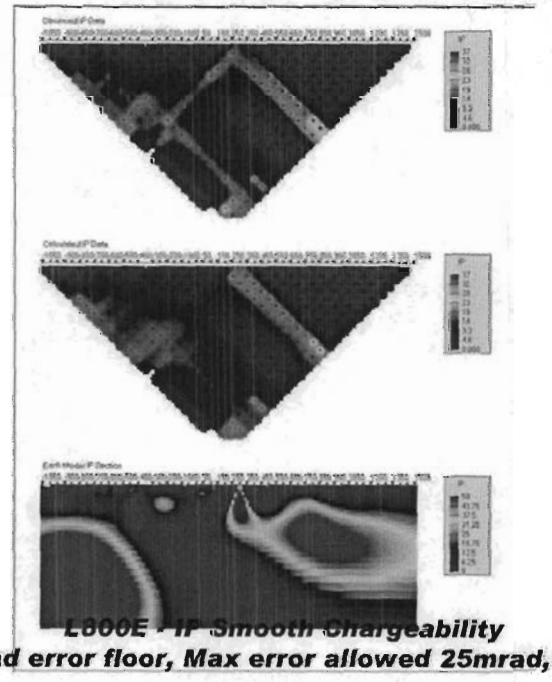

Figure 61: Line 800E – UBC 2D Smooth model IP Inversion results.

MT Resistivity

The raw (measured) MT frequency pseudosections for Line 800E are presented in – shown Figure 62 from top to bottom: a) the In-line (XY) apparent resistivity, b) In-line (XY) phase, c) Cross-line (YX) apparent resistivity and d) Cross-line (YX) phase. The corresponding EVA processed Along-strike (TE) and Across-strike (TE) MT pseudosections are shown in Figure 63. The excellent data quality is clearly evident.

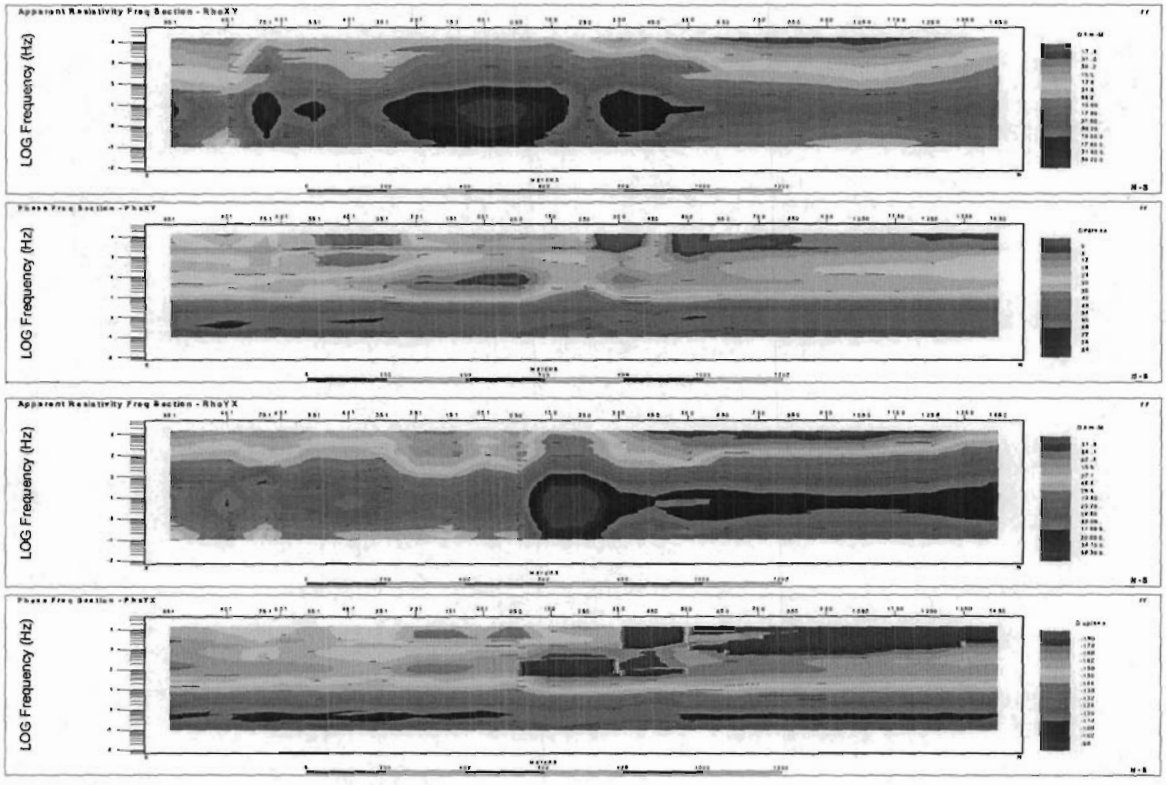

Figure 62: L800E - Raw MT Apparent Resistivity and Phase Frequency Pseudosections.

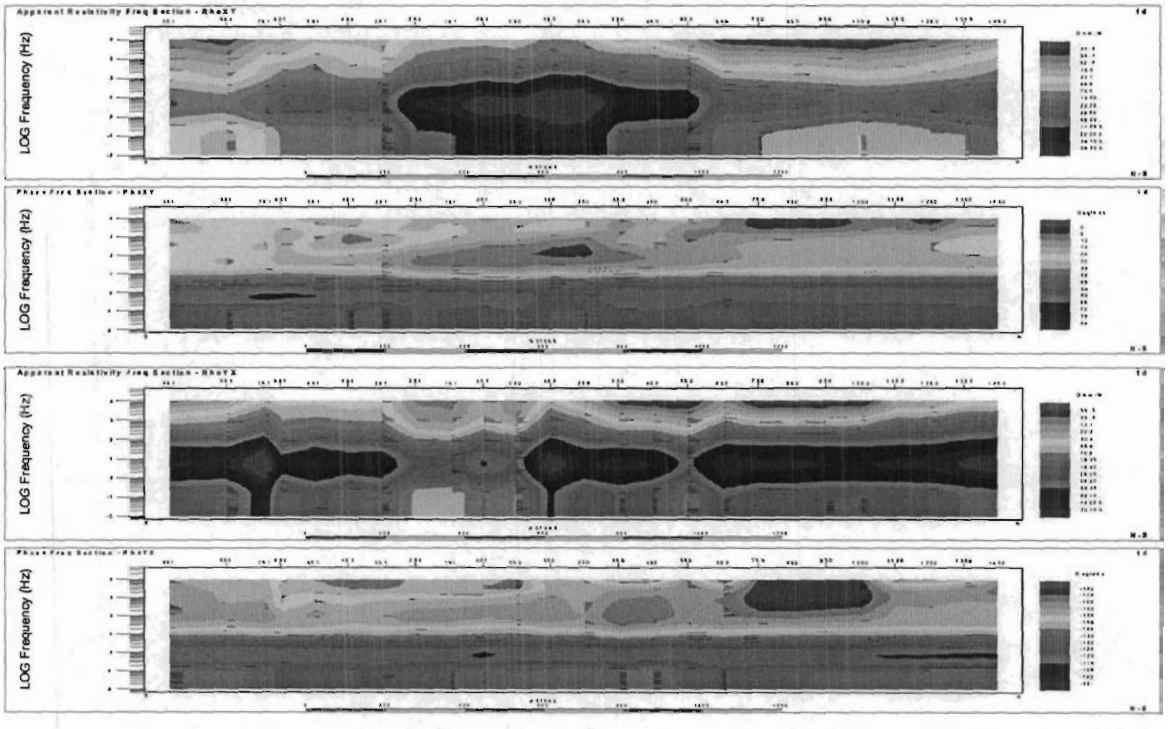

Figure 63: L800E - EVA-processed MT Apparent Resistivity and Phase Frequency Pseudosections

The 2D smooth-conjugate RLM MT resistivity inversion results for Line 800E are shown in Figure 64 and the corresponding 2D Gauss-Newton PW MT resistivity inversion results are shown in Figure 65. Relatively good (~8% rms) model-convergences were obtained.

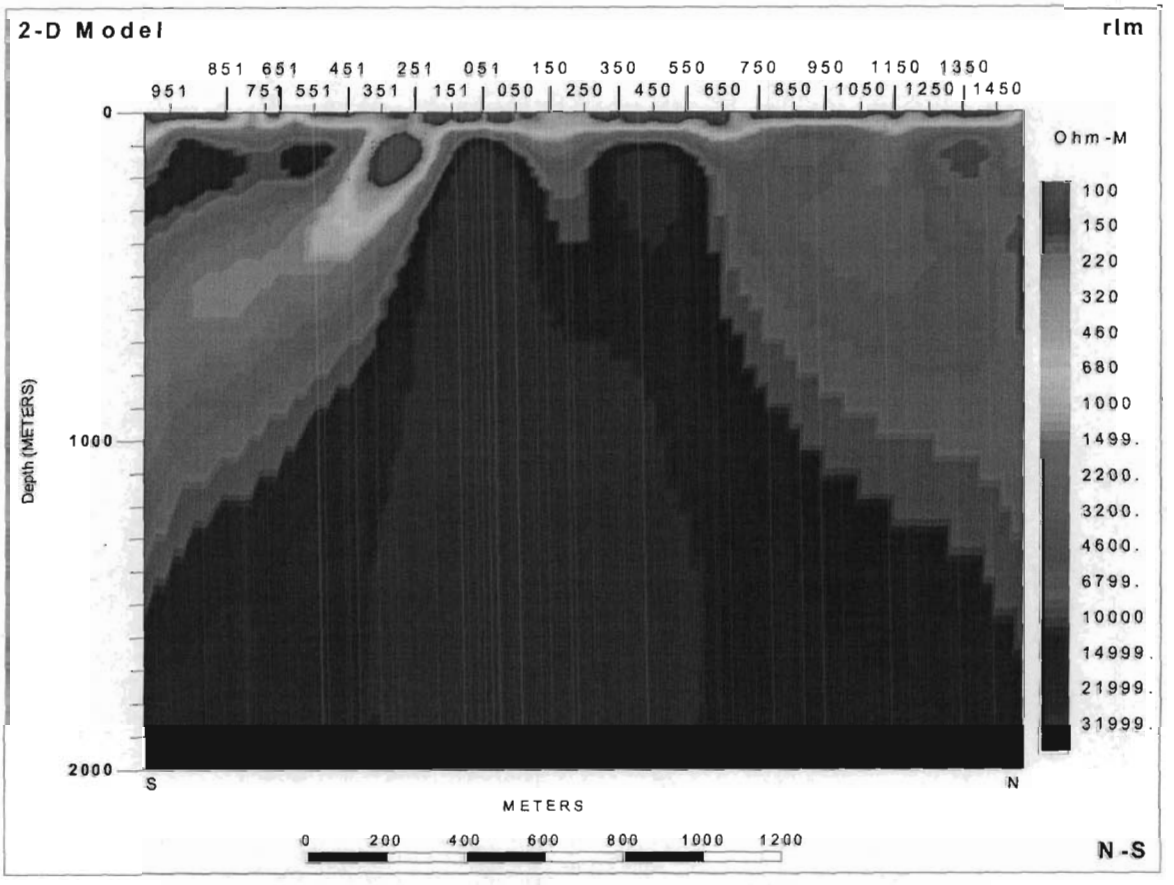

Figure 64: L800E - 2D RLM Smooth-Conjugate MT Resistivity Inversion.

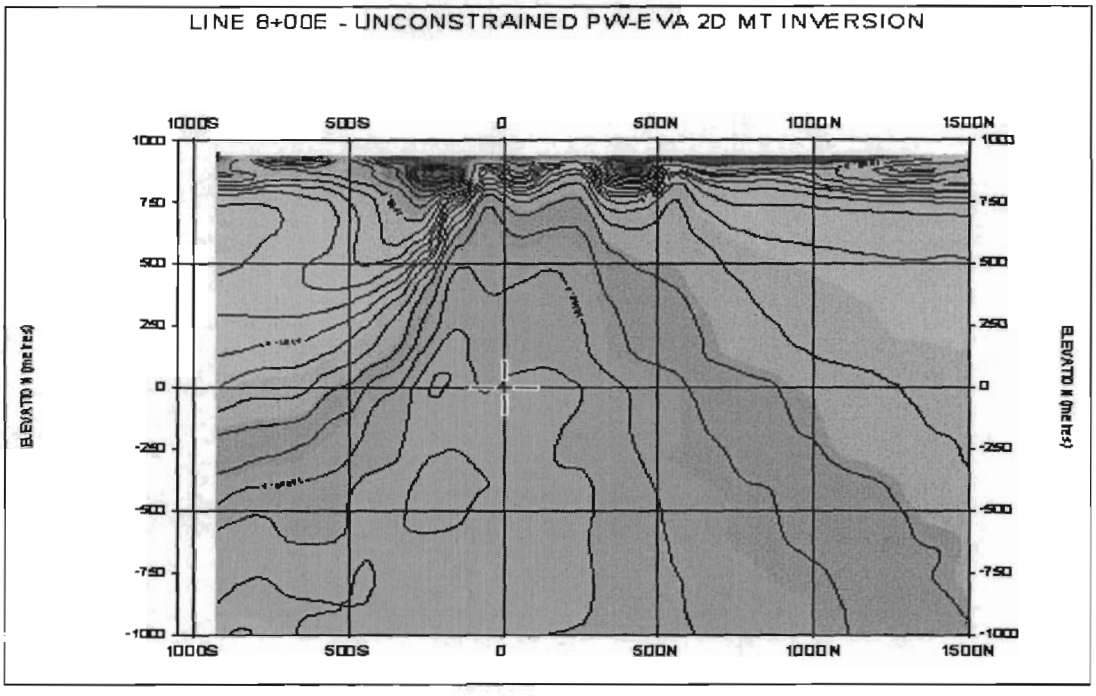

Figure 65: L800E - 2D PW Gauss Newton MT Resistivity Inversion.

Discussion of Results

This line shows a good correlation of resistivities derived from DC, PW and RLM of MT. There are low resistivity features at 250S and 450N and high resistivity in between. Comparing the two IP inversions concludes that there are two chargeable anomalies in close proximity to resistivity contacts. The top of the northern anomaly is close to the surface and the top of the southern anomaly is about 250 m.

LINE 10+00 E

DC Resistivity

The observed and calculated DC Apparent Resistivity pseudosections and the final 2D smooth body DC Resistivity inversion, for Line 1000E, are shown in Figure 66. The excellent quality of the data and the model fits are clearly evident.

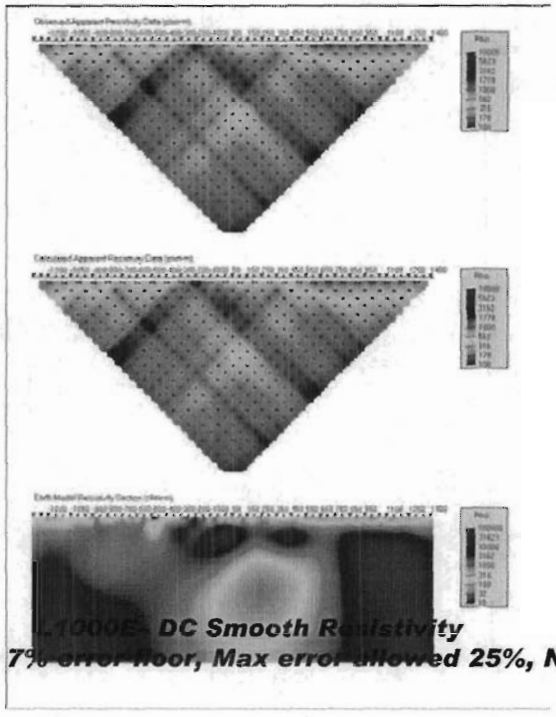

Figure 66: Line 1000E – UBC 2D Smooth DC Inversion Results.

IP Chargeability

The observed and calculated IP Phase pseudosections and the final 2D sharp body IP Chargeability inversion, for Line 1000E, are shown in Figure 67. The corresponding 2D smooth body inversion results are shown in Figure 68. The good to excellent quality of the data and the model fits are clearly evident.

Comparing the two proceeding IP inversions leads to the impression that there are three IP anomalies with the major one sits on the southern side of the MT resistivity contact.

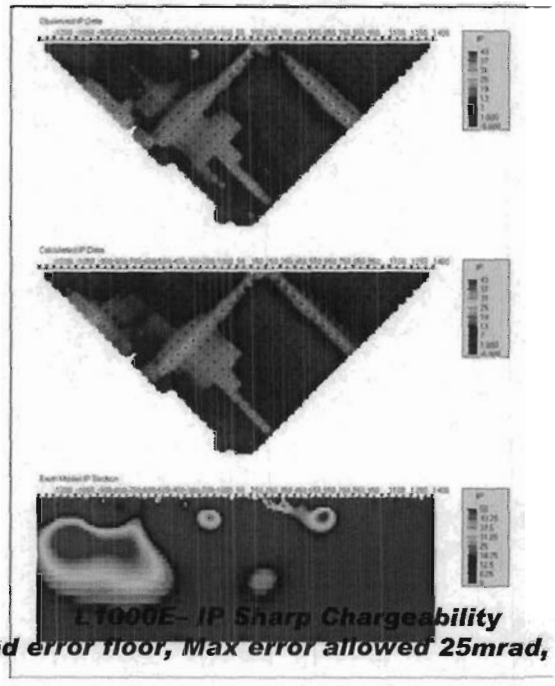

Figure 67: Line 1000E – UBC 2D Sharp model IP Inversion results.

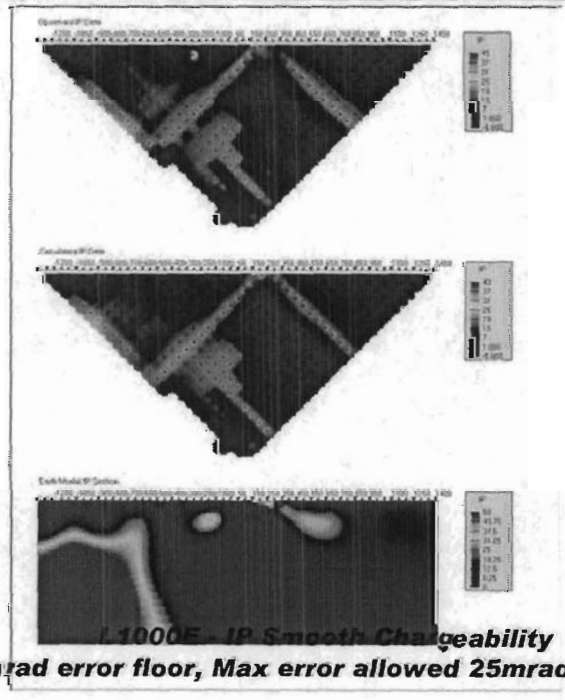

Figure 68: Line 1000E – UBC 2D Smooth model IP Inversion results.

MT Resistivity

The raw (measured) MT frequency pseudosections for Line 1000E are presented in – shown Figure 62 from top to bottom: a) the In-line (XY) apparent resistivity, b) In-line (XY) phase, c) Cross-line (YX) apparent resistivity and d) Cross-line (YX) phase. The corresponding EVA processed Along-strike (TE) and Across-strike (TE) MT pseudosections are shown in Figure 63. The excellent data quality is clearly evident.

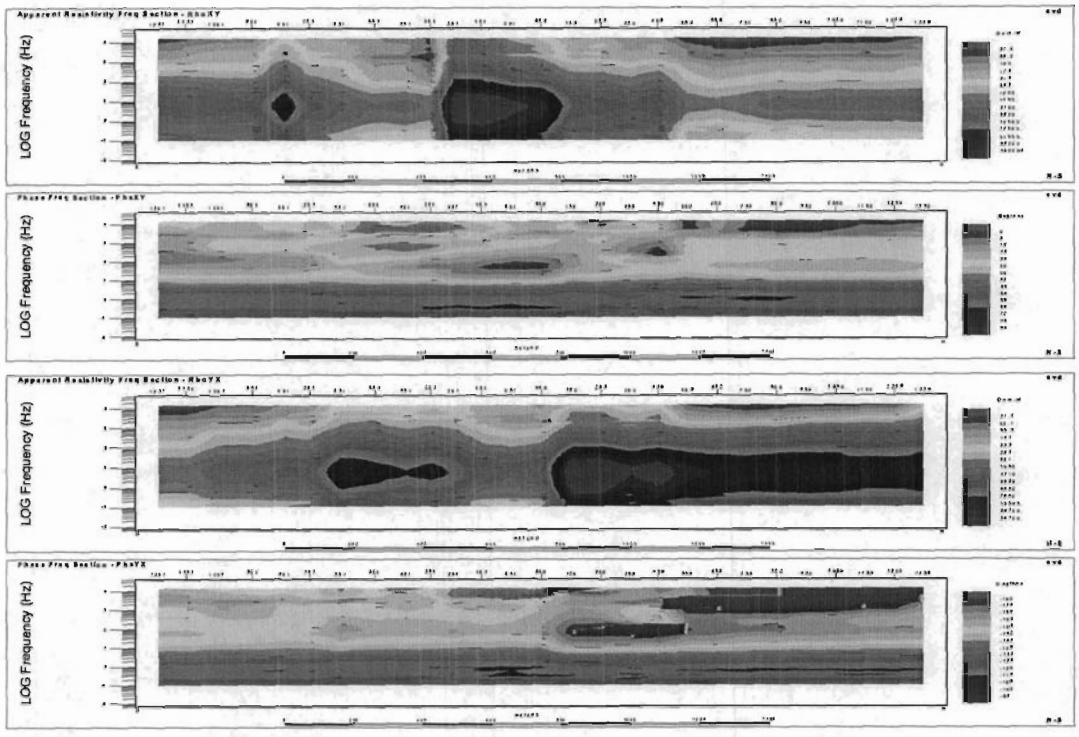

Figure 69: L1000E - Raw MT Apparent Resistivity and Phase Frequency Pseudosections.

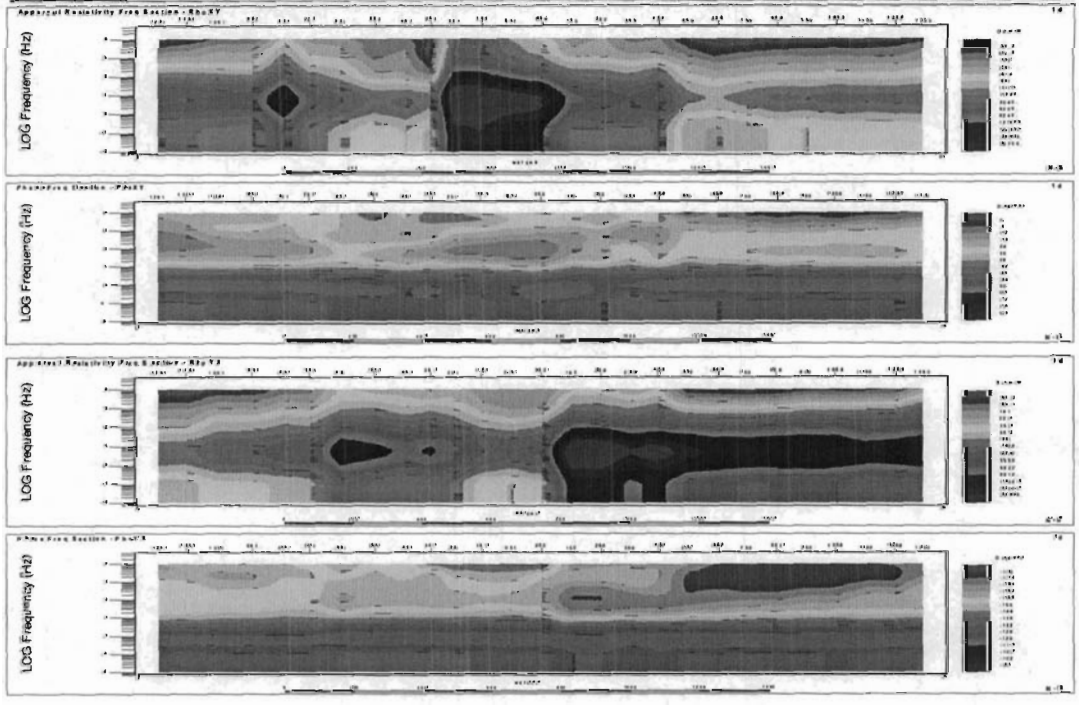

Figure 70: L10E - EVA-processed MT Apparent Resistivity and Phase Frequency Pseudosections

The 2D smooth-conjugate RLM MT resistivity inversion results for Line 1000E are shown in Figure 71 and the corresponding 2D Gauss-Newton PW MT resistivity inversion results are shown in Figure 72. Relatively good (~8% rms) model-convergences were obtained.

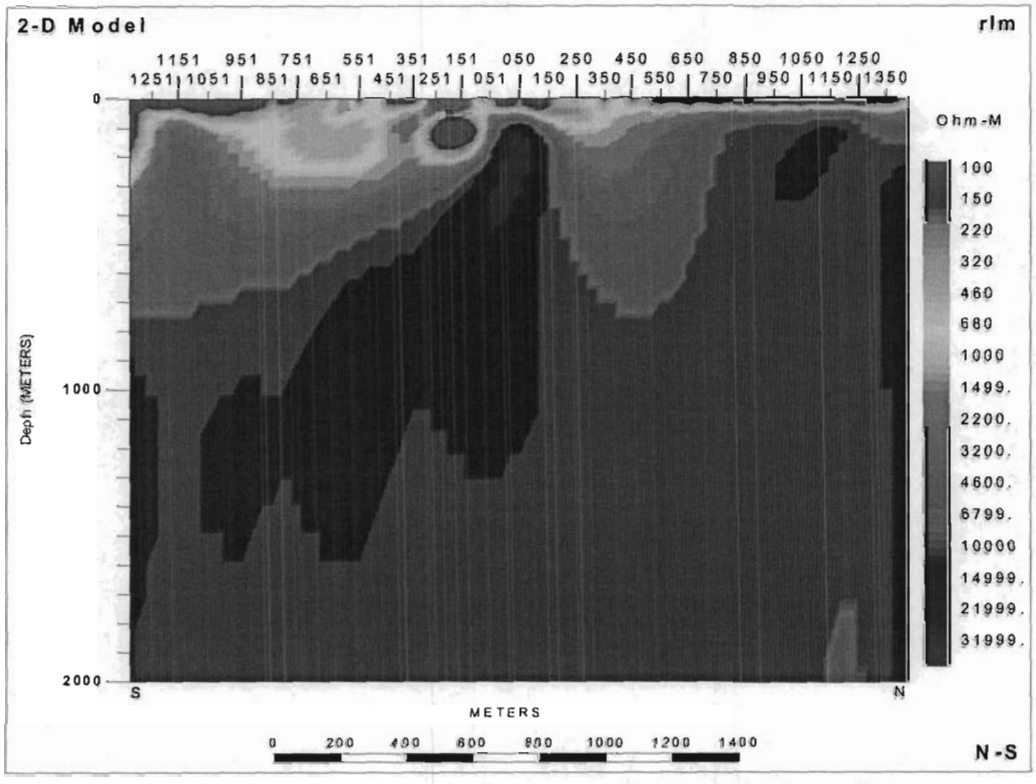

Figure 71: L1000E - 2D RLM Smooth-Conjugate MT Resistivity Inversion.

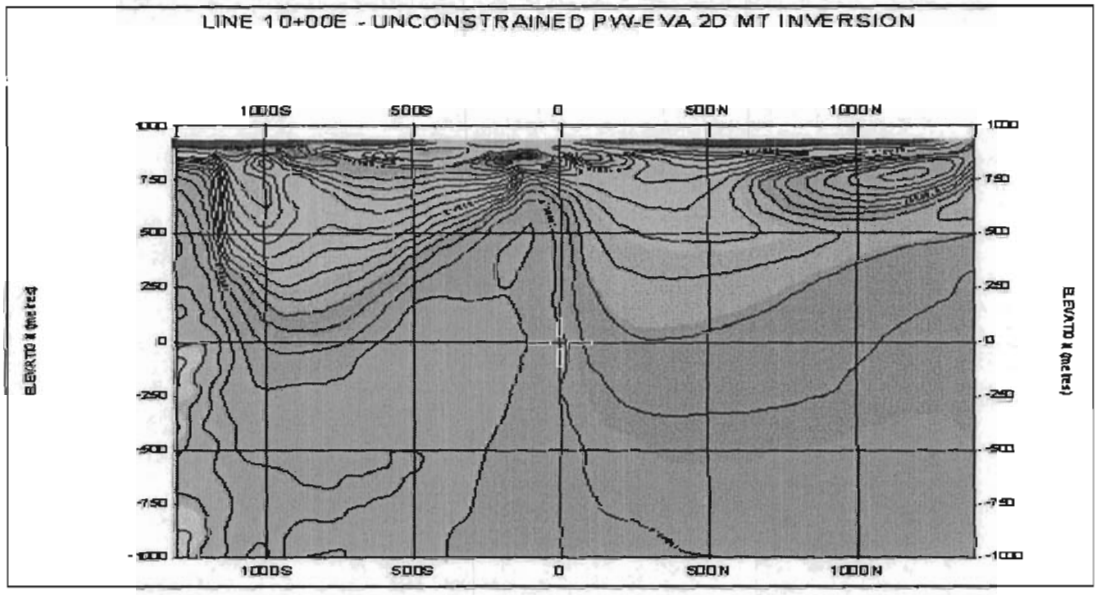

Figure 72: L1000E - 2D PW Gauss Newton MT Resistivity Inversion.

Discussion of Results

The DC model suggests that there is a significant conductive feature underneath 0 – 500N. This anomaly shows up on RLM, but on the PW section, it becomes insignificant. The IP sections show three anomalies with two sit on the resistivity contact clearly defined by the PW model.

LINE 12+00 E

DC Resistivity

The observed and calculated DC Apparent Resistivity pseudosections and the final 2D smooth body DC Resistivity inversion, for Line 1200E, are shown in Figure 73. The good to excellent quality of the data and the model fits are clearly evident.

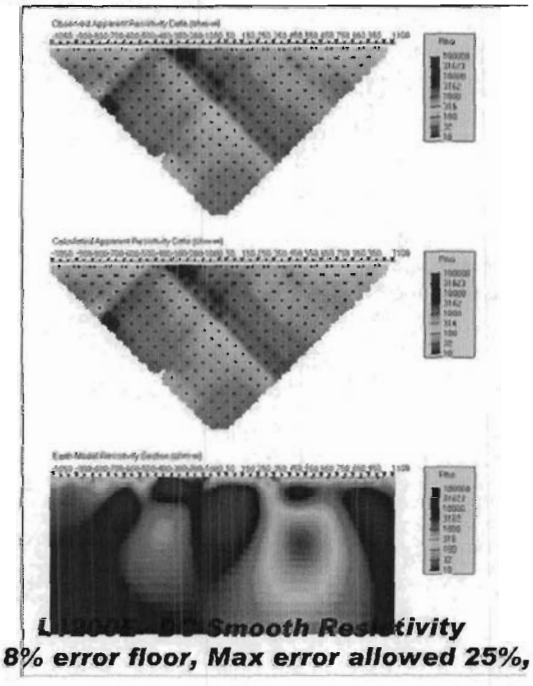

Figure 73: Line 1200E – UBC 2D Smooth DC Inversion Results.

IP Chargeability

The observed and calculated IP Phase pseudosections and the final 2D sharp body IP Chargeability inversion, for Line 1200E, are shown in Figure 74. The corresponding 2D smooth body inversion results are shown in Figure 75. The good to excellent quality of the data and the model fits are clearly evident.

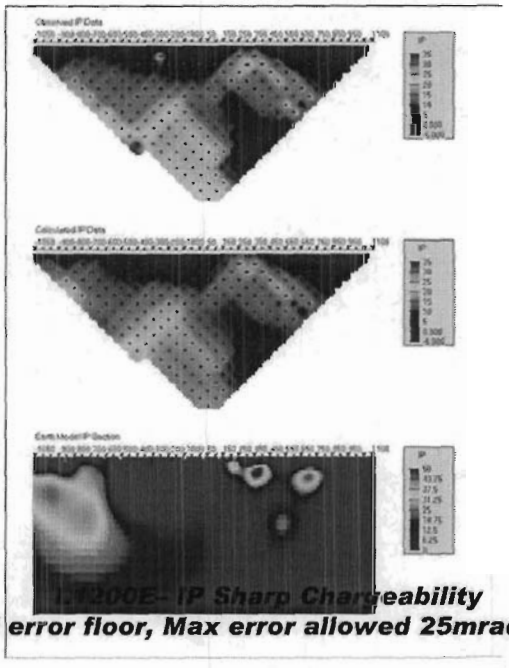

Figure 74: Line 12000E – UBC 2D Sharp model IP Inversion results.

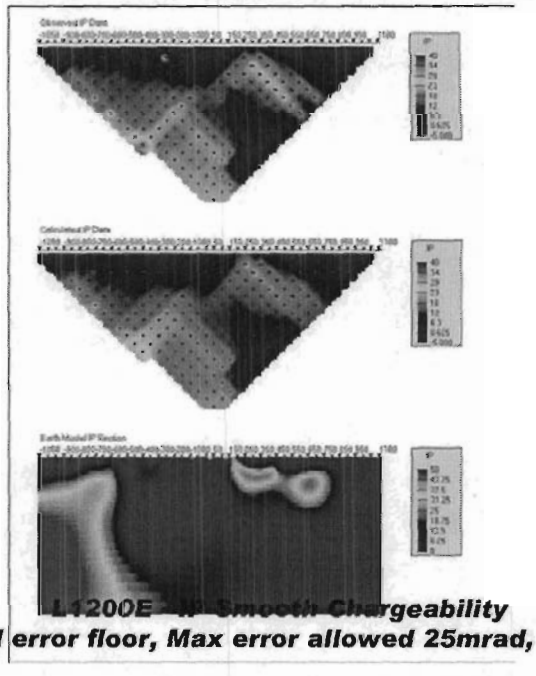

Figure 75: Line 1200E – UBC 2D Smooth model IP Inversion results.

MT Resistivity

The raw (measured) MT frequency pseudosections for Line 1200E are presented in – shown Figure 76 from top to bottom: a) the In-line (XY) apparent resistivity, b) In-line (XY) phase, c) Cross-line (YX) apparent resistivity and d) Cross-line (YX) phase. The corresponding EVA processed Along-strike (TE) and Across-strike (TE) MT pseudosections are shown in Figure 77. The excellent data quality is clearly evident.

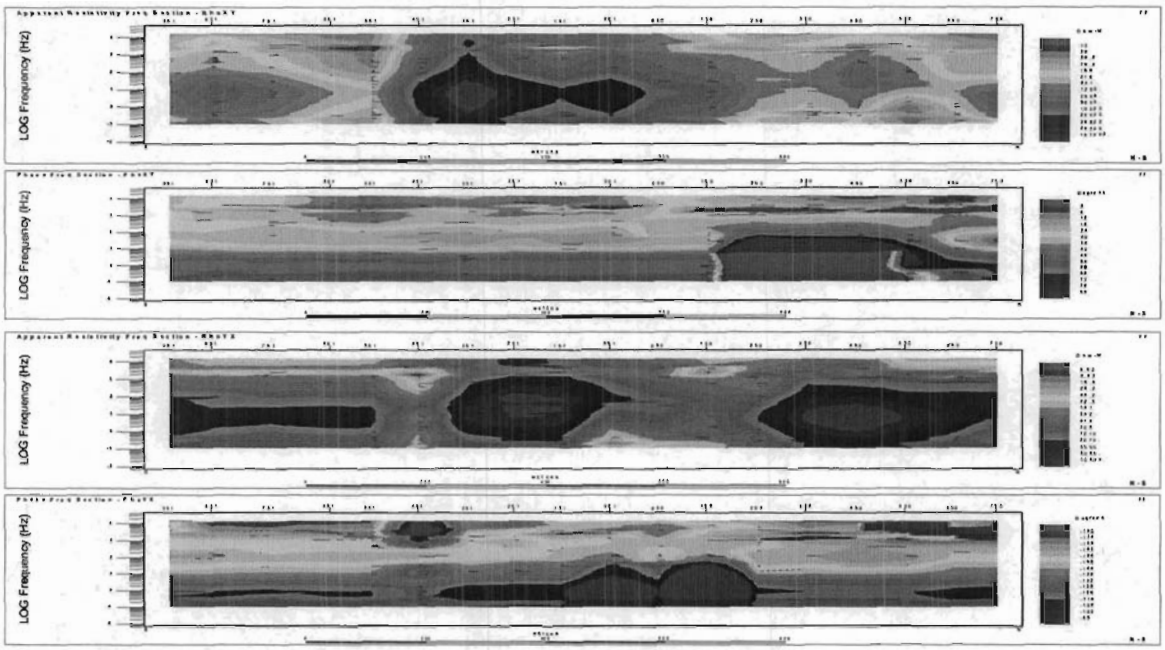

Figure 76: L1200E - Raw MT Apparent Resistivity and Phase Frequency Pseudosections.

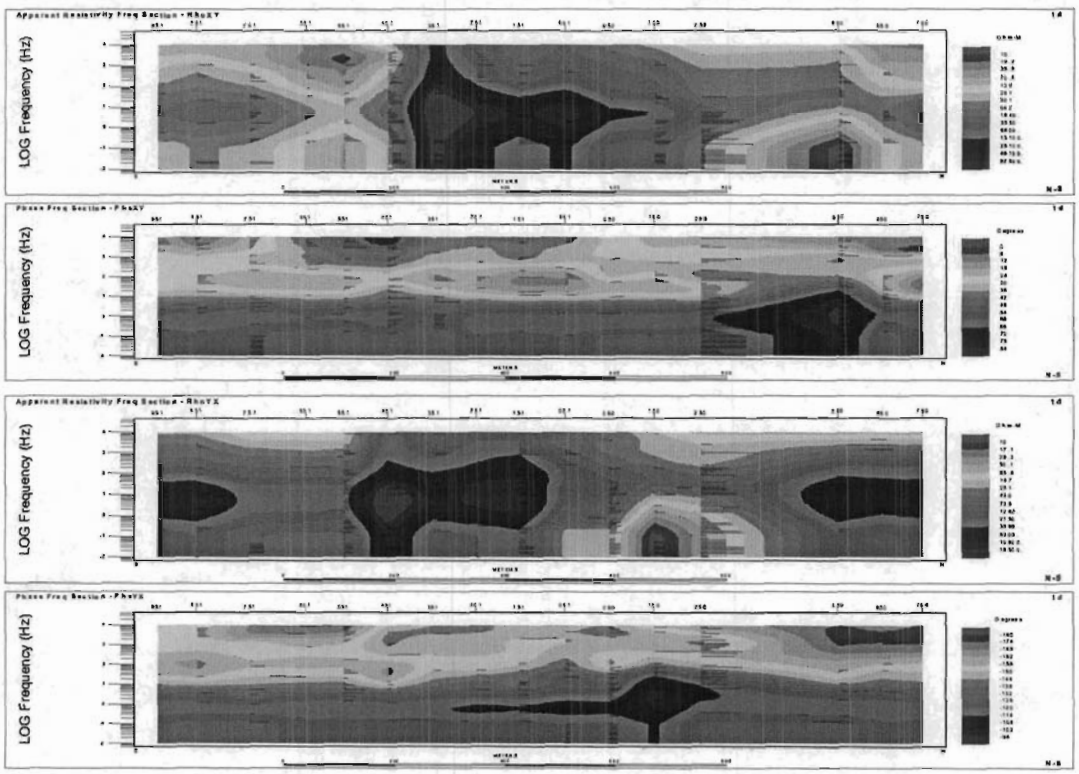

Figure 77: L12E - EVA-processed MT Apparent Resistivity and Phase Frequency Pseudosections

The 2D smooth-conjugate RLM MT resistivity inversion results for Line 1200E are shown in Figure 71 and the corresponding 2D Gauss-Newton PW MT resistivity inversion results are shown in Figure 72. Relatively good (~8% rms) model-convergences were obtained.

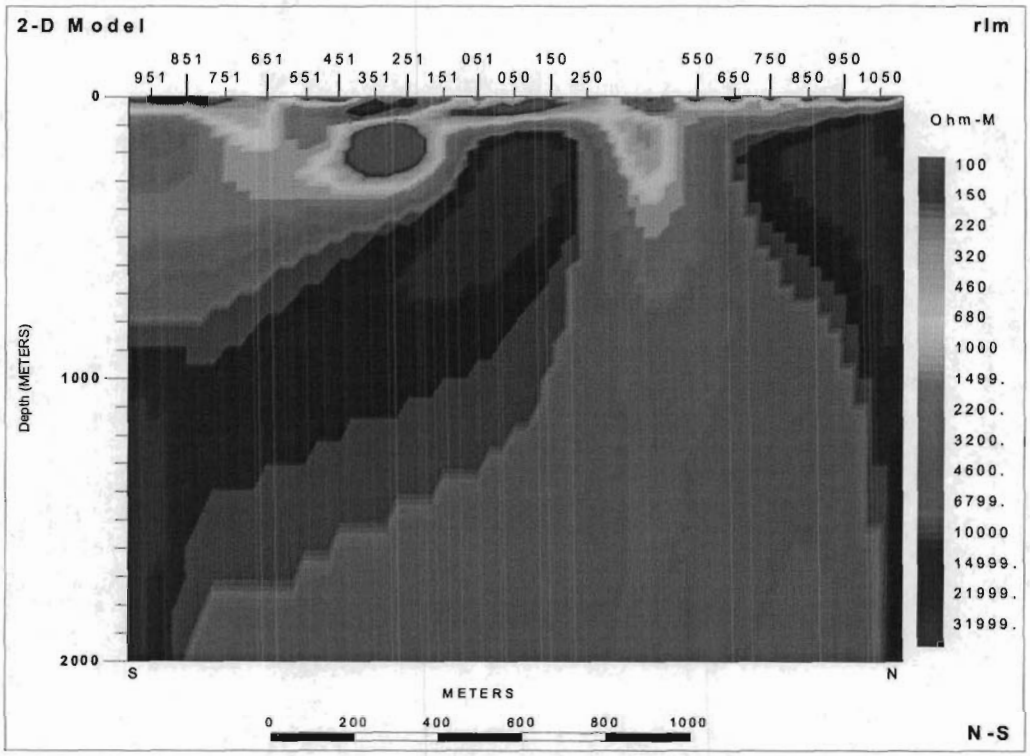

Figure 78: L1200E - 2D RLM Smooth-Conjugate MT Resistivity Inversion.

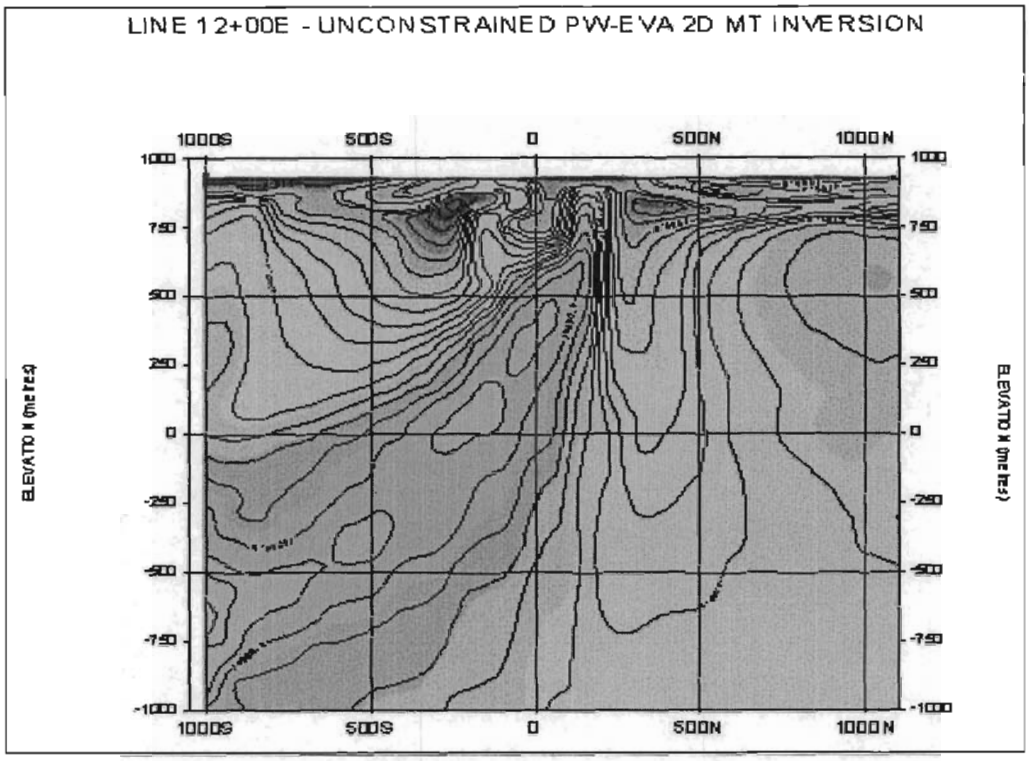

Figure 79: L1200E - 2D PW Gauss Newton MT Resistivity Inversion.

Discussion of Results

The RLM model clearly defines the two contacts at 400S and 250N. On the north side of 250N, there is a low resistive feature showing up in DC, RLM and PW. The PW and DC model didn't define the southern contact clearly. There are IP anomalies associated with contacts and northern low resistivity feature.

LINE 14+00 E

DC Resistivity

The observed and calculated DC Apparent Resistivity pseudosections and the final 2D smooth body DC Resistivity inversion, for Line 1400E, are shown in Figure 80. The excellent quality of the data and the model fits are clearly evident.

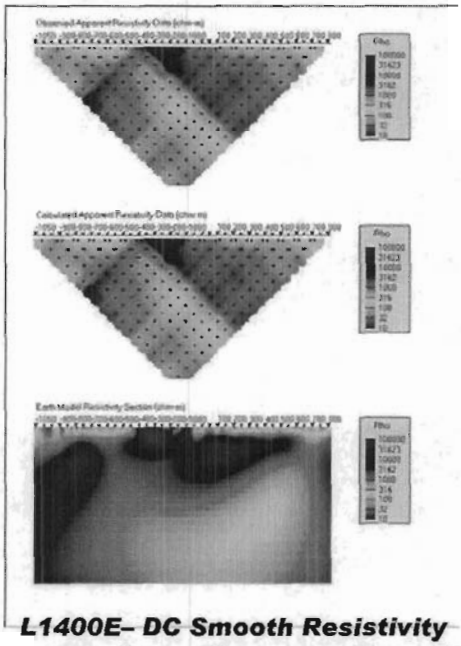

Observed

Calculated

2D Res

L1400E– DC Smooth Resistivity
(10k start, 3% error floor, Max error allowed 25%, 5x Cull)

Figure 80: Line 1400E – UBC 2D Smooth DC Inversion Results.

IP Chargeability

The observed and calculated IP Phase pseudosections and the final 2D sharp body IP Chargeability inversion, for Line 1400E, are shown in Figure 81. The corresponding 2D smooth body inversion results are shown in Figure 82. The good to excellent quality of the data and the model fits are clearly evident.

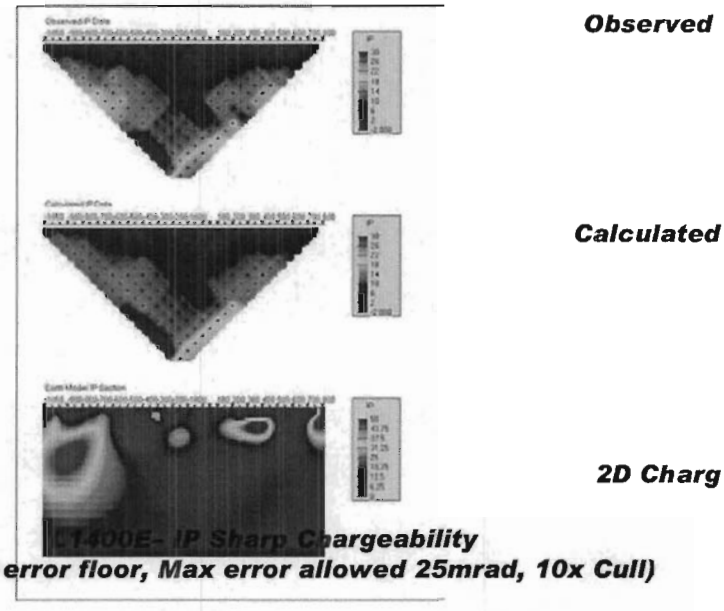

Figure 81: Line 1400E – UBC 2D Sharp model IP Inversion results.

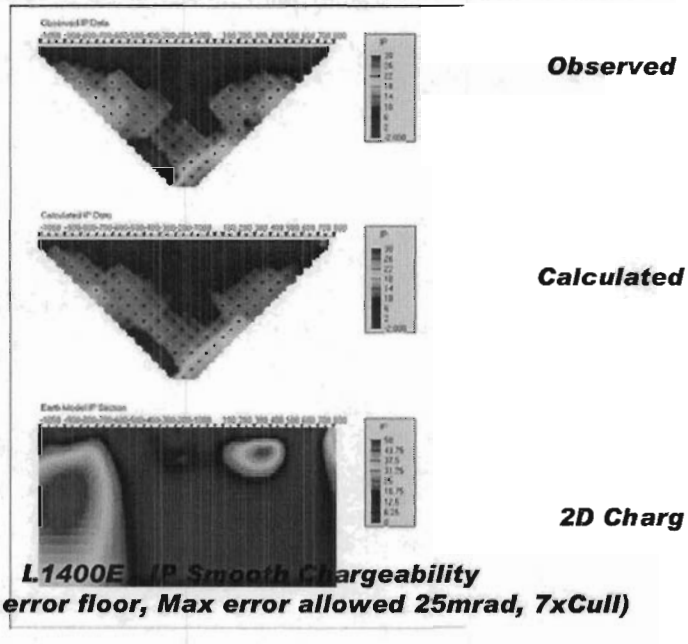

Figure 82: Line 1400E – UBC 2D Smooth model IP Inversion results.

MT Resistivity

The raw (measured) MT frequency pseudosections for Line 1400E are presented in Figure 83 – shown from top to bottom: a) the In-line (XY) apparent resistivity, b) In-line (XY) phase, c) Cross-line (YX) apparent resistivity and d) Cross-line (YX) phase. The corresponding EVA processed Along-strike (TE) and Across-strike (TE) MT pseudosections are shown in Figure 84. The excellent data quality is clearly evident.

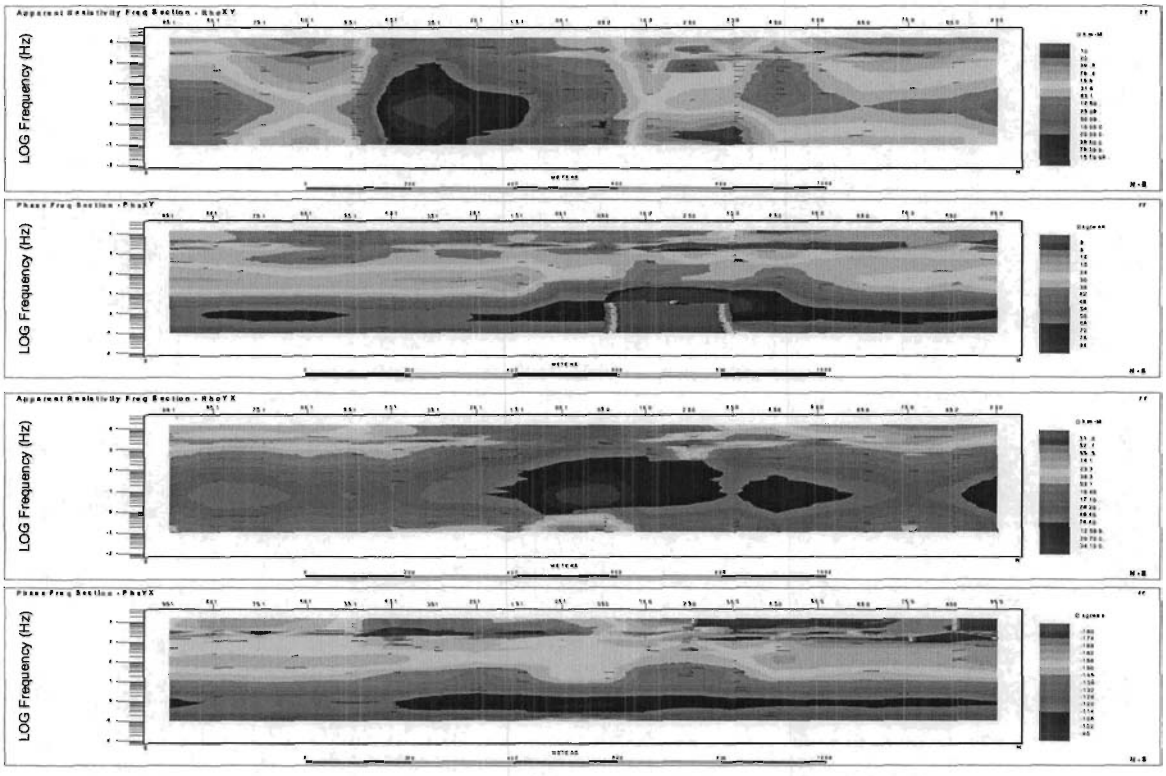

Figure 83: L1400E - Raw MT Apparent Resistivity and Phase Frequency Pseudosections.

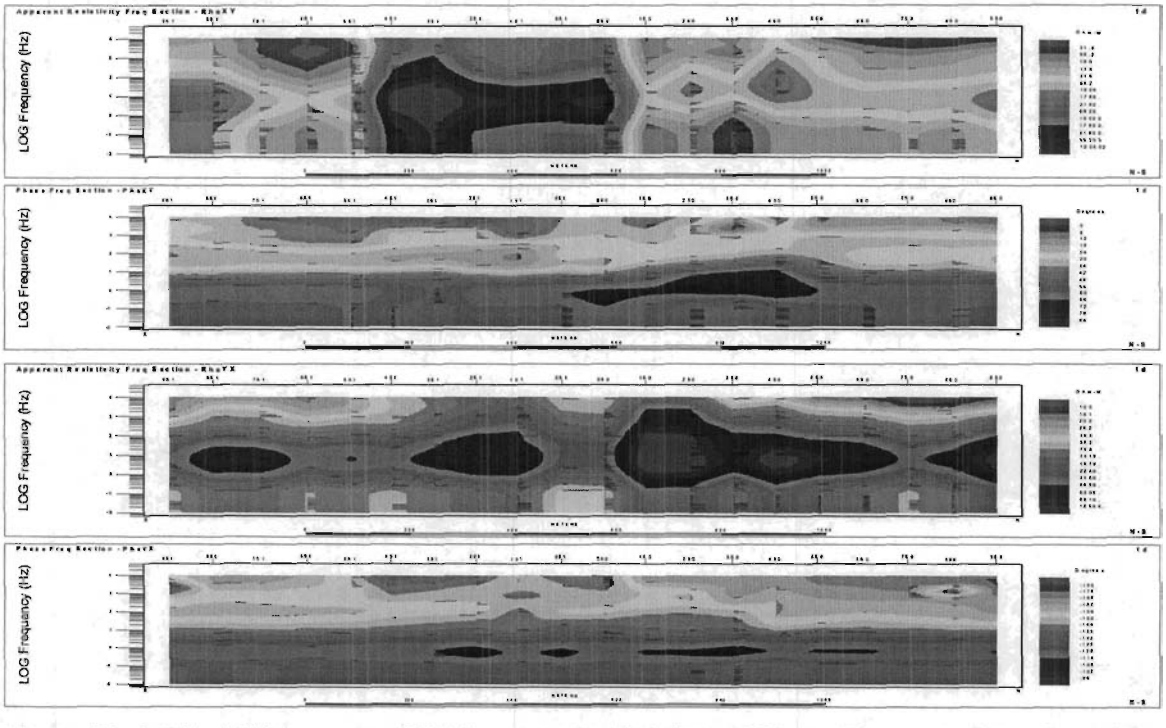

Figure 84: L14E - EVA-processed MT Apparent Resistivity and Phase Frequency Pseudosections

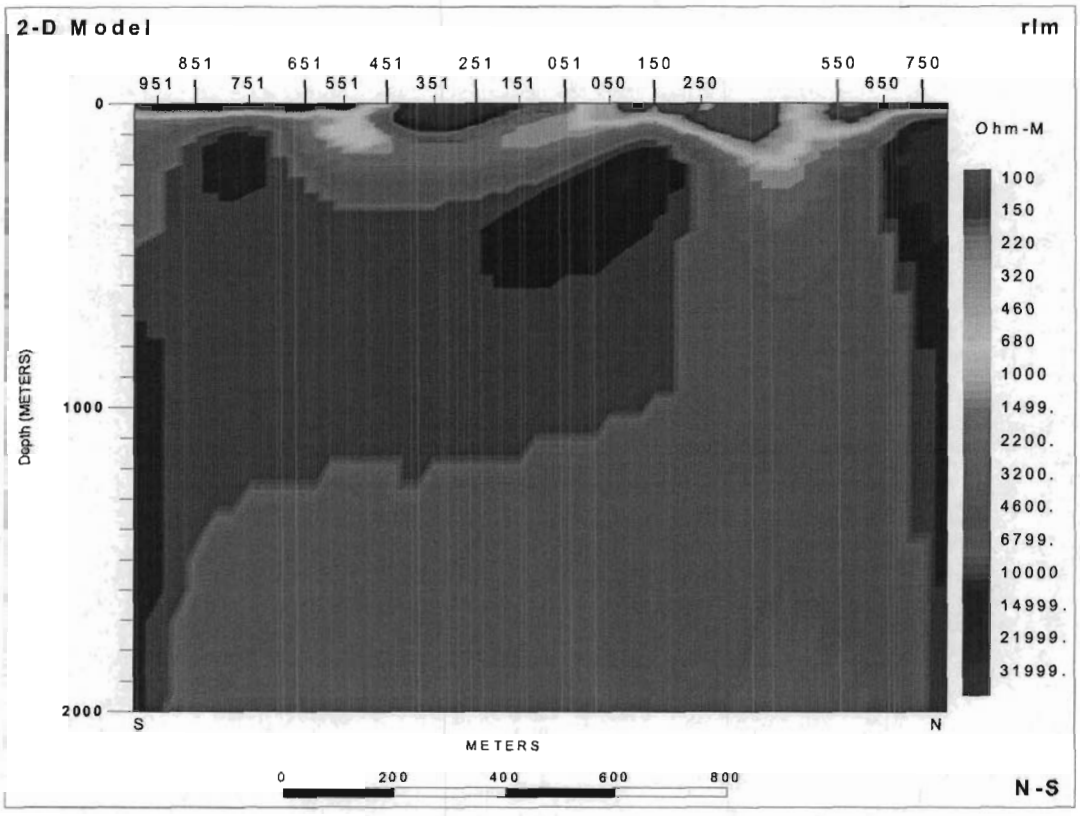

Figure 85: L1400E - 2D RLM Smooth-Conjugate MT Resistivity Inversion.

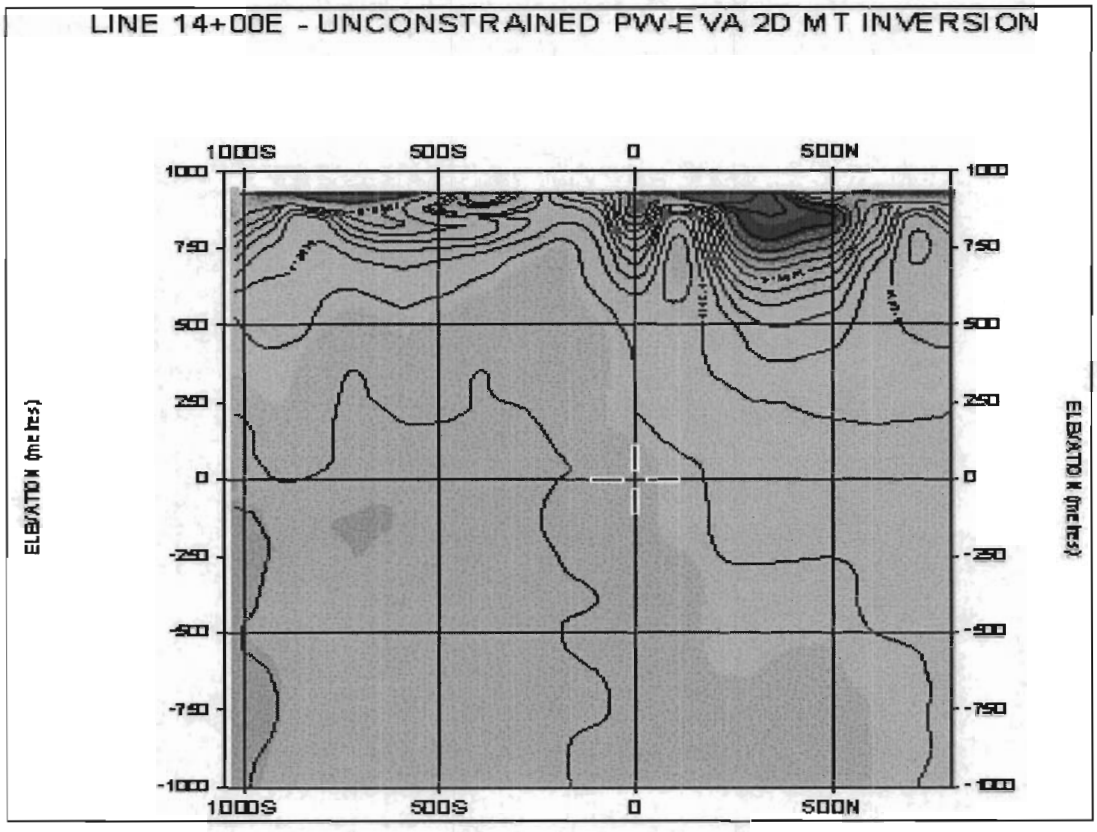

Figure 86: L1400E - 2D PW Gauss Newton MT Resistivity Inversion.

Discussion of Results

The correlation of resistivities derived from RLM and PW is excellent at this line. The south dipping conductive feature on DC at 400N shows up vaguely on RLM and PW. This can well explained by the low resolution of MT compared to DC. The IP shows anomalies on contacts.

LINE 16+00E

DC Resistivity

The observed and calculated DC Apparent Resistivity pseudosections and the final 2D smooth body DC Resistivity inversion, for Line 1600E, are shown in Figure 87. The excellent quality of the data and the model fits are clearly evident.

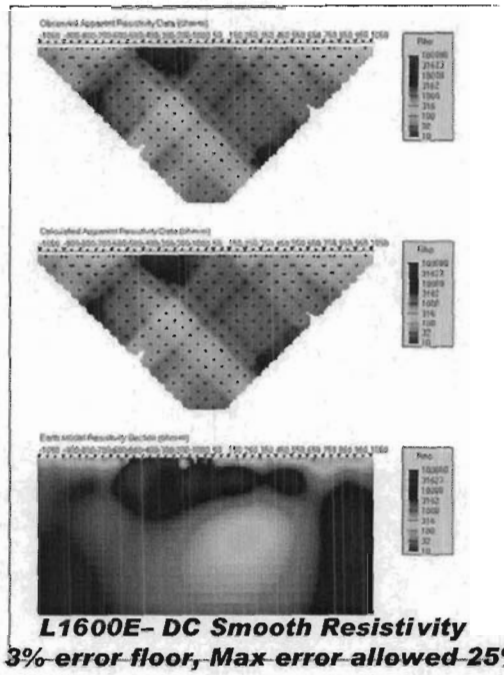

Figure 87: Line 1600E – UBC 2D Smooth DC Inversion Results.

IP Chargeability

The observed and calculated IP Phase pseudosections and the final 2D sharp body IP Chargeability inversion, for Line 1600E, are shown in Figure 88. The corresponding 2D smooth body inversion results are shown in Figure 89. The excellent quality of the data and the model fits are clearly evident.

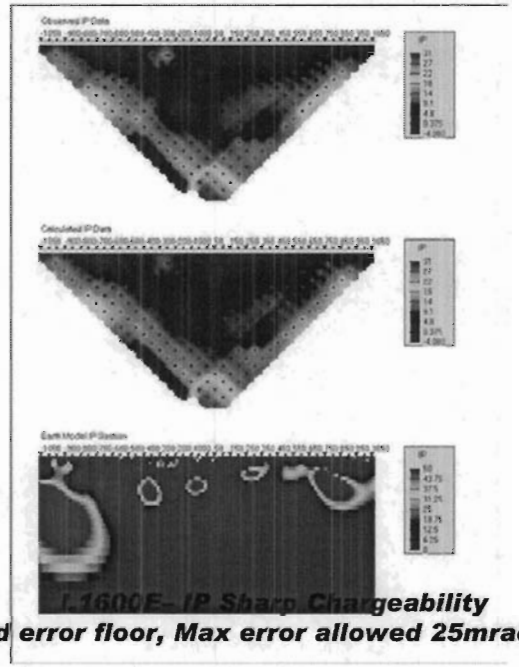

Figure 88: Line 1600E – UBC 2D Sharp model IP Inversion results.

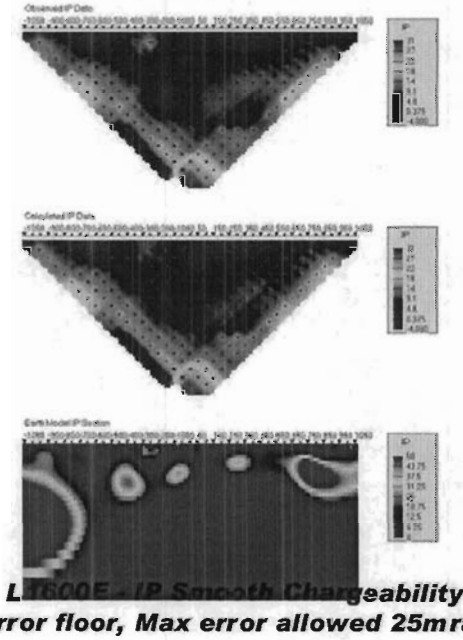

Figure 89: Line 1600E – UBC 2D Smooth model IP Inversion results.

MT Resistivity

The raw (measured) MT frequency pseudosections for Line 1600E are presented in Figure 90 – shown from top to bottom: a) the In-line (XY) apparent resistivity, b) In-line (XY) phase, c) Cross-line (YX) apparent resistivity and d) Cross-line (YX) phase. The corresponding EVA processed Along-strike (TE) and Across-strike (TE) MT pseudosections are shown in Figure 91. The excellent data quality is clearly evident.

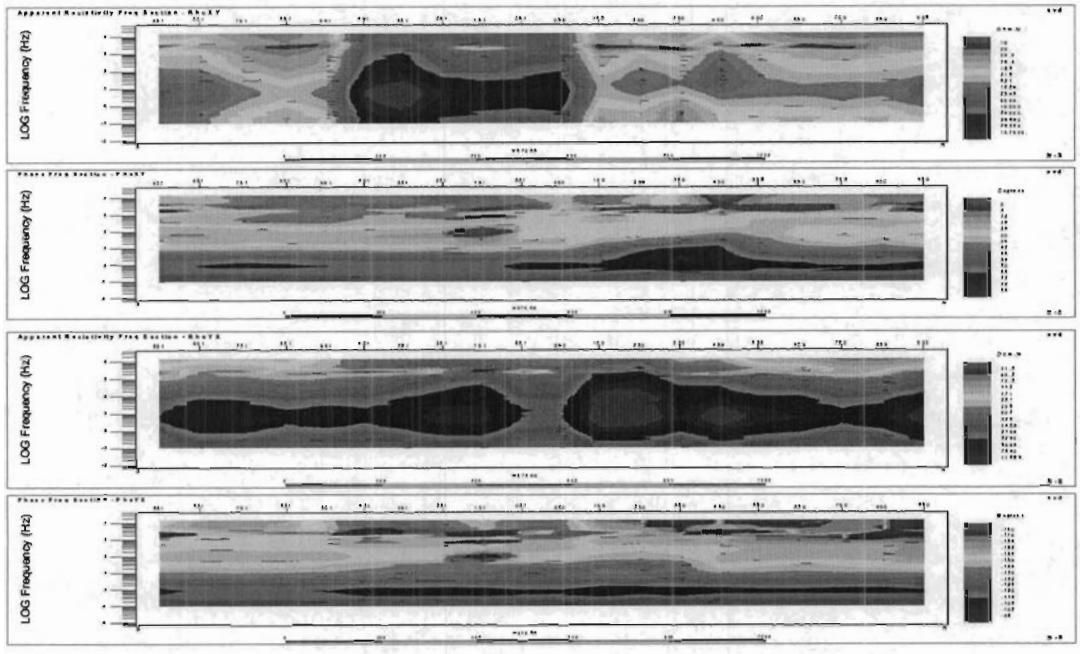

Figure 90: L1600E - Raw MT Apparent Resistivity and Phase Frequency Pseudosections.

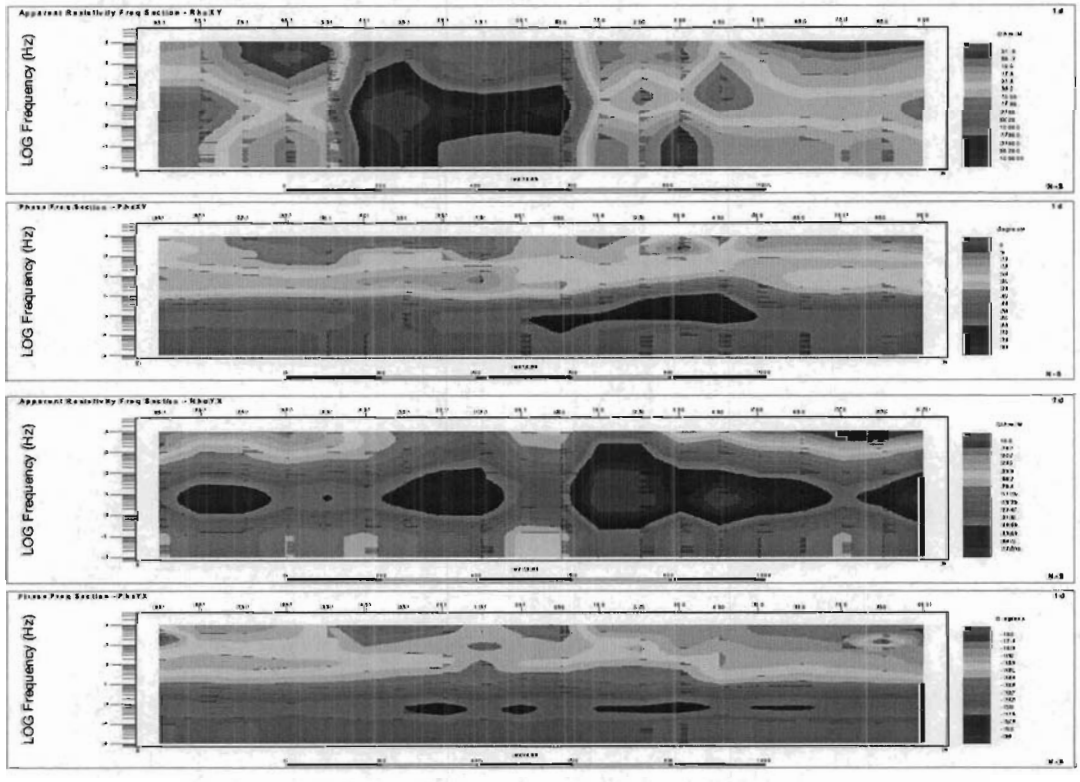

Figure 91: L16E - EVA-processed MT Apparent Resistivity and Phase Frequency Pseudosections

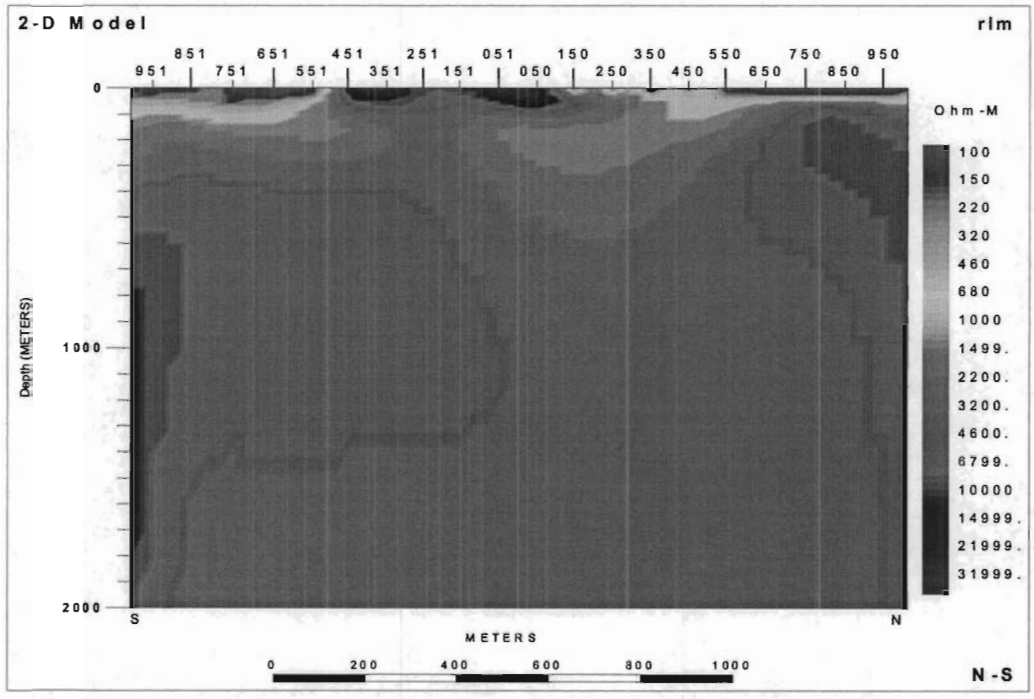

Figure 92: L1600E - 2D RLM Smooth-Conjugate MT Resistivity Inversion.

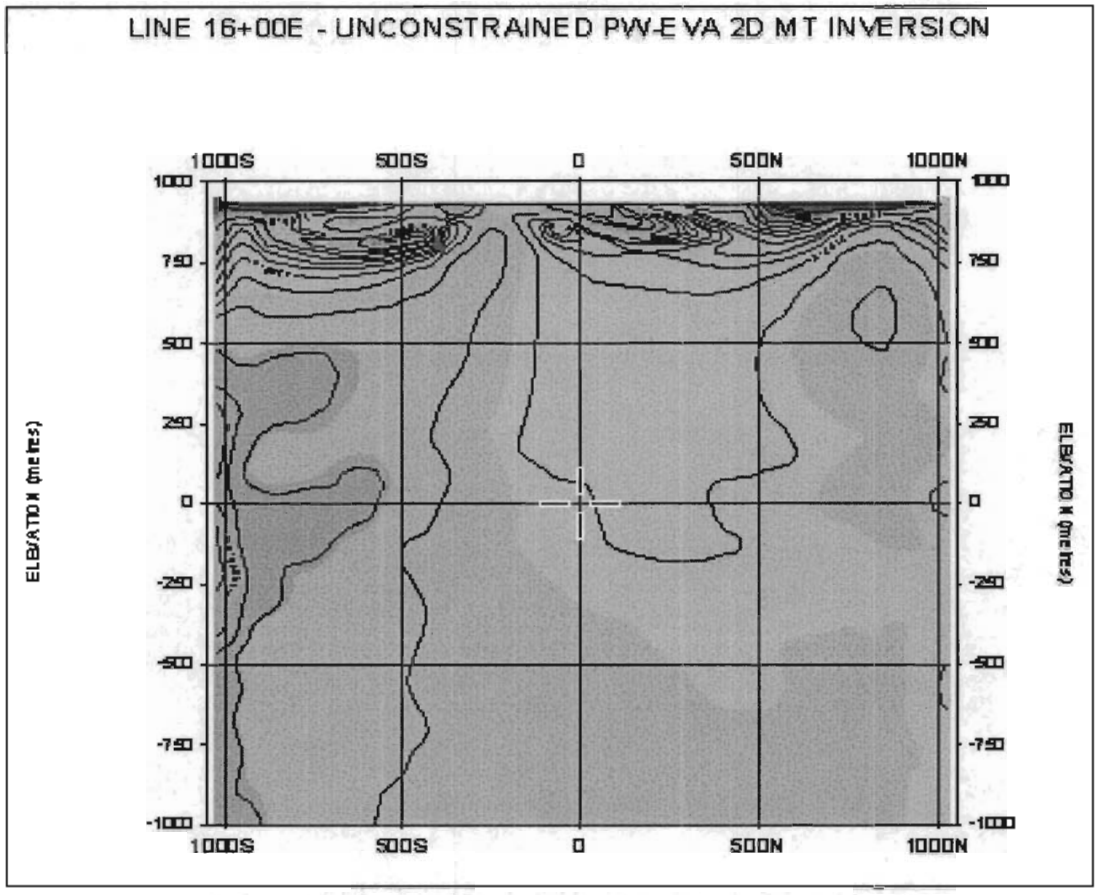

Figure 93: L1600E - 2D PW Gauss Newton MT Resistivity Inversion.

Discussion of Results

The correlation of resistivities derived from RLM and PW is slightly worse than the previous line, but the south dipping conductive feature from DC at 400N shows up better on RLM and PW. The IP shows up anomalies in both conductive and resistive regions.

PLAN VIEW

100m Levels

Depth-level plans of the final 2D sharp model IP chargeability, smooth model DC Resistivity, and PW Gauss-Newton MT inversion results, at 100m depth, are shown in Figure 94.

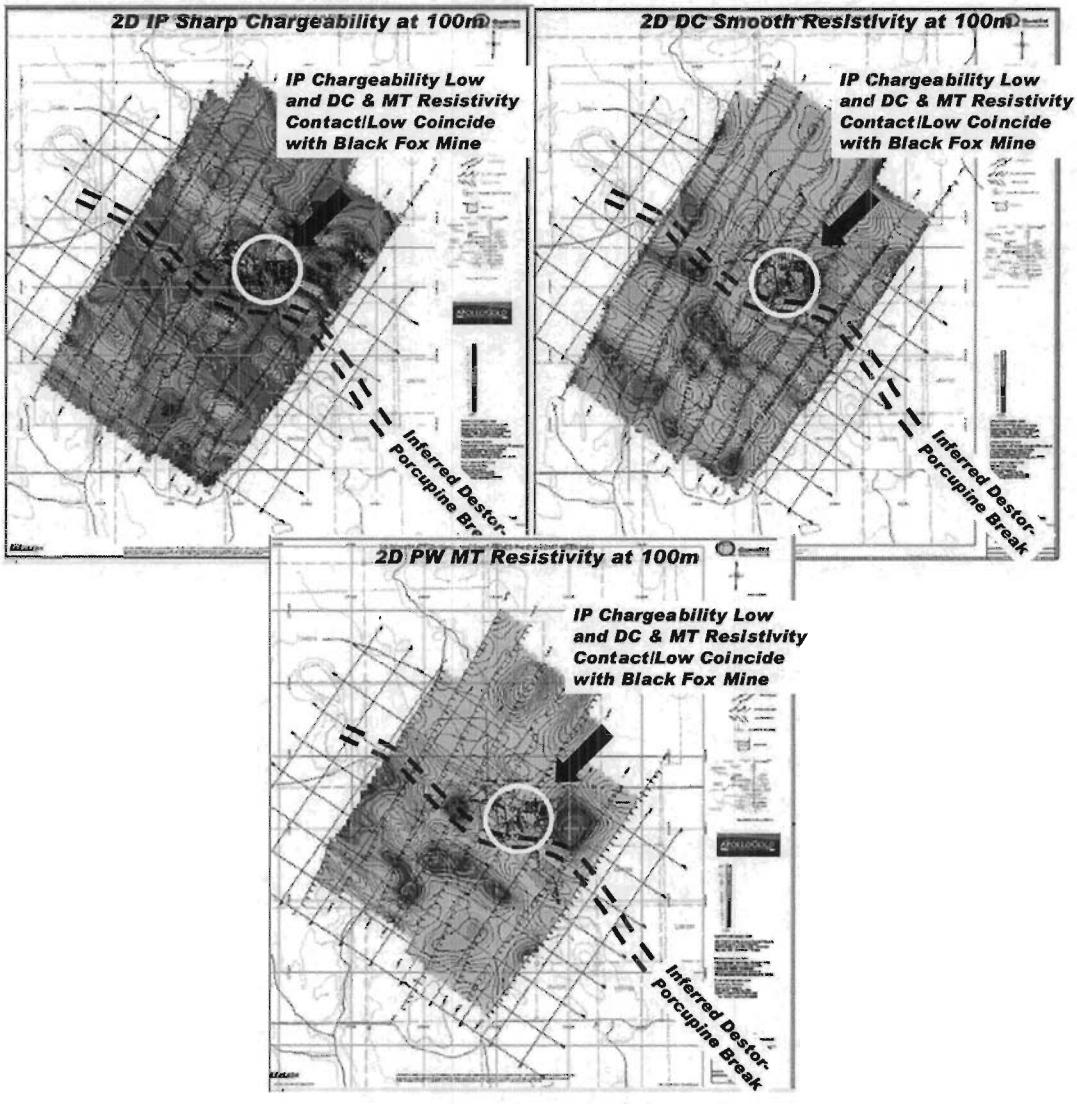

Figure 94: Plan-view Depth Level Plans of Titan 2D Inversion Results, at 100m.

250m Levels

Depth-level plans of the final 2D sharp model IP chargeability, smooth model DC Resistivity, and PW gauss-Newton MT inversion results, at 250m depths, are shown in Figure 95.

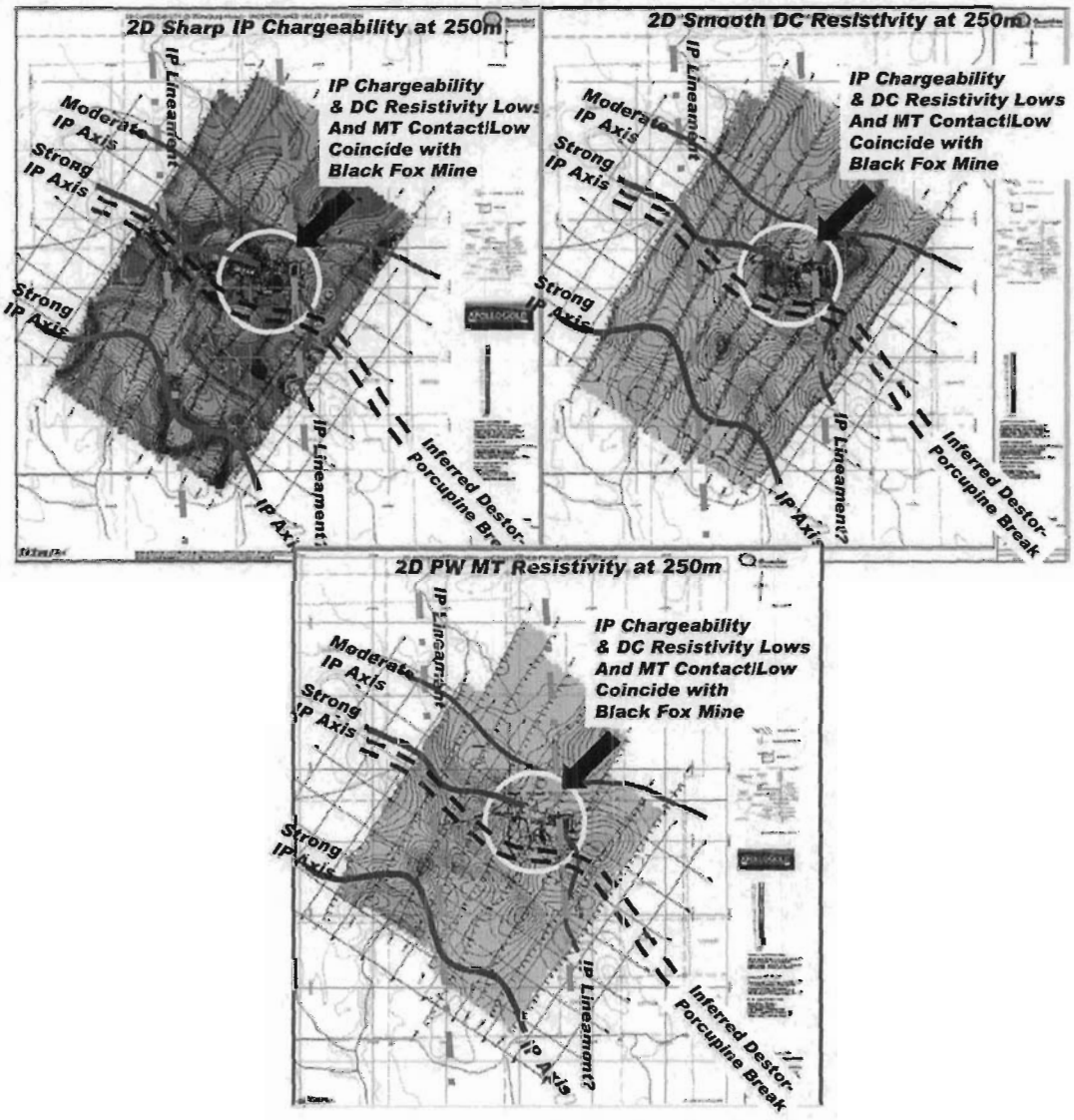

Figure 95: Plan-view Depth Level Plans of Titan 2D Inversion Results, at 250m

500m Levels

Depth-level plans of the final 2D sharp model IP chargeability, smooth model DC Resistivity, and PW gauss-Newton MT inversion results, at 500m depths, are shown in Figure 96.

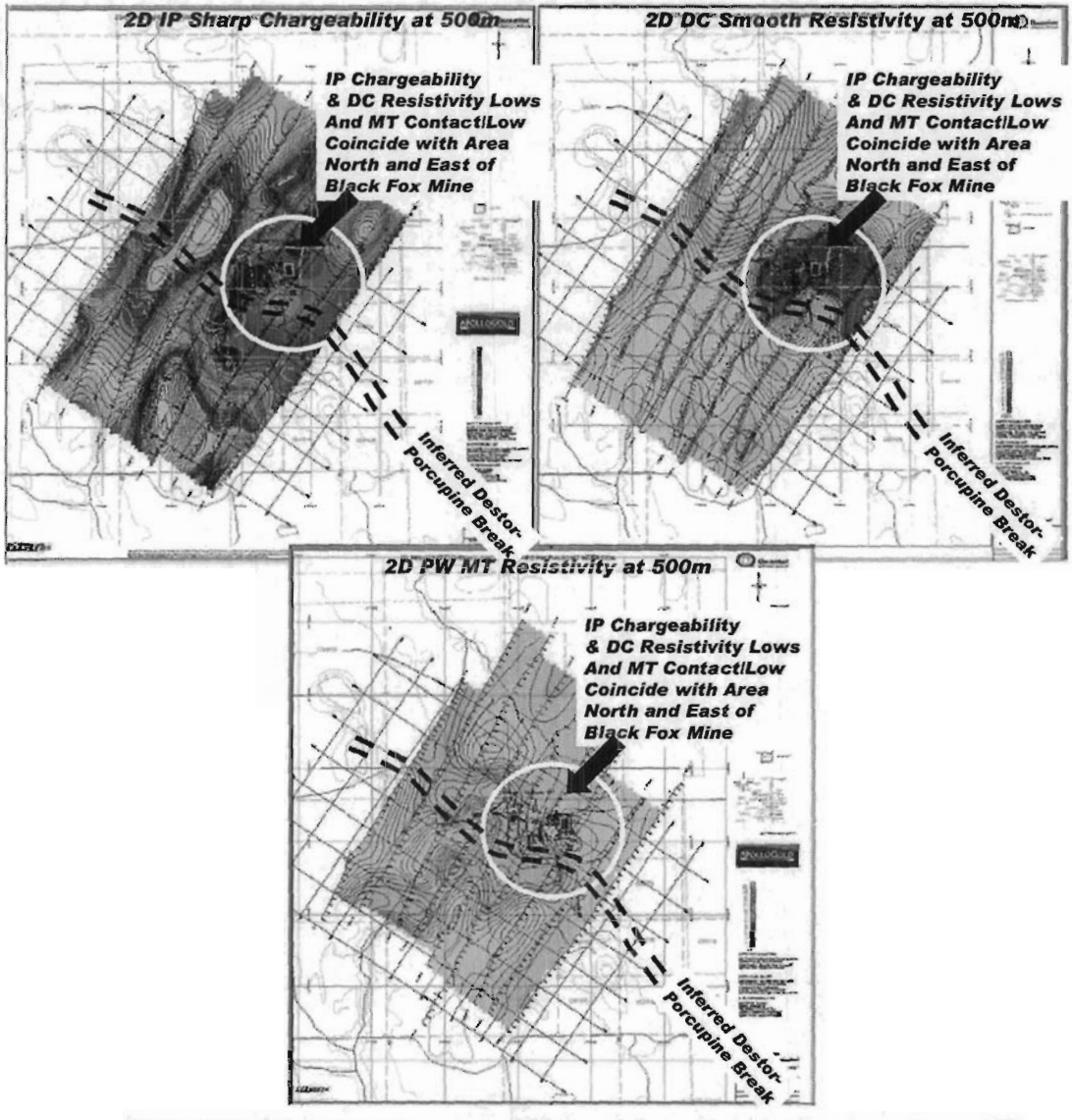

Figure 96: Plan-view Depth Level Plans of Titan 2D Inversion Results, at 500m

1000m Levels

The depth-level plan of the final 2D PW gauss-Newton MT inversion results, at the 1000m depths is shown in Figure 97. The corresponding sharp IP and smooth DC resistivity levels are not presented.

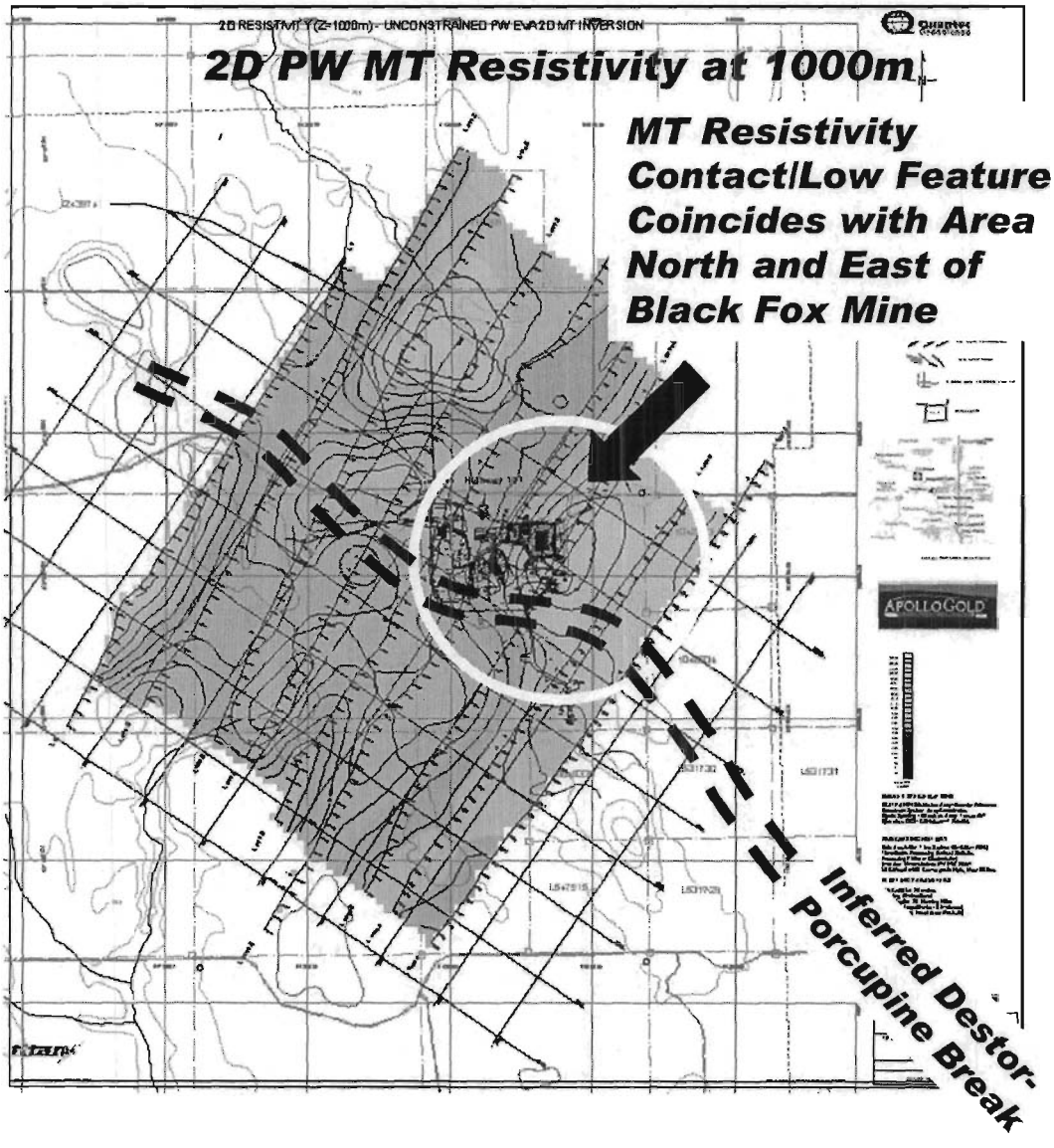

Figure 97: Plan-view Depth Level Plans of Titan 2D MT Inversion Results at 1000m

BOREHOLE PHYSICAL PROPERTY LOGGING[7]

Hole 03BF063

The borehole petrophysical logs for hole 03BF063 are presented in Figure 98, along with the accompanying geologic logs and interpretative comments. The hole is situated at mine grid 10037E/9739N (Titan Grid ≈ 1037E/146S), with Azimuth 40deg, Dip 70deg and length 491m.).

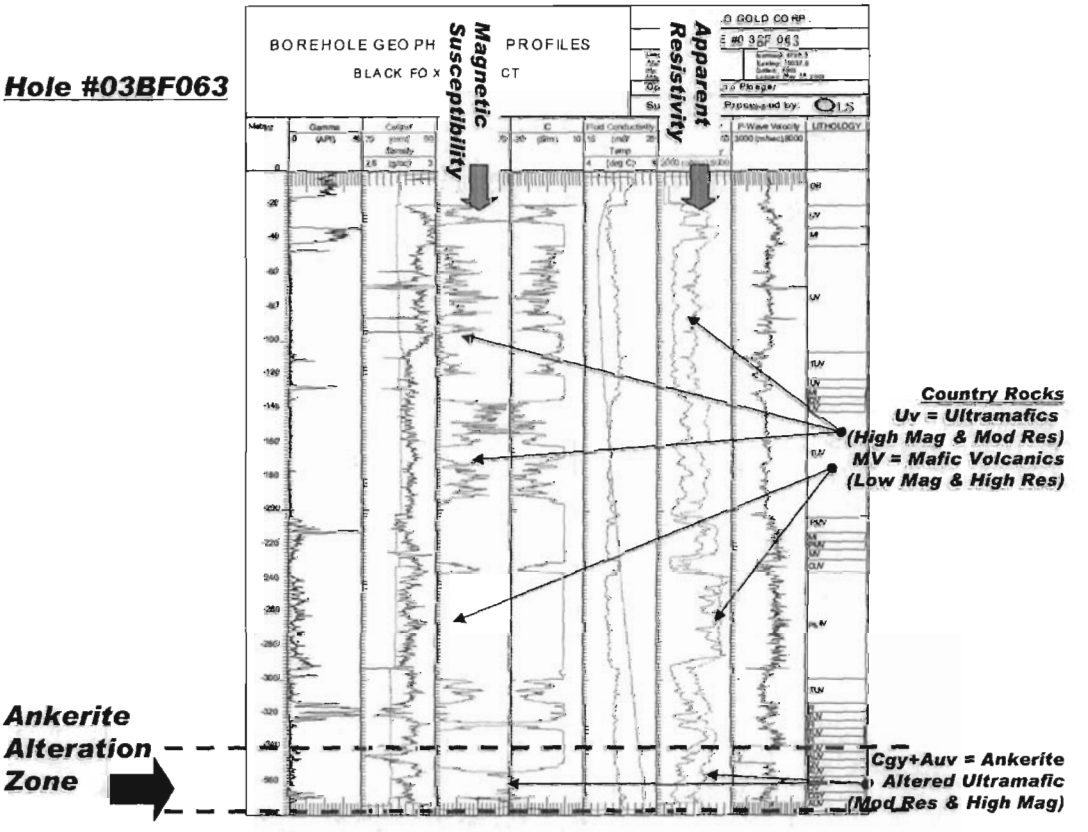

Figure 98: VIEWlogTM Borehole Petrophysical Logs for Hole 03BF063

[7] Note: More complete description of survey parameters and results provided in Quantec Logging Services logistics report L139 (May, 2003).

Hole 03BF109

The borehole petrophysical logs for hole 03BF109 are presented in Figure 98, along with the accompanying geologic logs and interpretative comments. The hole is situated at mine grid 10012E/9740N (Titan Grid ≈ 1012E/145S), with Azimuth 40deg, Dip 70deg and length 440m.).

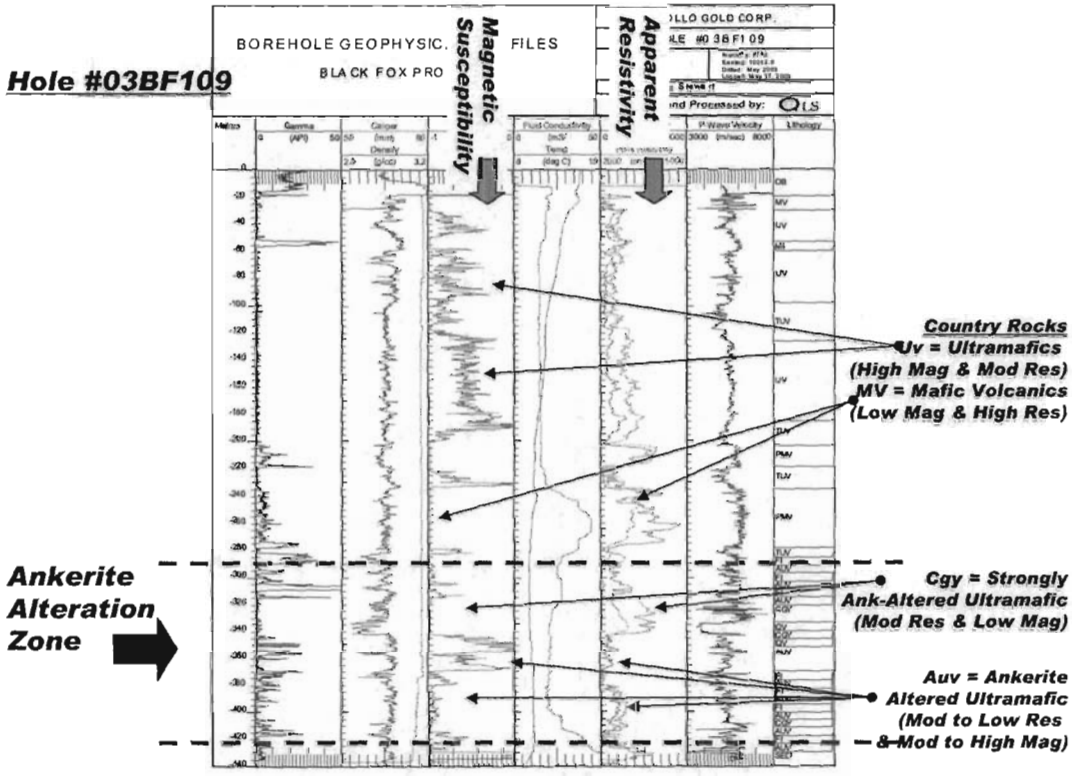

Figure 99: VIEWlogTM Borehole Petrophysical Logs for Hole 03BF109

Hole 03BF113

The borehole petrophysical logs for hole 03BF113 are presented in Figure, along with the accompanying geologic logs and interpretative comments. The hole is situated at mine grid 10000E/10110N (Titan Grid ≈ 1000E/225N), with Azimuth 40deg, Dip 45deg and length 145m.).

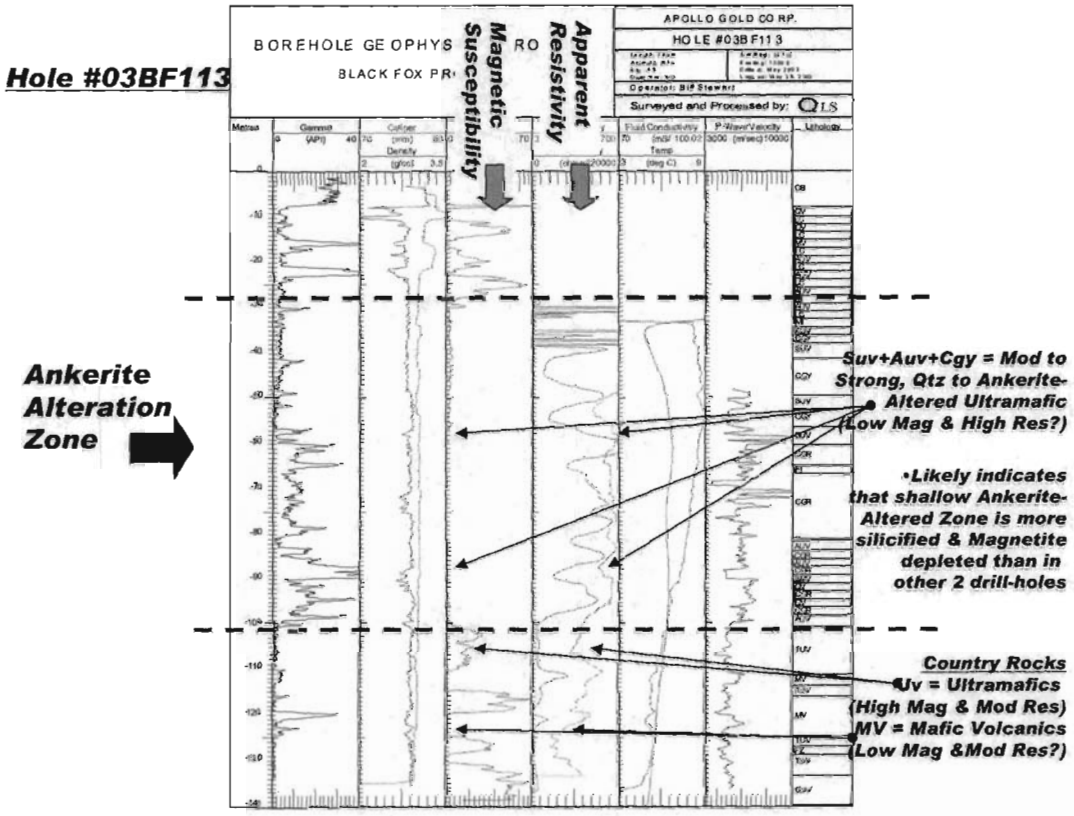

Figure 100: VIEWlogTM Borehole Petrophysical Logs for Hole 03BF113

APPENDIX C : STATEMENT OF QUALIFICATIONS

I, Wei Qian, declare that:

1. I am a consulting geophysicist, with residence in Markham, Ontario and am presently employed in this capacity with Quantec Geoscience Ltd., Toronto, Ontario.

2. I obtained a Bachelor's Degree of Science (B.Sc.), in Geophysics, from the University of Beijing, China. I later obtained my Ph.D in Geophysics, from the University of Uppsala, Sweden, in autumn, 1992.

3. I have practiced my profession continuously since December, 1992, in North America.

4. I am a member of the Society of Exploration Geophysicist (SEG) and the Secretary of Treasure of Canadian Exploration Geophysical Society (KEGS).

5. I have no interest, nor do I expect to receive any interest in the properties or securities of **Apollo Gold Corp.**, its subsidiaries, or its joint-venture partners.

6. I am a senior geophysicist associated with this study and am responsible for the creation, verification and presentation of the MT interpretation results contained in this report. The results presented represent my professional opinion based on my consideration of the information available to me at the time of writing this report.

Toronto, Ontario
July, 2003

Wei Qian
Senior Geophysicist
Quantec Geoscience

APPENDIX C : STATEMENT OF QUALIFICATIONS

I, Jean M. Legault, declare that:

1. I am a consulting geophysicist with residence in Waterdown, Ontario and am presently employed in this capacity with Quantec Geoscience Ltd., Toronto, Ontario.

2. I obtained a Bachelor's Degree, with Honours, in Applied Science (B.A.Sc.), Geological Engineering (Geophysics Option), from Queen's University at Kingston, Ontario, in Spring 1982.

3. I am a registered professional engineer (# 90531542), since 1985, and a registered professional geoscientist (#0948), since 2003, with license to practice in the Province of Ontario.

4. I have practiced my profession continuously since May, 1982, in North America, South-America and North Africa.

5. I am a member of the Association of Professional Geoscientists of Ontario, the Association of Professional Engineers of Ontario, the Northern Prospectors Association, the Association des Prospecteurs du Quebec, the Prospectors and Developers Association of Canada, and the Canadian Society of Exploration Geophysicists.

6. I have no interest, nor do I expect to receive any interest in the properties or securities of **Apollo Gold Corp.**, its subsidiaries or its joint-venture partners.

7. I am the qualified person for this project and am the co-author of the interpretation portion of the report. I have reviewed the survey results and the current report, and can attest to that these accurately and faithfully reflect the data acquired on site. I am responsible for the creation, verification and presentation of the DCIP interpretation results contained in this report, as well as the targeting portion of the study. The statements made in this report represent my professional opinion based on my consideration of the information available to me at the time of writing this report.

Toronto, Ontario
August, 2003

Jean M. Legault, P.Eng., P.Geo. (ON)
Senior Geophysicist
Quantec Geoscience Ltd.

APPENDIX D: DCIP SURVEY PROCEDURE AND THEORETICAL PRINCIPLES

Introduction

The resistivity is among the most variable of all geophysical parameters, with a range exceeding 10^6. Because most minerals are fundamentally insulators, with the exception of massive accumulations of metallic and submetallic ores (electronic conductors), which are rare occurrences, the resistivity of rocks depends primarily on their porosity, permeability and particularly the salinity of fluids contained (ionic conduction), according to Archie's Law. In contrast, the chargeability responds to the presence of polarize able minerals (metals, submetallic sulphides and oxides, and graphite), in amounts as minute as parts per hundred. Both the quantity of individual chargeable grains present, and their distribution with in subsurface current flow paths are significant in controlling the level of response. The relationship of chargeability to metallic content is straightforward, while the influence of mineral distribution can be understood in geologic terms by considering two similar, hypothetical volumes of rock in which fractures constitute the primary current flow paths. In one, sulphides occur predominantly along fracture surfaces. In the second, the same volume percent of sulphides are disseminated throughout the rock. The second example will, in general, have significantly lower intrinsic chargeability.

More detailed descriptions on the theory and application of the IP/Resistivity method can be found in the following reference papers:

Cogan, H., 1973, Comparison of IP electrode arrays, Geophysics, 38, p 737 - 761.

Langore, L., Alikaj, P., Gjovreku, D., 1989, Achievements in copper sulphide exploration in Albania with IP and EM methods, Geophysical Prospecting, 37, p 925 - 941.

Arrays and Survey Methodology

Direct current resistivity (DC) is one of the simplest geophysical methods. A current is injected into the ground using two electrodes connected by a wire with a current source. The resulting electric potentials are measured at several locations, again using two electrodes connected by a wire through some type of voltmeter.

Many different geometries of transmitter and receiver electrodes have been proposed and used over the years. These different geometries represent different compromises in depth of penetration, target resolution, and cost. Some of the familiar geometries might include pole-dipole, dipole-dipole, gradient, Schlumberger, and Wenner. The Schlumberger and some variants are "sounding arrays" intended to measure the resistivity at a site. Gradient arrays and some variants are "profiling arrays" intended to measure resistivity at a fixed depth down a profile or throughout an array. Perhaps the most common and effective exploration arrays are those that combine "sounding" and "profiling" characteristics, such as pole-dipole and dipole-dipole.

The Titan-24 system could be used to record any array, but for cost and efficiency reasons it is most appropriate for deep penetrating sounding-profiling arrays. The most obvious example of this would be the pole-dipole array. This uses an array of receiver dipoles (measuring voltage, or potential) laid out along a profile. The transmitter consists of a single electrode moving through the array, centered on each receiver dipole. The second transmitter electrode, for the return or back current, is located "infinitely" far away. The practical implementation of "infinite" is somewhat vague, generally ranging from 3 to 10 times the array length.

This array can be illustrated schematically as:

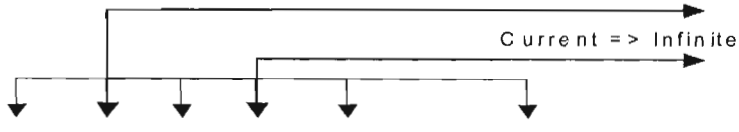

In this illustration the voltage (potential) receiver dipoles are shown in black. All of the receivers are usually recorded simultaneously, although this is not required. Two different transmit current are show (in blue), with one electrode centered in a receiver dipole and the other at "infinity".

For the Titan-24 system it is often cost effective and convenient to modify this array somewhat. The "infinite" current electrode is moved into the center of the array. We refer to this as a "center pole" or "QARA" array. There are

numerous advantages to this approach:

- No "infinite" wire. For 2500-meter array this eliminates 7500-25,000m of wire. For multi-setup profiles the back-current would be untenable, and would have to move.
- Operational efficiency as "bunny chews" is minimized. This can be substantial.
- Safer operations, all "hot" current electrodes and wire is local to survey area.
- Higher transmit currents due to reduced back-current wire resistance.
- All 4 receiver and transmitter poles are on the profile and modeled, eliminating uncertainty about "infinity".

However there are drawbacks:

- Reduced current penetration. For "N" of 1-6 measured potentials (for same transmit current) are larger for QARA array, for "N" of 6-8 potentials are comparable, but for "N" greater than 8 the pole-dipole array is superior, up to 50x at "N" of 20.
- Center pole moves with each setup. Fixed center pole for profile would be superior for multiple setup profiles.
- No standard plotting conventions.
- Some reduction in data coverage. Basically, one "pant-leg" is missing in each direction off the center pole.

The relative merits of each array need to be evaluated for the logistics, budget, and targets of each exploration program.

An important consideration may be the expected improvement, and ultimate interpretational value, of the large "N" spacing data. In practice the necessary large back-current wire can impose substantial resistance in the transmitter circuit, reducing actual transmit currents by 5-10x. This can substantially reduce the advantage of the pole-dipole array in practice. This can be overcome by using large diameter wire (8-10 gauge), using multiple transmitter wires in parallel (also helping the "bunny-chew" problem), and taking extra care installing the electrodes. Again, all of the factors impact survey cost.

Another consideration is that even perfect large "N" data may not provide a substantial difference in the resolution of deep targets. In effect the current paths asymptote out at depth, and larger "N" spacing may not provide much deeper sensing. The data at "N=10" and "N=20" are generally indistinguishable; the current paths are essentially identical.

Principles of Reciprocity and Superposition

There are two fundamental geophysical principals that are helpful in understanding the DC/IP data. First is the principal of reciprocity. Reciprocity states that replacing the transmitter location with a receiver, and the receiver with a transmitter, will produce the same measurement of resistivity and chargeability. This principal is most often applied in optimizing field logistics in "sounding" arrays.

The second principal is superposition. Superposition of data is a common procedure in Titan-24 surveys and data analysis. Superposition is equivalent to linearity. It simply states that the measured potentials can be summed, and the sum is identical to making a direct measurement of the summed electrode. This principal is apparent to most people for apparent resistivity, but it is also applicable to chargeability.

Superposition can be most effectively used to **display** the data in different formats. It is also possible to invert the data in different formats. There should be no advantage, or disadvantage, to inverting the data in any particular array through superposition. The information remains the same. Despite the obvious temptation, combining the data in various superposed geometries will not lead to a better inversion, only a slower inversion. In general, it is best to simply invert the data in the native array geometry, although it is reasonable to transform the array geometry to satisfy the requirements of specific inversion programs.

The most common application of superposition in the Titan-24 data is in transforming the data and model responses for comparison. The data and responses are most commonly transformed to dipole-dipole data. The advantage of this is that the dipole-dipole data display is widely understood by geophysicists, and it is relatively easy to see how the data and models are related. So where there is a misfit in the data and model responses the geologic significance is easily evaluated.

The following illustration shows how two transmitter events of pole-dipole data can be combined to create equivalent dipole-dipole data:

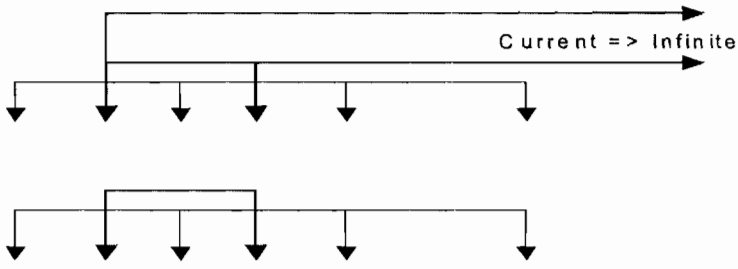

The earlier illustration of the pole-dipole array has now been modified to indicate how two pole-dipole transmitter "events" can be subtracted to generate a dipole-dipole measurement.

The Titan-24 system also records orthogonal potential dipoles for each current transmit. These dipoles are not being used in the inversion or interpretation at present. The orthogonal voltages are quite small, and are generally contaminated by telluric noise (MT signal). Efforts are underway to implement telluric cancellation, which may open the possibility of more accurate analysis of the DC/IP data. There are good indications that the same current rotations seen in the MT data occur in the DC/IP data, and could be accounted for in the data processing and inversion.

2D Inversion Procedure

The approach to interpreting the DC/IP data relies primarily on 2D inversions. There is little pre-processing of the data. The steps are:

- Edit data to remove extreme outliers. This is commonly done by deleting data where the repeatability errors are > 10% of the data value.
- Assign realistic data errors. The repeatability errors from the field observations are generally about 10,000x smaller than the data. These small repeatability errors are dominated in reality by uncertainty in electrode positioning, topographic effects, multidimensional effects, and inaccuracies in the modeling and inversion programs. Errors of about 3% of the measured data value often work well, and are consistent with the expected numerical modeling errors.
- Invert the data.
- Evaluate "convergence" of the inversion. The inversion approach focuses initially on fitting the data. Once convergence is obtained (the data are "fit") additional iterations of the inversion are necessary to reduce the model norm – remove structure from the inversion that is not required by the data.
- Presuming the inversion has not converged the data are "culled". This involves removing a small percentage of the data that are most inconsistent with the inversion model. These are, presumably, data that are biased or have 3D effects. However, some care must be taken as this approach presumes that the inversion has fit the "good" data.
- Re-invert the "culled" data, starting from the original (halfspace or geologic) model. This will generally provide the necessary convergence.
- Several inversions are run on the "culled" data, using different "model norms", or target models. This is important in exploring the range of models consistent with the data.
- Invert the IP data in much the same way.
- Convert data and model responses to dipole-dipole for display.

Several different inversion models are produced. Several models are "smooth" inversions starting from a half-space. These models will vary in the "model norm", the balance between model smoothness and data misfit. Additionally, several GoCad geologically constrained inversion models are typically run. The geophysicist selects one, representative, model as "the" inversion.

APPENDIX E: MT SURVEY PROCEDURES AND GENERAL THEORY

The magnetotelluric (MT) method measures time-variations in the Earth's natural electric (E) and magnetic (H) fields to image the subsurface resistivity structure. No source or transmitter is used. These natural fields penetrate much deeper than is practical with a transmitter. At the same time the natural signals are a plane-wave source. The plane-wave source is much simpler to model than complex transmitter geometries and signals.

The E and H fields are measured over a broad range of frequencies. Typically, the frequencies can range from above 10kHz to below 0.001Hz. High frequency signals are attenuated more rapidly in the subsurface. High frequency data are indicative of shallow resistivity structure while low frequency data are indicative of deep resistivity structure.

At frequencies below 1Hz the signal source is due to oscillations of the Earth's ionosphere as it interacts with the solar wind. At frequencies above 1Hz the signal source is due to worldwide lightning activity. There is a lack of signal around 1Hz, often referred to as the "hole". Modern 24-bit recording hardware and signal processing techniques have largely eliminated the data quality problems that have been traditionally seen around the 1Hz signal hole.

Between about 8Hz and 300Hz the signal from worldwide lightning activity propagates in a "resonant" cavity (the resistive atmosphere) between the conductive ionosphere and the Earth's surface. Above 3kHz the signal propagates as a ground wave. Between 300Hz and 3kHz there is a "dead-band" where the signal does not propagate well. Despite hardware and signal processing improvements this dead-band remains problematic. When signal (atmospheric activity) is present within several hundreds of miles of the survey area the data is quite good. When no signal is being generated in the vicinity data quality is poor.

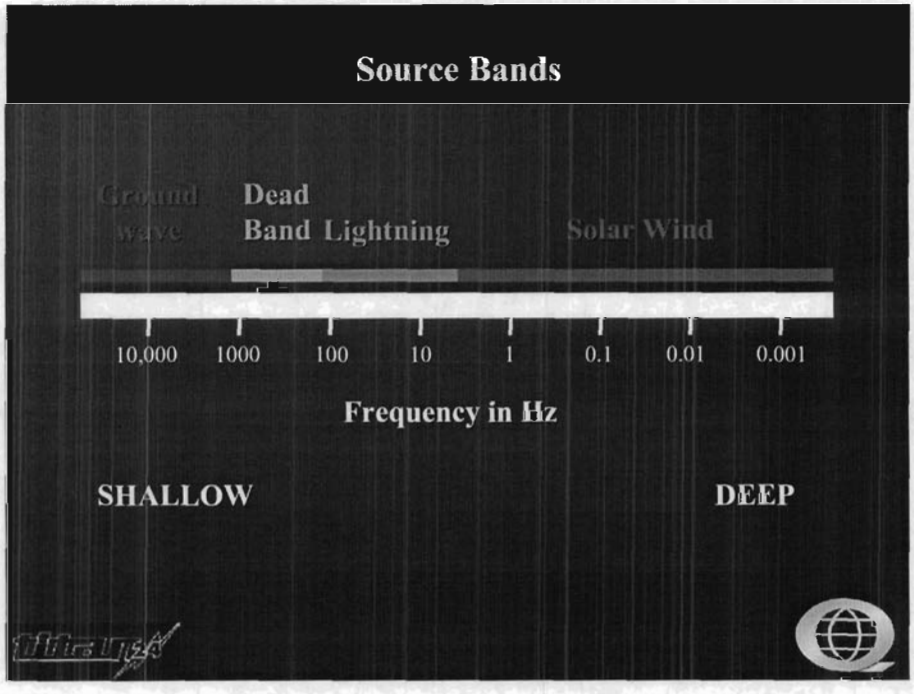

Both the electric and magnetic fields are measured. The measured fields depend on the ionosphere and lightning, and are essentially random. While the E and H fields are random the ratio of the fields depends on the subsurface resistivity structure. Note that it is primarily the orthogonal E and H fields that are related. The magnetic field must be measured perpendicular to the electric field. It is possible for complex subsurface resistivity structure to rotate the fields, and full tensor data are usually measured.

It is often useful to think of the magnetic field as the source signal and the electric field as the response. Time variations in the magnetic field induce currents to flow in the ground.

In the field the electric and magnetic fields are measured as a function of time. The electric field is measured using two orthogonal dipoles consisting of a wire connecting two grounded electrodes. In essence, the recording system consists of a voltmeter between the electrodes. The voltage measured depends on the electric field strength and the length of the dipole. The magnetic field is measured using an induction coil.

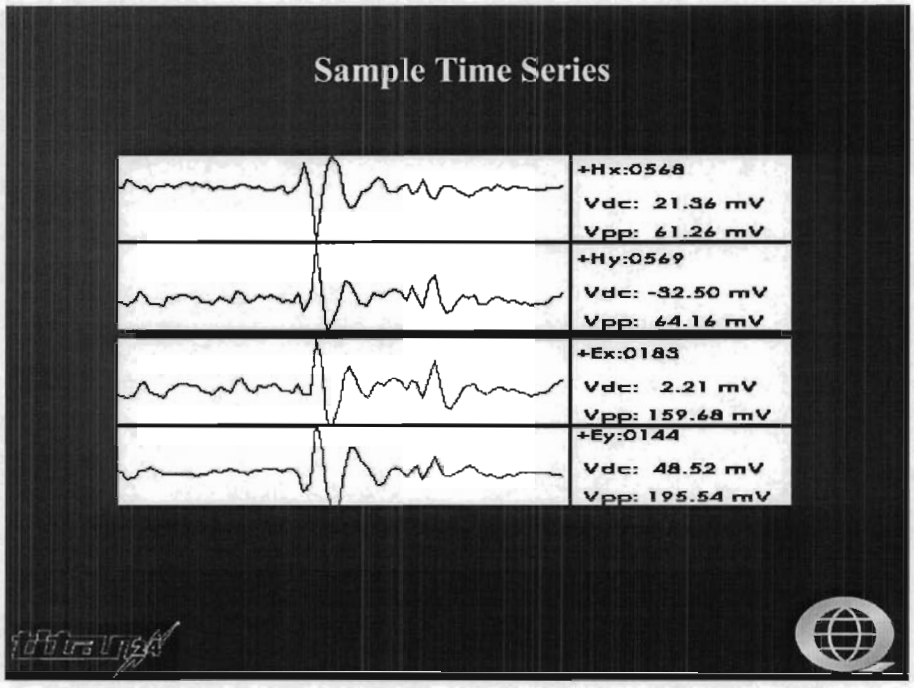

While the actual fields that are measured vary randomly (with solar and lightning activity), the relationship between the measured magnetic and electric fields is constant and depends on the subsurface resistivity structure. Extracting the subsurface resistivity structure from the measured magnetic and electric fields is a multi-step process. First timeseries processing techniques are used to derive geophysical parameters from the electric and magnetic fields. Then geophysical processing and inversion techniques are used to convert the geophysical parameters to a subsurface resistivity image. Finally, the resistivity image must be interpreted in terms of geologic units.

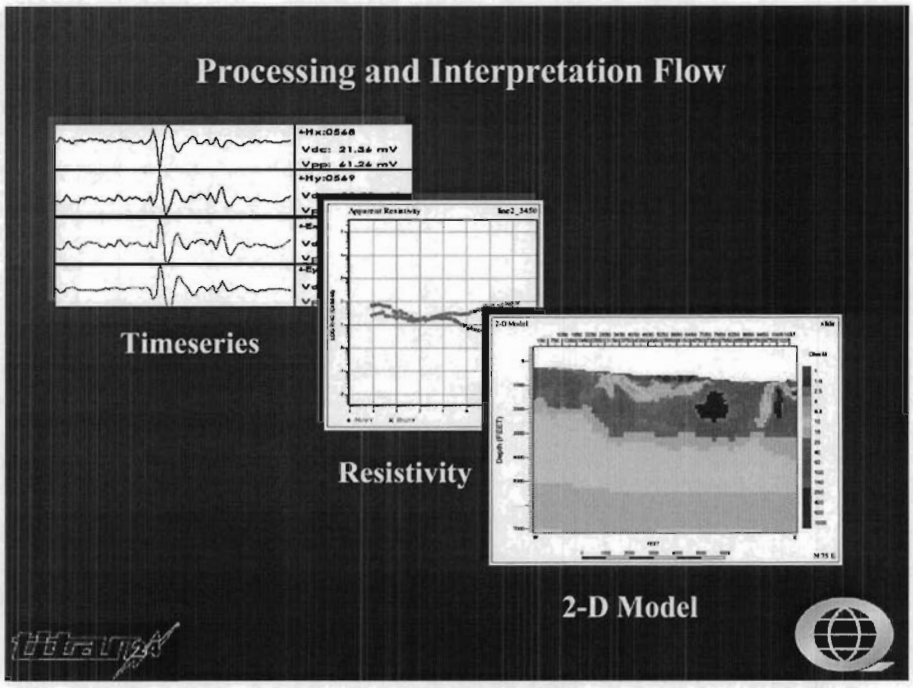

The measured magnetic and electric fields are Fourier transformed into the frequency domain. The system response is removed from the data (making the measurement independent of the hardware system). The Fourier coefficients represent the amplitude and phase of the electric and magnetic fields as a function of frequency.

Data Processing and Inversion

A variety of signal processing techniques are used to minimize noise and bias in the estimation of geophysical parameters from the measured fields. The details are complex, but the approach is easily understood. Philosophically, the idea is to use multiple approaches to noise and bias reduction, not letting any one statistical approach have too much impact on the data, but relying on the combination of approaches to produce good estimates. The approaches include:

1. Spatial isolation of noise. A remote reference magnetic station is used to separate widely distributed signal from local noise.
2. Coherency sieves to find coherent signal. First the local and remote magnetic field measurements are compared and coherent signal kept. Then the local magnetic and electric fields are compared for coherency.
3. Frequency isolation of noise. Long Fourier transforms are used to provide extremely sharp isolation of noise in frequency.
4. Time isolation of noise. Short Fourier transforms are used to remove noise that is isolated in time (noise spikes, or noise that is randomly turning off and on).
5. Robust statistics that minimize biasing effects of a few isolated measurements.

Once the time series processing is complete geophysical parameters can be estimated. The primary geophysical parameters for MT are typically the apparent resistivity versus frequency and phase versus frequency.

The apparent resistivity and phase curves are the primary parameters used in the interpretation of MT data. For a layered (1D) earth the apparent resistivity and phase data can be converted into intrinsic resistivity versus depth simply by accounting for the volume averaging nature of the method. There are a variety of algorithms for doing the conversion. The conversion is not unique. Some algorithms provide smoothly varying intrinsic resistivity versus depth functions (Occam inversion, Bostick transform). Others

provide distinct layered solutions (Marquardt inversion).

1D modeling and inversion raises the following points:

- A single MT site provides information about resistivity versus depth. This is a major distinction from potential fields techniques that only provide information about relative variations along a profile.
- The conversion from apparent resistivity versus frequency to intrinsic resistivity versus depth is not unique. It is susceptible to equivalence. In particular any sharp resistivity contrast can be replaced by an equivalent transition zone.
- In a layered model the thickness of a resistive layer is well resolved. The resistivity of a resistive layer is poorly resolved.
- In a layered model the conductance (conductivity*thickness) of a layer is resolved. Neither the thickness nor the conductivity is uniquely resolved.
- Once the constraint that the subsurface is composed of distinct, resolvable, units is imposed the 1D inversion of MT data is essentially unique. Resolution is excellent (better than 5% of depth).

Apparent resistivity versus frequency is the most fundamental way of looking at the data in the interpretation phase. While the overall process is complex, with advanced processing techniques and inversions, it is important to keep in mind that the subsurface structures are apparent in the raw data – the apparent resistivity plots.

The following sequence (a to f) of illustrations is intended to introduce the apparent resistivity versus frequency sounding curves. But it is also intended to highlight the relatively complex, but understandable, relationships between the observed data and subsurface structure.

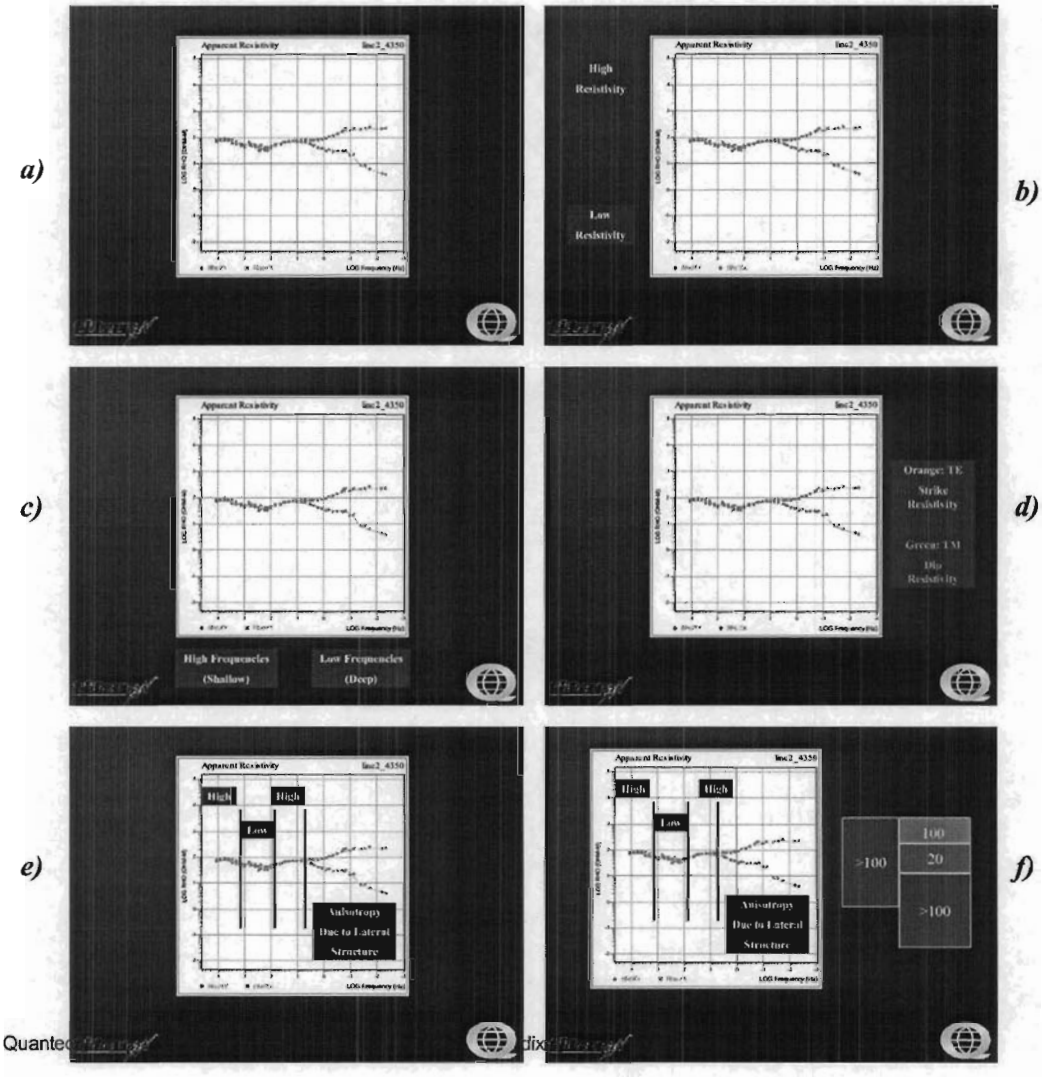

A simple layered subsurface structure is not generally the problem of immediate interest in exploration. In the case of more complex two-dimensional (2D) or three-dimensional (3D) structure the MT response will be affected by lateral resistivity variations.

The MT measurement relies on natural, plane-wave, source signals. The measured response depends on lateral resistivity variations as much as (or more than) resistivity variations below the immediate sounding site.

Full tensor measurements of the E and H fields are made at every site. For each site there are two apparent resistivity sounding curves (or modes) and phase curves. These two modes are arbitrarily labeled Rho-XY and Rho-YX. Rho-XY refers to the apparent resistivity (Rho) calculated from Ex and Hy.

Once full tensor measurements are made in the field it is possible to mathematically rotate the fields to any arbitrary coordinate system. Traditionally, the data are rotated independently at each frequency to maximize the difference between the two apparent resistivity sounding curves. This puts the data into "geologic" or "principal" coordinates.

One sounding curve will have the electric field in the geologic strike direction and is referred to as "Transverse Electric" or TE. The other mode will have the electric field in the geologic dip direction and is referred to as "Transverse Magnetic" or TM. Note that TE and TM are interpretive designations, and refer to geologic strike. XY and YX were simply geometric designation.

For a layered (1D) earth the two measurements are identical. When the structure is 2D or 3D the lateral resistivity variations will distort (often severely) the simple 1D response. The distortion of the fields by complex structure is realized in the apparent resistivity data as "anisotropy". This is a divergence between the two apparent resistivity sounding curves.

The measurement of two orthogonal apparent resistivity sounding curves provides valuable information. Both curves reflect the resistivity structure underlying the site. Both curves will show increasing or decreasing resistivity at a frequency in response to resistivity structure under a site. The two apparent resistivity curves will diverge in response to lateral resistivity variations.

If the site is located on the resistive side of a lateral resistivity contrast the TE mode will be slightly suppressed due to the contact and the TM mode will be significantly biased up by the contact. If the site is located on the conductive side of a lateral resistivity contrast the TE mode will be slightly biased up while the TM mode will be significantly biased down by the contact.

For a 2D resistivity structure the TE mode is always providing an indication of the integrated conductance of the volume being sampled. It will always be a slowly varying function of position. The TM mode is responding dramatically to the presence of charges on the lateral resistivity boundaries, and will dramatically overshoot on the resistive side of a contact and undershoot on the conductive side. The anisotropy (divergence of the two sounding curves) is diagnostic of a lateral resistivity contrast.

The following simple model demonstrates most of the critical 2D behaviours. The model consists of a 100 Ohm-m host with a 10 Ohm-m basin on the right. There is a 1 Ohm-m layer buried within the host and below the basin. The response is shown at two sites, one immediately on the resistive side of the basin contact and the other immediately on the conductive side of the contact.

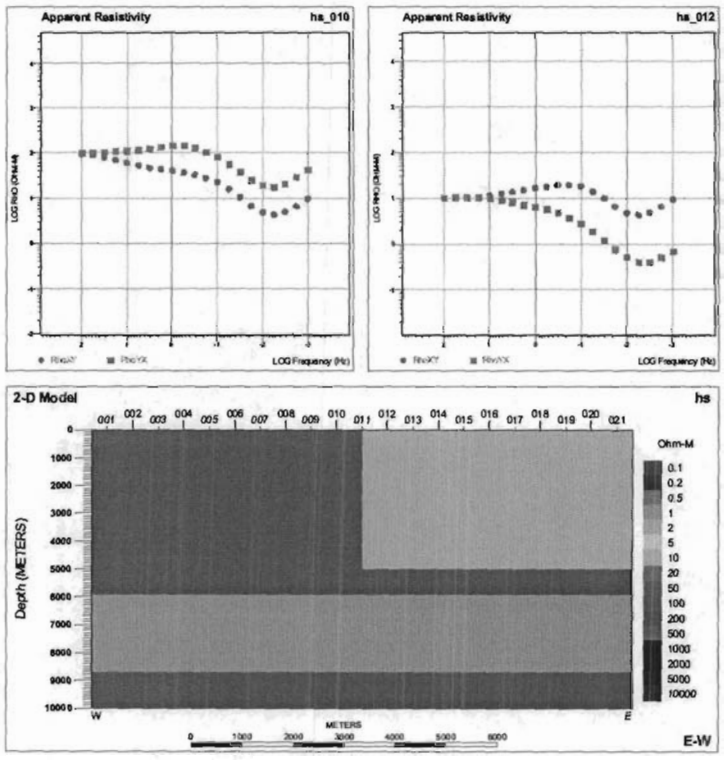

The following observations summarize the behavior of 2D MT responses:

- The apparent resistivity at high frequencies reflects the true shallow resistivity.
- The apparent resistivities converge at high frequencies to the true shallow resistivity.
- The divergence in apparent resistivities occurs at a higher frequency for the site on the resistive side of the contact. Because the skin depth is larger in the resistive media the site on the resistive side of the contact is effectively "closer" to the contact than the site on the conductive side of the contact. The TE mode is constrained to the range of physical resistivities actually present in the model
- The TE mode "volume averages" the intrinsic resistivity. The TM mode exhibits apparent resistivities outside the range of physical resistivities in the model. Note that for the site on the right the TM mode indicates resistivities below 1 Ohm-m.
- Both the TE and TM modes respond in tandem, at the same frequency, to resistivity structure under the site. At both sites both the TE and TM modes indicate the top and bottom of the 1 Ohm-m layer. While 1D inversions of the TE and TM modes would place different apparent depths to the 1 Ohm-m layer the response is at the same frequency in both modes indicating it is the response of one layer.
- The intrinsic resistivity of the 1 Ohm-m layer is difficult or impossible to discern. Without physical property data only the conductance of the layer can be resolved.

These effects can also be clearly seen in pseudo-sections of the TE and TM apparent resistivity response of the model:

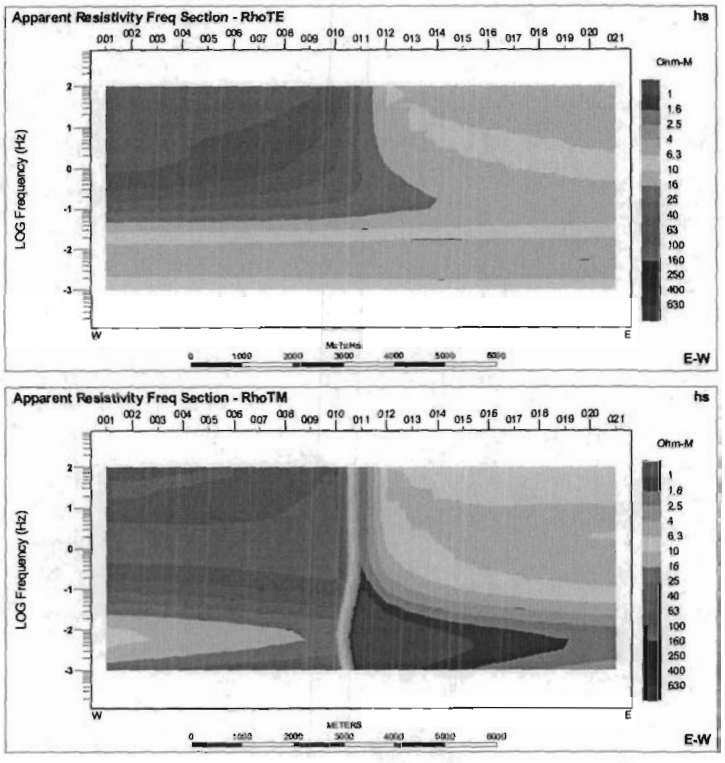

The apparent resistivity data at each site have been contoured, as a function of frequency. The inherent smoothness of the TE section can be clearly discerned. The distinctive "undershoot" of the TM response on the conductive side of the contact can be clearly seen.

One of the key factors in multidimensional MT data is "static shifts". The apparent resistivity sounding curves can be biased, up or down, by lateral resistivity contrasts too small to be resolved by the MT data. The curve is essentially DC shifted on the log-log apparent resistivity plot. This can be seen by examining the sounding curves from the previous 2D model. Assuming data had not been acquired above 1Hz the two sounding modes would be seen to be separated in the highest frequency data. Note that there are no static shift effects in the phase data.

Inversions and forward modeling are used to derive the subsurface resistivity structure from the data. The primary interpretation tools are 2D inversions. Problems emerge when the real world, complex, data are not consistent with the simplistic 2D assumptions. In a perfect world we would use modeling and inversion programs capable of reflecting the full complexity of the subsurface. However, in practice incorporating too much complexity in the modeling and inversion programs results in very coarse models, which are incapable of resolving exploration targets. Instead, we must find ways to remove some of the complexity from the actual data. We employ a number of techniques to this end:

- Topographic tensor stripping. The topography is well known and unchanging. By running models of the topography we can uniquely determine the topographic response and remove it from the data.
- Rotation to principal coordinates. The inversion algorithms presume that we have acquired a true geologic dip profile. In reality, geologic dip is often difficult define, and seldom known prior to acquisition. However, because we have acquired full tensor data we can rotate our data to the geologic dip direction after acquisition.
- Static stripping. Unlike topography, the static shifts are not known. However, once the "best" static correction is determined it can be "stripped" from the data. The impact can be very dramatic; by removing shallow complexity the deeper sounding curves can change, sometimes significantly.
- Eigenvector processing. 3D structures can introduce complex "rotations" of the electrical currents. These rotations produce effects; such as excessively steep resistivity curves and out-of-range phases that would be impossible to fit with 2D modeling programs. By relaxing the assumption that the electric and magnetic fields are orthogonal eigenvector analysis provides a unique and trivial methodology for simplifying complex 3D data.

- 1D inversion for curve fitting. Real data are often noisy, and inconsistent. Out-of-range phases are a typical example of features seen in real data that cannot be fit using 2D inversion. It is often best to make use 1D inversion to make interpretative decisions about how to "best" fit the data, rather than letting the 2D inversion thrash trying to fit inconsistent data.

Once these data processing techniques have been completed the data are inverted. Generally, two inversions of the MT data are done. The first inversion uses an approach (a model norm) that explicitly looks for the "smoothest" model consistent with the data. This approach essentially finds the minimal subsurface structure consistent with the data. The second inversion uses an approach (a model norm) that looks for a model most consistent with the known geology.

For the geologically constrained inversion we use a proprietary approach developed by Dr. Phil Wannamaker. This approach uses the geologic constraints as a target, while not imposing any intrinsic smoothing on the inversion. The approach finds the maximum structural information, at the risk of sometimes including structure not required by the data. It represents an effort to extract the maximum exploration information from the data.

Both approaches are valid, and important. A smooth model approach to inversion can be viewed as finding the least possible useful exploration information. However, it does provide an independent assessment of what the data actually require. The geologically constrained inversion will provide a much sharper subsurface image. But it will also reproduce the known geology where the data does not require a change to the model. Without an independent smooth model inversion it can be hard to determine whether a geologically constrained inversion has confirmed the geologic interpretation, or simply doesn't have information either way.

References:

1. Cagniard, L. (1953). Basic theory of the magnetotelluric method of geophysical prospecting. Geophysics, v. 18, pp. 605-635.
2. Chouteau, M. (1985b). Magnetotelluric measurements in La Malbaie area (Québec): the anomalous vertical magnetic field. Canadian Journal of Earth Sciences, v. 22, pp. 1530-1536.
3. Eggers, D.E. (1982). An eigenstate formulation of the magnetotelluric impedance tensor. Geophysics, v. 47, pp. 1204-1214.
4. Fischer, G. (1985). Some remarks on the behaviour of the magnetotelluric phase. Geophysical Prospecting, v. 33, pp. 716-722.
5. Garland, G.D. (1979). Introduction to Geophysics – Mantle, Core and Crust. W.B. Saunders Company, Toronto, ON, 494 pp.
6. Goldstein, M.A., and Strangway, D.W. (1975). Audio frequency magnetotellurics with a grounded dipole source. Geophysics, v. 40, pp. 669-683.
7. Hoover, D.B., Frischknecht, F.C., and Tippens, C.L. (1976). Audiomagnetotelluric sounding as a reconnaissance exploration technique in Long Valley, California. Journal of Geophysical Research, v. 81, pp. 801-809.
8. Jones, A.G. (1983). On the equivalence of the "Niblett" and "Bostick" transformations in the magnetotelluric method. Letter to the editor, Geophysics v. 53, pp. 72-73.
9. Jones, A.G. (1988). Static shift of magnetotelluric data and its removal in a sedimentary basin environment. Geophysics, v. 53, pp. 967-978.
10. Kaufman, A.A., and Keller, G.V. (1981). The Magnetotelluric Sounding Method. Elsevier, New York, 595 pp.
11. Keller, G.V., and Frischknecht, F.C. (1966). Electrical Methods in Geophysical Prospecting. Pergamon Press, New York, 519 pp.
12. Park, S.K., and Livelybrooks, D.W. (1989). Quantitative interpretation of rotationally invariant parameters in magnetotellurics. Geophysics, v. 54, pp. 1483-1490.
13. Prugger, A.F., and Woods, D.V. (1984). The pattern of anomalous geomagnetic variation fields over the Mid-continent Gravity High. Journal of Geophysical Research, v. 89, pp. 773-382.
14. Ranganayaki, R.P. (1984). An interpretive analysis of magnetotelluric data. Geophysics, v. 49, pp. 1730-1748.
15. Spitz, S. (1985). The magnetotelluric impedance tensor properties with respect to rotations. Geophysics, v. 50, pp. 1610-1617.
16. Strangway, D.W., Redman, J.D., Holladay, S., and Horne, C. (1980). Audio frequency magnetotelluric soundings at the Whiteshell nuclear research establishment and Chalk River nuclear laboratories. AECL, Technical Record, TR-71, 58 pp.
17. Strangway, D.W., Swift, C.M., and Holmer, P.C. (1973). The application of audio frequency magnetotellurics to mineral exploration. Geophysics v. 38, pp. 1159-1175.
18. Vozoff, K. (1972). The magnetotelluric method in the exploration of sedimentary basins. Geophysics, v. 37, pp. 98-141.
19. Waeselynck, M. (1974). Magnetotellurics - principle and outline of the recording technique - a case history. Geophysical Prospecting, v. 22, pp. 107-121.
20. Word, D.R., Smith, H.W., and Bostick, F.X. (1971). Crustal investigations by the magnetotelluric tensor impedance method. In: Geophysical Monograph Series, v. 14: The Structure and Physical Properties of the Earth's Crust, Heacock, J.G., ed., pp. 145-167.
21. Young, C.T. (1981). Principles of Phoenix Geophysics real time remote reference magnetotelluric system. Phoenix Geophysics, Denver, vers. 3.2, 51 pp., based on: Magnetotelluric measurements of conductivity anomalies in northern Wisconsin (1977). Ph.D. dissertation, Department of Geology and Geophysics, University of Wisconsin, Madison.

APPENDIX F: INVERSION THEORY

An excellent overview and introduction to both the philosophy and use of inversions in geophysics is available on the University of British Columbia (UBC) website (http://www.geop.ubc.ca/ubcgif/).

Several points, detailed on the website, are crucial to understanding the 3D-Quest and Titan-24 approach to exploration:

- Inversion is a powerful 'tool', not a 'solution'.
- Inversion is not normally "unique". Given noisy and incomplete data of inherently limited resolution there are usually an 'infinite' range of models that 'fit' the data equally well. Recognition of this inherent non-uniqueness is why inversion must be viewed as a tool rather than a solution. Understanding and exploration of this non-uniqueness is an important part of the interpretive process.
- Inversion finds a model that 'fits' the data. The precise definition of 'fit' can be critical in the actual model that is found.
- The inversion depends on the data, and the data errors. The importance of the data errors is often overlooked.
- Inversion depends on a "model norm" – the mathematical definition of which model the inversion should try to find. This definition is almost as important as the actual data in determining the final inversion model.

Mathematically, inversion is the process of minimizing a function. The choice of which function to minimize ultimately defines the inversion model. Schematically, this function might be expressed:

$$\phi = \phi_d + \beta \phi_m = \text{(misfit)} + \beta \text{(model norm)}$$

$$0 < \beta < \infty \text{ is a constant}$$

This defines a function to be minimized that consists of some function that minimizes the data misfit, combined with some function that finds a "smooth" model. Beta represents a relative weighting between fitting the data and smoothing the model.

Clearly, the data misfit function must be defined in more detail. One approach might be:

$$\phi_d = \sum_{i=1}^{N} \left(\frac{F_i[m] - d_i^{obs}}{\varepsilon_i} \right)^2$$

This function defines the data misfit as the sum of the individual misfits squared, normalized by the errors associated with each data point. It is a very common, and stable, definition of the data misfit.

An important point not made on the UBC website is that the errors depend on many factors. The most common measure of data errors is simply the repeatability of the voltage and current measurements in the field. This may be misleading as there are also "errors" associated with electrode positioning, geologic complexity (2D vs 3D, but also coupling of shallow and deeper structure), and errors in the numerical calculation of model responses and inversion.

Another point not sufficiently detailed on the UBC site is the importance of not overestimating the data errors and fitting the data as closely as possible. Most geophysical techniques, but particularly electrical techniques, have large responses to shallow structure. This is expressed as "pant legs" in DC/IP, or "statics" in MT. The response to deep structure is generally a very subtle component of the data, compared to the sensitivity to shallow structure. Without excellent data, and an excellent match between the data and model response, the deep structure will not be imaged to the degree necessary for commercial exploration.

The model misfit function must also be defined in more detail. One of the most flexible definitions is the one used by UBC:

$$\phi_m(m,m_0)=\alpha_s\int_{vol}(m-m_0)^2dv+\alpha_x\int_{vol}\left(\frac{\partial(m-m_0)}{\partial x}\right)^2dv+\alpha_z\int_{vol}\left(\frac{\partial(m-m_0)}{\partial z}\right)^2dv$$

In this definition there are three components to the "model norm" (or "smoothness" constraint, or "regularization"). The first component is simply an overall difference between the model and a "target" model, the second component is a horizontal smoothness, and the third component is a vertical smoothness. The three "alpha" parameters represent a relative weighting of each component.

The UBC website provides an excellent example of the importance of selecting an appropriate "model norm", reproduced here:

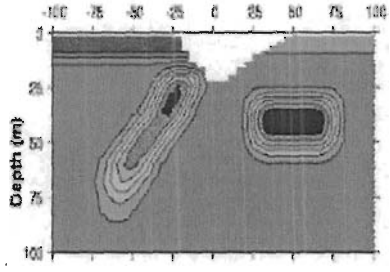

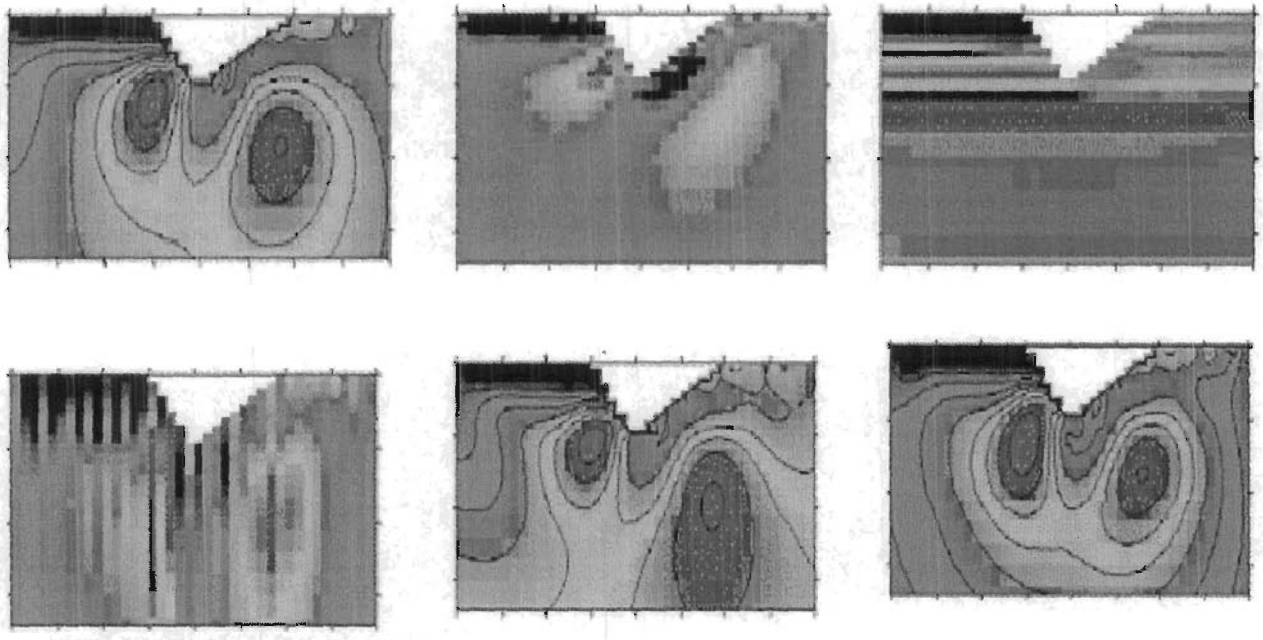

In this example the expected response of the top figure was computed. These 'data' were then inverted six times, using different "model norms". The lower six figures show the range of valid inversion models that can be produced. Note that six of these models are essentially mathematically equivalent, they all "fit" the data.

An important philosophy, driving much of the academic communities approach to inversion for the last two decades, is that the "best" model is the "smoothest" model consistent with the data. There are good reasons for taking this approach. However, from an exploration viewpoint this philosophy can be rephrased to "find the model with the least exploration value" – perhaps not reflecting the real goal of an exploration program.

Recently, several groups have taken major steps towards developing inversion approaches more tuned to exploration needs. Instead of using "smooth" model norms, they are being replaced with "focused (minimum transition zone)

inversion, or smoothing to a geologic "target" model.

For exploration smoothing to a geologic target model makes sense. It requires good geologic control, and some understanding of the rock physical properties. There are three drawbacks to the geologic target approach:

- The geologic information is incomplete or inaccurate.
- Physical property data are incomplete.
- It is difficult to determine whether the geophysical data support the geologic model, or simply provide no information.

The most sensible approach is to combine smooth model inversion with geologic target inversion. For now, we are focusing on providing inversions using both approaches. It is up to the project geologist and geophysicist to review these inversions and develop a final interpretation.

APPENDIX G: PRODUCTION SUMMARY

DATE	DESCRIPTION	LINE	START	END	IP EVENTS	MT EVENTS		SUBTOTAL(m)		TOTAL (km)	
						BASE	REMOTE	IP	MT	IP	MT
04/25/03	• Looking for remote site • Coils parallel sensor test • Infinite wire out										
04/26/03	• Setup • Record DCIP • Record MT	L0E	1000S	1000N	1007-1047	1057-1069	003-016	2000	1900	2.0	1.9
04/27/03	• Record DCIP • Record MT	L200E	750S	1500N	1003-1052	1056-1064	020-028	2250	2250	4.25	4.15
04/28/03	• Record DCIP • Record MT	L400E	800S	1500N	1007-1057	1066-1077	045-057	2300	2300	6.55	6.45
04/29/03	• Record DCIP • Record MT	L600E	800S	1300N	1005-1047	1052-1065	060-075	2100	2100	8.65	8.55
04/30/03	• Record DCIP • Record MT	L800E	1000S	1500N	1009-1061	1072-1082 2015-2019	076-092	2400	2500	11.05	11.05
05/01/03	• Record DCIP • Record MT	L1000E	1300S	1400N	1007-1066	1069-1082 2002-2012	098-109	2700	2700	13.75	13.75
05/02/03	• Record DCIP • Record MT	L1200E	1000S	1100N	1004-1046	1051-1061 2002-2010	115-124	2100	2100	15.85	15.85
05/03/03	• Record DCIP • Record MT	L1400E	1000S	800N	1007-1043	1046-1061 2002-2015	128-141	1800	1800	17.65	17.65
05/04/03	• Record DCIP • Record MT	L1600E	1000S	1000N	1006-1049	1053-1066 2002-2013	146-158	2100	2000	19.75	19.65
05/05/03	• Pick gear up • Demobilization Matheson-Timmins										

TOTAL PRODUCTION: IP: 19.75 km
MT: 19.65 km

SURVEY DAYS: 11
DOWN DAYS: 0
MOBILIZATION DAYS: 0

APPENDIX H: INSTRUMENT SPECIFICATIONS

INSTRUMENT SPECIFICATIONS

REF TEK – 120 Data Acquisition System
Acquisition Module (AM)

SPECIFICATIONS

Physical	
Size:	♦ 267 x 248 x 184 mm ♦ 10.5 x 9.75 x 7.25 in.
Weight:	♦ 3.7kg ♦ 305 g ♦ 8 lbs (2-Channels maximum weight))
Temperature:	♦ -40°C to 60°C operating range.
Environmental:	♦ Operates in 1m of water without leaking for 48 hours. ♦ Airtight to 1.0 psi.
Shock:	♦ Remains operational after 1m drop (any corner) onto cement floor.
Connectors	
Line A & Line B:	♦ A pair of identical 10 pin U77/U style connectors. ♦ Each connector provides 3 pairs of lines (±): — A (+)/B (-) Receive telemetry data and/or commands — C (+)/D (-) Transmit telemetry data and/or commands — E (+)/F (-) Sync
Power:	♦ PTO7A12-8S style connector. ♦ Provides input +12 VDC supplied from battery.
Sensor:	♦ PU283/U style connector. ♦ Provides for a direct connection from the AM to the sensor.
Power Requirements	
Battery:	♦ Two 12 volt lead acid battery (7 Ah).
Signal Input	
Input Impedance:	♦ 10 megohms, 330pF, differential
Broadband Dynamic Range:	♦ 130dB (noise power ratio test @ 125 sample per second [sps])
ADC Type:	♦ Delta-sigma modulation
Sample Rage:	♦ Multiple 50 to 48,000
Gain Settings:	♦ Four – programmable for 1, 4, 16 and 64.

Sensor Input Signal Range:

Gain	*24-Bit High Speed A/D*		*24-Bit Low Speed A/D*	
	Actual	*Reported*	*Actual*	*Reported*
1	1.192μV	78.12mV	1.907μV	125.0mV
4	298.0nV	19.53mV	476.8nV	31.25mV
16	74.51nV	4.883mV	119.2nV	7.812mV
64	18.63nV	1.221mV	29.80nV	1.953mV

Data Storage	
Data Size:	♦ 32-bit two's compliment.
Base Memory:	♦ 128K EPROM ♦ 6.5Mb SRAM
Base Capacity:	♦ Better than 1.5 million samples or approximately 3 hours 10 minutes continuous data @ 125 sps.
AM Telemetry	
Protocol:	♦ Full duplex synchronous data link control (SDLC).
Error Correction:	♦ Packet acknowledge with modulo 8 sliding window.
Speed	♦ 3.072Mb/second
Encoding:	♦ Bi-phase pulse = 1, missing pulse = 0
Line Impedance:	♦ 100 Ohm
Synchronization	
Timing:	♦ Each AM on-line is timed and synchronized for simultaneous sampling within ± 1.50 μsecond.
Protection	
Electrical Protection:	♦ Line A and Line B signals circuits are protect by: — A surge arrestor located on the RT514 board (SS1-14). — A line isolation transformer located on the RT514 board (T1-6) with over-voltage diodes (D1-4) on both sides of each secondary windings.
State-of-Health	
Information Provided:	♦ The AM reports information on battery status, clock setting, gain setting, calibration mode and the communications link.

ACQUISITION PARAMETERS

Acquisition parameters include the sample rate, transmitter frequency and number of samples desired. The operator can also determine whether the AMs calibration signal is activated during data colletcion.
In typical use, the acquisition parameters are set according to the specific application configuration and event type. For each event type, several recording sessions are made, each at a different transmitter frequency and sample rate. The recording period is set based on event type and transmitter frequency.
The listing below shows several examples of event type, typical transmitter frequency (Hz), sample rates (with applicable ADC resolution) and the corresponding number of samples (record period).

Event Type	Transmit Frequency	Sample Rate	ADC Resolution	Number of Sample
Geophysical Response	375 Hz	48,000	24	124,032
Gain Test	375	48,000	24	65,536
Geophysical Response	75	9,600	24	130,176
Gain Test	75	9,600	24	65,536
Geophysical Response	25/8	3,200	24	139,264
Gain Test	25/8	3,200	24	32,768
Sensor Impedance	N/A	1,600	24	8,704
Ambient Noise	N/A	1,600	24	8,192
Geophysical Response	25/128	800	24	147,456
Gain Test	25/128	800	24	16,384
Geophysical Response	25/2048	100	24	212,992
Gain Test	25/256	100	24	4,096
Gain Test	N/A	50	24	4,096
Geophysical Response	N/A	50	24	65,536

SENSOR CALIBRATION

The AM can source a 12.5Hz, 50μA signal to the sensor input for measuring the source impedance of the attached sensor. The user can also specify frequency in amplitude of calibration signal.

TELEMETRY CABLE

The telemetry cable is a *Category V* specification cable and is supplied by the customer.

SAMPLE RATES

The following table shows all available sample rates, based on a 12.288 Mhz oscillator. A 24-bit resolution ADC is used for sample rates 48000 through 4800 and a 24-bit resolution ADC is used for sample rates 3200 and below. The correct ADC is selected automatically by the AM, based on the sample rate.

Typically, different sample rates and transmitter frequencies are used in 50 Hz and 60 Hz power environments to minimize AC power effects on the data. In the table, the shaded areas indicate the sample rates typically used in a 60 Hz power environment. A few rates are typically used in both environments.

Sample Rate	*Power Line*
48000	50 & 60
24000	50 & 60
19200	60
16000	50
12000	50 & 60
9600	50 & 60
6400	50
4800	60
3200	50
1920	60
1600	50
960	60
800	50
480	60
400	50
240	60
200	50
120	60
100	50
60	60
50	50
60/2	60
50/2	50
60/4	60
50/4	50
60/8	60
50/8	50
60/16	60
50/16	50
60/32	60
50/32	50

APPENDIX F

INSTRUMENT SPECIFICATIONS

EMI – ELECTROMAGNETIC INSTRUMENTS INC. – BERKELEY, CA

BF-4 Series Magnetic Sensors

Specifications

Magnetic Sensors

BF-4 Magnetic Field Induction Sensor

Features

- High sensitivity
- Very low noise
- Magnetic feedback design
- Chopper stabilized amplifier for best low frequency performance
- Ruggedized and waterproof
- Light weight and compact design
- Low power consumption (290 mW)
- Stable phase response

Applications

- Geophysical surveys: MT, AMT, CSAMT, MMR, MIP, CSEM
- Marine surveys
- Atmospheric studies
- Earthquake studies
- High accuracy magnetic field studies

Options

- Marine connector for underwater applications

EMI

BF-4 Noise Spectrum

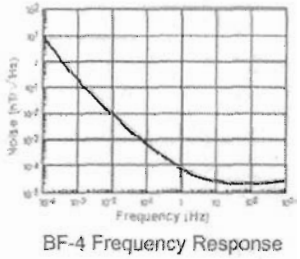

BF-4 Frequency Response

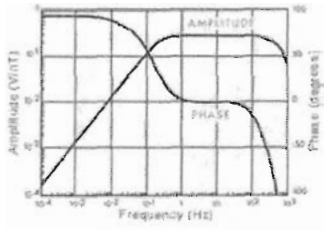

The BF-4 sensor design utilizes a magnetic feedback design to provide a stable flat respose over several decades of frequency. The sensors respond as a B field detector over the flat band regions. Both the amplitude and phase responses are highly stable with variations of less than 0.1 dB in amplitude and +/- 1 degree in phase between sensors. For the frequencies below the flat response region the sensor response is proportional to signal frequency so that the sensor acts as a dB/dt detector. The coil is sealed in epoxy inside a rugged impact resistant Nema G-10 fiberglass tube. A matched low-noise preamplifier is connected to the coil inside the waterproof case and is powered from the connector using a nearby +/- 12V power supply.

Technical Specifications

PERFORMANCE

Frequency Range:
0.0001 to 1000 Hz

3 dB frequency corners:
0.2 Hz, 500 Hz

Sensitivity (flat region):
0.3 V/nT (standard)

Power consumption:
12 mA at +/- 12V

MECHANICAL

Case style:
Nema G-10 Straight Tube

Length:
142 cm (56 in.)

Diameter:
6 cm (2.4 in.)

Weight:
7.9 Kg (17.4 Lbs)

Connector:
8 pin Waterproof Tajimi

For further information please contact gg@emiinc.com

Last modified: March, 2001

APPENDIX F

INSTRUMENT SPECIFICATIONS

EMI – Electromagnetic Instruments Inc. – Berkeley, CA
BF-6 Series Magnetic Sensors

SPECIFICATIONS

Magnetic Sensors

BF-6 Magnetic Field Induction Sensor

Features

- High sensitivity
- Very low noise
- Magnetic feedback design
- Ruggedized and waterproof
- Light weight and compact design
- Low power consumption (210 mW)
- Stable phase response

Applications

- Geophysical surveys: MT, AMT, CSAMT, MMR, MIP, CSEM, TSHMT, Stratagem™
- Marine surveys
- Earthquake studies
- High accuracy magnetic field studies

Options

- Marine connector for underwater applications

BF-6 Noise Spectrum

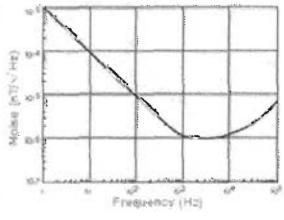

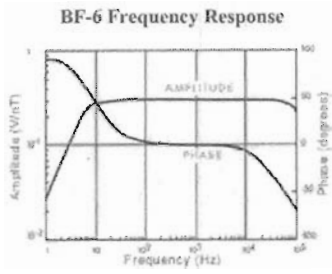

The BF-6 sensor design utilizes a magnetic feedback design to provide a stable flat respose over several decades of frequency. The sensors respond as a B field detector over the flat band regions. Both the amplitude and phase responses are highly stable with variations of less than 0.1 dB in amplitude and +/- 1 degree in phase between sensors. For the frequencies below the flat response region the sensor response is proportional to signal frequency so that the sensor acts as a dB/dt detector. The coil is sealed in epoxy inside a rugged impact resistant ABS tube. A matched low-noise preamplifier is connected to the coil inside the waterproof case and is powered from the connector using a nearby +/- 12V power supply.

Technical Specifications

PERFORMANCE

Frequency Range:
1 Hz to 25 kHz or 1 Hz to 100 kHz

3 dB frequency corners:
10 Hz, 25kHz or 10 Hz, 100 kHz

Sensitivity (flat region):
0.3 V/nT (standard)

Power consumption:
9 mA at +/- 12V

MECHANICAL

Case style:
High Impact ABS Straight Tube

Length:
73 cm (29 in.)

Diameter:
5 cm (2 in.)

Weight:
1.7 Kg (3.7 Lbs)

Connector:
8 pin Waterproof Tajimi

For further information please contact gg@emiinc.com

Last modified: March, 2001

NOTE:

THE AREAS SHOWN ON THIS MAP REPRESENT OWNERSHIP BY APOLLO MINES. THE AREAS SHOWN HAVE BEEN BASED UPON TOWNSHIP MAPS AND ARE NOT, IN ANY MANNER, ATTEMPTING TO SHOW LEGAL PROPERTY BOUNDARIES.

LEGEND:

- APOLLO GOLD OWNED PROPERTIES
- APOLLO GOLD UNPATENTED CLAIMS (PENDING DISPUTE RESOLUTION)
- APOLLO GOLD MINERAL RIGHTS
- APOLLO GOLD SURFACE RIGHTS

W.0780.02012

CON 2

CON 1

CON 6

LOT 5
CON 5

BEATTY
TWP

HISLOP
TWP

PARCEL 3524
Mining Rights
Only

L-1115059
Unpatented

PARCEL 24577
Surface Rights
Only

PARCEL 14572
Surface+Mining
Rights

PARCEL 24577
Surface+Mining
Rights

PARCEL 11720
Mining Rights
Only

Leach
Lake

HWY 101

Froome
Lake

L-1113087
Patented

PARCEL 15466
Surface Severance

PARCEL 7745
Surface+Mining
Rights

PARCEL 4707
Surface+Mining
Rights

PARCEL 2582
Surface+Mining
Rights

L-1048333
Unpatented

L-1048334
Unpatented

PARCEL 11511
Surface+Mining
Rights

PARCEL 3393
Surface+Mining
Rights

L-1048335
Unpatented

PARCEL 388
Surface+Mining
Rights

PARCEL 6413
Surface+Mining
Rights

Lawlar
Lake

9 8 7 6 4 3

0 200 400m
APPROXIMATE SCALE

ApolloGold amec

BLACK FOX PROJECT

LAND TENURE

SCALE: AS SHOWN	DATE: FEBRUARY 2007
PROJECT NUMBER: TC51500	**FIGURE 1-2**

P:\EARD\PROJECTS\TC51500 (Apollo - ENV)\Project Description - Updated for Small Pit\Drawings & Figures - updated 2007\Figure 1-2 Land Tenure.dwg Feb 22/2007 4:01:04 PM EST